

**INVESTIGATION OF DESIGN AND ANALYSES PRINCIPLES
OF
HONEYCOMB STRUCTURES**

**A THESIS SUBMITTED TO
THE GRADUATE SCHOOL OF NATURAL AND APPLIED SCIENCES
OF
MIDDLE EAST TECHNICAL UNIVERSITY**

BY

İLKE AYDINCAK

**IN PARTIAL FULFILLMENT OF THE REQUIREMENTS
FOR
THE DEGREE OF MASTER OF SCIENCE
IN
AEROSPACE ENGINEERING**

NOVEMBER 2007

Approval of the thesis:

**INVESTIGATION OF DESIGN AND ANALYSES PRINCIPLES
OF
HONEYCOMB STRUCTURES**

submitted by **İLKE AYDINCAK** in partial fulfillment of the requirements for
the degree of **Master of Science in Aerospace Engineering Department,**
Middle East Technical University by,

Prof. Dr. Canan Özgen _____
Dean, Graduate School of **Natural and Applied Sciences**

Prof. Dr. İsmail Hakkı Tuncer _____
Head of Department, **Aerospace Engineering**

Assoc. Prof. Dr. Altan Kayran _____
Supervisor, **Aerospace Engineering Dept., METU**

Examining Committee Members:

Prof. Dr. Ozan Tekinalp _____
Aerospace Engineering Dept., METU

Assoc. Prof. Dr. Altan Kayran _____
Aerospace Engineering Dept., METU

Asst. Prof. Dr. Melin Şahin _____
Aerospace Engineering Dept., METU

Dr. Güçlü Seber _____
Aerospace Engineering Dept., METU

Dr. Gökmen Mahmutyazıcıoğlu _____
TÜBİTAK-SAGE

Date: _____

I hereby declare that all information in this document has been obtained and presented in accordance with academic rules and ethical conduct. I also declare that, as required by these rules and conduct, I have fully cited and referenced all material and results that are not original to this work.

Name, Last name: İlke AYDINCAK

Signature:

ABSTRACT

INVESTIGATION OF DESIGN AND ANALYSES PRINCIPLES OF HONEYCOMB STRUCTURES

Aydıncak, İlke

M.Sc., Department of Aerospace Engineering

Supervisor: Assoc. Prof. Dr. Altan Kayran

November 2007, 177 pages

In this thesis, design and analyses of honeycomb structures are investigated. Primary goal is to develop an equivalent orthotropic material model that is a good substitute for the actual honeycomb core. By replacing the actual honeycomb structure with the orthotropic model, during the finite element analyses, substantial advantages can be obtained with regard to ease of modeling and model modification, solution time and hardware resources . To figure out the best equivalent model among the approximate analytical models that can be found in the literature, a comparison is made. First sandwich beams with four different honeycomb cores are modeled in detail and these are accepted as reference models. Then a set of equivalent models with the same dimensions is generated. The material properties of the equivalent models are taken from different studies performed in the literature. Both models are analyzed under the same loading and the boundary conditions. In finite element analyses, ANSYS finite element program is used. The results are compared to find out the best performing equivalent model. After three major analyses loops, decision on the equivalent model is made. The differences between the total reaction forces calculated by the equivalent model and the actual honeycomb model are all found to be within 10%. The equivalent model gives stress results at the macro-

scale, and the local stresses and the strains can not be determined. Therefore it is deemed that for stress analysis, equivalent model can be used during the preliminary design phase. However, the equivalent model can be used reliably for deflection analysis, modal analysis, stiffness determination and aero-elastic analysis.

Keywords: Honeycomb, Sandwich Structures, Equivalent Model, Orthotropic Material, Finite Element Method

ÖZ

BALPETEĞİ MALZEMELERİN TASARIM VE ANALİZ YÖNTEMLERİNİN İNCELENMESİ

Aydıncak, İlke

Yüksek Lisans, Havacılık ve Uzay Mühendisliği Bölümü

Tez Yöneticisi: Doç. Dr. Altan Kayran

Kasım 2007, 177 sayfa

Bu tezde, balpeteği malzemelerin tasarım ve analiz yöntemleri incelenmiştir. Birincil amaç, balpeteği malzemenin yerini tutacak iyi bir ortotropik denk model geliştirmektir. Sonlu elemanlar analizleri sırasında bu malzemenin ortotropik model ile değiştirilmesi modellemedeki ve modelin değiştirilmesindeki kolaylık, çözüm zamanı ve donanım ihtiyacı gibi konular dikkate alındığında büyük avantajlar sağlamaktadır. Literatürde bulunan yaklaşık analitik modeller arasından en iyi denk modeli belirlemek için bir karşılaştırma yapılması gerekmektedir. İlk olarak dört farklı balpeteği ile sandviç kirişler detaylı olarak modellenmiş ve bunlar referans modeller olarak kabul edilmiştir. Daha sonra aynı ölçülere sahip bir set denk model hazırlanmıştır. Bu denk modellerin malzeme özellikleri literatürde bulunan çalışmalardan alınmıştır. Her iki model de aynı yük ve sınır şartlarında analiz edilmiştir. Analizlerde ANSYS sonlu elemanlar programı kullanılmıştır. Analiz sonuçları, en iyi başarıma sahip denk modeli bulmak için karşılaştırılmıştır. Üç ana analiz döngüsünden sonra denk model üzerinde karara varılmıştır. Balpeteği model ve denk modelde elde edilen toplam tepki kuvvetleri arasındaki fark %10'luk aralık içerisindeydir. Denk model gerilmeleri makro ölçekte verdiği için bölgesel gerilme ve uzamalar belirlenmemektedir. Bu sebeple, denk modelin ön tasarım aşamasında

kullanılabileceđi varsayılmıřtır. Bununla birlikte, denk model güvenilir bir řekilde eđilme analizlerinde, modal analizlerde, rijitlik belirlenmesinde ve aero-elastik analizlerde kullanılabilir.

Anahtar Kelimeler: Balpeteđi Malzemeler, Sandviç Yapılar, Denk Model, Ortotropik Malzeme , Sonlu Elemanlar Yöntemi

Now and Ever

ACKNOWLEDGMENTS

I would like to express my special thanks and gratitude to my supervisor Assoc. Prof. Dr. Altan KAYRAN for his guidance, motivation and patience.

I would like to thank my coordinator Dr. Mehmet Ali AK and my chiefs Rıza GENÇ and M.Cengizhan YILDIRIM for their support and understanding.

My dear colleagues Mete AYDEMİR, Raci GENÇ and Ayça ÇEKİÇ are gratefully acknowledged for their motivation and help.

I owe a special to thank Özlem SÖKMEN for her technical advices, help and discussions during my studies

I also wish to thank my dear friends İ. Evrim DİZEMEN, Yücel DEVELLİOĞLU, A. Bahar HASER, K. Efe KAFDAĞLI and Argün KATIRCI for their help and support through my studies.

I would also like to express my very special thanks to my dear Aunt Fatma GÜRER for proof – reading my thesis and guiding me in grammatical issues.

I would like to thank my family for their endless love, support, patience and encouragement throughout my all education. I wish to thank and to express my love to my beloved grandmother who raised me. Rest in peace grandma.

Finally, I would like express my very special thanks to Aysun, for her endless support, faith in me, patience and love from the very beginning of this thesis. Her motivation, threats and encouragements kept me going on during times “I was in serious trouble”. Words are not enough to express my gratefulness to her, without her, none of these would have been possible.

TABLE OF CONTENTS

ABSTRACT	iv
ÖZ	vi
ACKNOWLEDGMENTS	ix
TABLE OF CONTENTS	x
LIST OF FIGURES	xii
LIST OF TABLES	xiv
LIST OF SYMBOLS AND ABBREVIATIONS	xviii

CHAPTERS

1. INTRODUCTION	1
1.1 COMPOSITE MATERIALS	3
1.2 SANDWICH STRUCTURES	5
1.2.1 FACE SHEET MATERIALS	7
1.2.2 CORE MATERIALS	8
1.2.3 ADHESIVES	8
1.3 MAIN APPLICATION AREAS OF HONEYCOMB SANDWICH STRUCTURES	9
1.3.1 COMMERCIAL AEROSPACE	9
1.3.2 SPACE & DEFENCE	13
1.3.3 MARINE & RAIL	16
1.3.4 AUTOMOTIVE	18
1.3.5 ELECTROMAGNETIC INTERFERENCE (EMI) FILTERING	20
1.4 MANUFACTURING OF HONEYCOMB CORES	20
1.5 FAILURE MODES OF HONEYCOMB SANDWICH STRUCTURES	25
1.6 ADVANTAGES OF USING HONEYCOMB STRUCTURES	27
2. THEORY	29
2.1 FUNDAMENTALS OF SANDWICH THEORY	29
2.2 RELATIVE STIFFNESS & RELATIVE STRENGTH	32
2.3 ANISOTROPY – ORTHOTROPY	36
2.4 ESTIMATION / CALCULATION OF THE ELASTIC CONSTANTS OF ORTHOTROPIC MATERIALS	38
2.4.1 CALCULATION OF E_3	40
2.4.2 CALCULATION OF E_1 & E_2	42
2.4.3 CALCULATION of $\nu_{12}, \nu_{13}, \nu_{23}$	47
2.4.4 CALCULATION of G_{12}, G_{13}, G_{23}	49
2.5 DIFFERENT MODELS ON THE NINE ELASTIC CONSTANTS:	50
3. MODELING	55
3.1 GEOMETRIC MODELING OF THE HONEYCOMB SANDWICH STRUCTURES	56
3.1.1 Full 3D Modeling	56

3.1.2	Shell Modeling	56
3.1.3	Mixed Modeling	58
3.2	FINITE ELEMENT MODELING OF THE HONEYCOMB STRUCTURES	59
3.2.1	ANSYS ELEMENTS USED IN ANALYSES	64
3.2.2	EFFECT OF NODE POSITIONS:.....	67
3.3	HONEYCOMBS USED IN THE ANALYSES:	71
4.	ANALYSES:.....	74
4.1	EQUIVALENT MODELING:.....	78
4.2	CANDIDATE EQUIVALENT MODELS:	78
4.3	MODEL GENERATION:.....	83
4.4	ASSUMPTIONS:	85
4.5	LOADS AND BOUNDARY CONDITIONS:.....	85
4.6	MESHING:.....	89
4.6.1	Meshing of the HC Models:.....	89
4.6.2	Meshing of the equivalent models:	91
5.	RESULTS & DISCUSSION:.....	93
5.1	RESULTS OF THE FIRST RUNS:.....	93
5.2	DISCUSSION ON THE FIRST RUNS:	99
5.2.1	CHECKING OF THE NUMERICAL RESULTS:	99
5.2.2	RE-MODELING OF THE REFERENCE MODELS-1:	101
5.2.3	RE-MODELING THE REFERENCE MODELS - 2:.....	102
5.3	DISCUSSION ON THE SECOND RUNS:.....	103
5.4	DECISION ON THE EQUIVALENT MODEL:.....	109
5.5	EQUIVALENT MODEL COEFFICIENTS:	112
5.6	COMPARISON OF REFERENCE AND EQUIVALENT MODELS:.....	113
6.	TEST CASE:.....	115
6.1	MODELING & ANALYSES OF THE WING:.....	116
6.2	RESULTS:	119
6.2.1	Weight:.....	119
6.2.2	Displacements & Stresses:	120
7.	CONCLUDING REMARKS AND FUTURE WORK:.....	130
	REFERENCES.....	134
	APPENDIX A	138
	APPENDIX B	150
	APPENDIX C	158
	APPENDIX D	170
	APPENDIX E.....	176

LIST OF FIGURES

Figure 1.1	Sandwich Panel	5
Figure 1.2	Mosquito Aircraft [7]	6
Figure 1.3	Natural Sandwich Structures	7
Figure 1.4	A Commercial Aircraft [14]	10
Figure 1.5	A Jet Engine [14]	11
Figure 1.6	A Helicopter [14]	12
Figure 1.7	A Fighter Aircraft [14]	13
Figure 1.8	A Launcher [14]	14
Figure 1.9	A Satellite [14]	15
Figure 1.10	Sail [14]	16
Figure 1.11	Train Wagon [14]	17
Figure 1.12	Crash Test Barriers [14]	18
Figure 1.13	Car [14]	19
Figure 1.14	Ventilation panel with EMI shielding [15]	20
Figure 1.15	Expansion Method [16]	21
Figure 1.16	Corrugation Method [17]	22
Figure 1.17	Router Bit Type Cutting Tools [18]	23
Figure 1.18	Unit HC Cell [19]	24
Figure 1.19	Failure Modes of HC Structures [6]	26
Figure 1.20	Advantages of Sandwich Structures [20]	28
Figure 2.1	Dimensions of A Sandwich Beam	29
Figure 2.2	Error due to neglecting the first term in Eq. 2.2	31
Figure 2.3	Error due to neglecting the first and third terms in Eq. 2.2	31
Figure 2.4	Relative I,S and W versus Face Sheet Thickness, Constant Core Thickness	35
Figure 2.5	Relative I,S and W versus Face Sheet Thickness, Constant Total Height	35
Figure 2.6	HC Axis System	38
Figure 2.7	Walls of HC	42
Figure 2.8	Deformation in 2 Direction [30]	42
Figure 2.9	Idealized Unit Cell [30]	43
Figure 2.10	Deformation in 1 Direction	46
Figure 3.1	Divided Face Sheets Area	57
Figure 3.2	Sheet Modeling	58
Figure 3.3	Mixed Modeling	59
Figure 3.4	Two Blocks	60
Figure 3.5	Meshed Two Blocks	61
Figure 3.6	Mesh of Single Volume	61
Figure 3.7	Divided Volume	62
Figure 3.8	Mapped Meshed Volumes	63
Figure 3.9	SHELL93 ELEMENT	64
Figure 3.10	SOLID 186 ELEMENT	65
Figure 3.11	MPC 184 RIGID LINK/RIGID BEAM ELEMENT	66
Figure 3.12	SHELL99 ELEMENT	67

Figure 3.13	Modified Unit Cell	68
Figure 3.14	Interference of the HC Core and the Face Sheet	68
Figure 3.15	Reduced Height Due to the Interference	69
Figure 3.16	Unit Cell Meshed with SHELL99 (Nodes are shifted)	69
Figure 3.17	Beams with different node locations	70
Figure 3.18	Effect of Node Locations	71
Figure 4.1	Flowchart of the Overall Process	77
Figure 4.2	HC model and the Equivalent Model	78
Figure 4.3	Sample Beam Geometry.....	83
Figure 4.4	The Analyzed Beam to Visualize the Waviness	86
Figure 4.5	The Deflections of the Analyzed Beam	86
Figure 4.6	The Deflections of the Analyzed Beam (Closer View).....	87
Figure 4.7	Faces of a Beam	87
Figure 4.8	Boundary Conditions for Load Case 2.....	88
Figure 4.9	A sample Beam, Meshed with Shell Elements	89
Figure 4.10	A sample Beam, Meshed with Shell Elements (Closer View).....	90
Figure 4.11	A sample Beam, Meshed with Shell and Solid Elements	90
Figure 4.12	A sample Beam, Meshed with Shell and Solid Elements (Closer View).....	91
Figure 4.13	A sample Equivalent Beam, Meshed with Solid Elements.....	91
Figure 4.14	A sample Equivalent Beam, Meshed with Solid Elements.....	92
Figure 5.1	A unit cell with MPC184 elements	102
Figure 6.1	V-n Diagram for the Tomahawk Cruise Missile [35]	116
Figure 6.2	Exploded View of The Wing	117
Figure 6.3	Meshed Wing	118
Figure 6.4	Pressure Distribution Over The Wing.....	119
Figure 6.5	Displacement of Solid Wing	121
Figure 6.6	Displacement of Sandwich Wing.....	122
Figure 6.7	Solid Wing Stress Distribution.....	124
Figure 6.8	Sandwich Wing Stress Distribution	124
Figure 6.9	Solid Wing Stress Distribution, Longitudinal Cut	125
Figure 6.10	Sandwich Wing, Stress Distribution, Longitudinal Cut.....	125
Figure 6.11	Solid Wing, Stress Distribution, Transverse Cut	126
Figure 6.12	Sandwich Wing, Stress Distribution, Transverse Cut.....	126
Figure 6.13	Deformation of The Solid and The Sandwich Wing, Mod 1, Bending.....	128
Figure 6.14	Deformation of The Solid and The Sandwich Wing, Mod 2, Bending.....	128
Figure 6.15	Deformation of The Solid and The Sandwich Wing, Mod 3, Torsion.....	128

LIST OF TABLES

Table 2.1	Formulas for E_1	50
Table 2.2	Formulas for E_2	51
Table 2.3	Formulas for E_3	51
Table 2.4	Formulas for ν_{12}	52
Table 2.5	Formulas for ν_{23}	52
Table 2.6	Formulas for ν_{13}	52
Table 2.7	Formulas for G_{12}	53
Table 2.8	Formulas for G_{23}	53
Table 2.9	Formulas for G_{13}	54
Table 3.1	The Selected Honeycombs	72
Table 3.2	Mechanical Properties of AA-5052 [33].....	72
Table 4.1	The Models and the Related References.....	75
Table 4.2	Orthotropic Material Properties for 10 Equivalent Models for CS1.....	79
Table 4.3	Orthotropic Material Properties for 10 Equivalent Models for CS2.....	80
Table 4.4	Orthotropic Material Properties for 10 Equivalent Models for CS3.....	81
Table 4.5	Orthotropic Material Properties for 10 Equivalent Models for CS4.....	82
Table 4.6	Dimensions of the Analyzed Beams	84
Table 4.7	Loads & Boundary Conditions.....	88
Table 5.1	The Load Cases and Corresponding FSUM Values.....	94
Table 5.2	The Relative difference between Honeycomb and Equivalent Models of CS1-H1 in the First Runs	95
Table 5.3	The Relative difference between Honeycomb and Equivalent Models of CS2-H1 in the First Runs	96
Table 5.4	The Relative difference between Honeycomb and Equivalent Models of CS3-H1 in the First Runs	97
Table 5.5	The Relative difference between Honeycomb and Equivalent Models of CS4-H1 in the First Runs	98
Table 5.6	Comparison of Calculations of ANSYS and Theory	101
Table 5.7	Comparison of the Total Reaction Forces- Shell Modeling and Mixed Modeling of the Honeycomb Structure for CS1-H1	103
Table 5.8	The Relative Difference between Mixed Honeycomb and Equivalent Models of CS1-H1 in the Second Runs	105
Table 5.9	The Difference between Mixed Honeycomb and Equivalent Models of CS2-H1 in the Second Runs	106
Table 5.10	The Relative Difference between Mixed Honeycomb and Equivalent Models of CS3-H1 in the Second Runs	107
Table 5.11	The Relative Difference between Mixed Honeycomb and Equivalent Models of CS4-H1 in the Second Runs	108
Table 5.12	New Candidate Models for the Third Runs	109

Table 5.13	The Relative Difference between the Honeycomb and Regenerated Equivalent Models of CS1-H1 in the Third Runs	110
Table 5.14	The Relative Difference between the Honeycomb and Regenerated Equivalent Models of CS2-H1 in the Third Runs	110
Table 5.15	The Relative Difference between the Honeycomb and Regenerated Equivalent Models of CS3-H1 in the Third Runs	111
Table 5.16	The Relative Difference between the Honeycomb and Regenerated Equivalent Models of CS4-H1 in the Third Runs	111
Table 5.17	The Material Coefficients Of The Model 13	112
Table 5.18	Comparison Of Reference and Equivalent Models.....	113
Table 6.1	Forces and Moments Acting On the Wing.....	116
Table 6.2	Mechanical Properties of AA-7075 [36].....	120
Table 6.3	Maximum Deflections for the Solid and the Sandwich Wing .	120
Table 6.4	Comparison of Wing Alternatives.....	122
Table 6.5	Maximum Stress Values for the Solid and the Sandwich Wing	123
Table 6.6	Margin of Safety of the Solid and the Sandwich Wing.....	123
Table 6.7	First Three Modal Frequencies	127
Table A.1	The Relative Difference between the Honeycomb and Regenerated Equivalent Models of CS1-H2 in the First Runs (h=7.938).....	138
Table A.2	The Relative Difference between the Honeycomb and Regenerated Equivalent Models of CS2-H2 in the First Runs (h=7.938).....	139
Table A.3	The Relative Difference between the Honeycomb and Regenerated Equivalent Models of CS3-H2 in the First Runs (h=7.938).....	140
Table A.4	The Relative Difference between the Honeycomb and Regenerated Equivalent Models of CS4-H2 in the First Runs (h=7.938).....	141
Table A.5	The Relative Difference between the Honeycomb and Regenerated Equivalent Models of CS1-H3 in the First Runs (h=21.813).....	142
Table A.6	The Relative Difference between the Honeycomb and Regenerated Equivalent Models of CS2-H3 in the First Runs (h=21.813).....	143
Table A.7	The Relative Difference between the Honeycomb and Regenerated Equivalent Models of CS3-H3 in the First Runs (h=21.813).....	144
Table A.8	The Relative Difference between the Honeycomb and Regenerated Equivalent Models of CS1-H3 in the First Runs (h=21.813).....	145
Table A.9	The Relative Difference between the Honeycomb and Regenerated Equivalent Models of CS1-H4 in the First Runs (h=31.750).....	146
Table A.10	The Relative Difference between the Honeycomb and Regenerated Equivalent Models of CS2-H4 in the First Runs (h=31.750).....	147
Table A.11	The Relative Difference between the Honeycomb and Regenerated Equivalent Models of CS3-H4 in the First Runs (h=31.750).....	148
Table A.12	The Relative Difference between the Honeycomb and Regenerated Equivalent Models of CS4-H4 in the First Runs (h=31.750).....	149
Table B.1	Comparison of the Total Reaction Forces- Shell Modeling and Mixed Modeling of the Honeycomb Structure for CS2-H1	150
Table B.2	Comparison of the Total Reaction Forces- Shell Modeling and Mixed Modeling of the Honeycomb Structure for CS3-H1	150

Table B.3	Comparison of the Total Reaction Forces- Shell Modeling and Mixed Modeling of the Honeycomb Structure for CS4-H1.....	151
Table B.4	Comparison of the Total Reaction Forces- Shell Modeling and Mixed Modeling of the Honeycomb Structure for CS1-H2.....	151
Table B.5	Comparison of the Total Reaction Forces- Shell Modeling and Mixed Modeling of the Honeycomb Structure for CS2-H2.....	152
Table B.6	Comparison of the Total Reaction Forces- Shell Modeling and Mixed Modeling of the Honeycomb Structure for CS3-H2.....	152
Table B.7	Comparison of the Total Reaction Forces- Shell Modeling and Mixed Modeling of the Honeycomb Structure for CS4-H2.....	153
Table B.8	Comparison of the Total Reaction Forces- Shell Modeling and Mixed Modeling of the Honeycomb Structure for CS1-H3.....	153
Table B.9	Comparison of the Total Reaction Forces- Shell Modeling and Mixed Modeling of the Honeycomb Structure for CS2-H3.....	154
Table B.10	Comparison of the Total Reaction Forces- Shell Modeling and Mixed Modeling of the Honeycomb Structure for CS3-H3.....	154
Table B.11	Comparison of the Total Reaction Forces- Shell Modeling and Mixed Modeling of the Honeycomb Structure for CS4-H3.....	155
Table B.12	Comparison of the Total Reaction Forces- Shell Modeling and Mixed Modeling of the Honeycomb Structure for CS1-H4.....	155
Table B.13	Comparison of the Total Reaction Forces- Shell Modeling and Mixed Modeling of the Honeycomb Structure for CS2-H4.....	156
Table B.14	Comparison of the Total Reaction Forces- Shell Modeling and Mixed Modeling of the Honeycomb Structure for CS3-H4.....	156
Table B.15	Comparison of the Total Reaction Forces- Shell Modeling and Mixed Modeling of the Honeycomb Structure for CS4-H4.....	157
Table C.1	The Relative Difference between the Honeycomb and Regenerated Equivalent Models of CS1-H2 in the First Runs (h=7.938).....	158
Table C.2	The Relative Difference between the Honeycomb and Regenerated Equivalent Models of CS2-H2 in the First Runs (h=7.938).....	159
Table C.3	The Relative Difference between the Honeycomb and Regenerated Equivalent Models of CS3-H2 in the First Runs (h=7.938).....	160
Table C.4	The Relative Difference between the Honeycomb and Regenerated Equivalent Models of CS4-H2 in the First Runs (h=7.938).....	161
Table C.5	The Relative Difference between the Honeycomb and Regenerated Equivalent Models of CS1-H3 in the First Runs (h=21.813).....	162
Table C.6	The Relative Difference between the Honeycomb and Regenerated Equivalent Models of CS2-H3 in the First Runs (h=21.813).....	163
Table C.7	The Relative Difference between the Honeycomb and Regenerated Equivalent Models of CS3-H3 in the First Runs (h=21.813).....	164
Table C.8	The Relative Difference between the Honeycomb and Regenerated Equivalent Models of CS4-H3 in the First Runs (h=21.813).....	165
Table C.9	The Relative Difference between the Honeycomb and Regenerated Equivalent Models of CS1-H4 in the First Runs (h=31.750).....	166
Table C.10	The Relative Difference between the Honeycomb and Regenerated Equivalent Models of CS2-H4 in the First Runs (h=31.750).....	167

Table C.11	The Relative Difference between the Honeycomb and Regenerated Equivalent Models of CS3-H4 in the First Runs (h=31.750).....	168
Table C.12	The Relative Difference between the Honeycomb and Regenerated Equivalent Models of CS4-H4 in the First Runs (h=31.750).....	169
Table D.1	The Relative Difference between the Honeycomb and Regenerated Equivalent Models of CS1-H2 in the Third Runs	170
Table D.2	The Relative Difference between the Honeycomb and Regenerated Equivalent Models of CS2-H2 in the Third Runs	170
Table D.3	The Relative Difference between the Honeycomb and Regenerated Equivalent Models of CS3-H2 in the Third Runs	171
Table D.4	The Relative Difference between the Honeycomb and Regenerated Equivalent Models of CS4-H2 in the Third Runs	171
Table D.5	The Relative Difference between the Honeycomb and Regenerated Equivalent Models of CS1-H3 in the Third Runs	172
Table D.6	The Relative Difference between the Honeycomb and Regenerated Equivalent Models of CS2-H3 in the Third Runs	172
Table D.7	The Relative Difference between the Honeycomb and Regenerated Equivalent Models of CS3-H3 in the Third Runs	173
Table D.8	The Relative Difference between the Honeycomb and Regenerated Equivalent Models of CS4-H3 in the Third Runs	173
Table D.9	The Relative Difference between the Honeycomb and Regenerated Equivalent Models of CS1-H4 in the Third Runs	174
Table D.10	The Relative Difference between the Honeycomb and Regenerated Equivalent Models of CS2-H4 in the Third Runs	174
Table D.11	The Relative Difference between the Honeycomb and Regenerated Equivalent Models of CS3-H4 in the Third Runs	175
Table D.12	The Relative Difference between the Honeycomb and Regenerated Equivalent Models of CS4-H4 in the Third Runs	175

LIST OF SYMBOLS AND ABBREVIATIONS

x,y,z	Rectangular Coordinates
$1,2,3$	Honeycomb Sandwich Beam Coordinates
FEM	Finite Element Method
HC	Honeycomb
EMI	Electromagnetic Interference
d	Honeycomb Cell Size
a	Honeycomb Cell Edge Length
t_c	Foil Thickness
L	Length
W	Width
h_c	Height of the Unit Cell.
t	Thickness
E	Modulus of Elasticity
E_f	Modulus of Elasticity of the Face Sheets
E_c	Modulus of Elasticity of the Core
I	Second Moment of Inertia
D	Flexural Rigidity
b	Width of the Beam
M	Applied Moment
M_{\max}	Maximum Moment
σ_{all}	Allowable Stress that the Material Can Resist
F	Applied Force
W	Weight
C_{ij}	is the stiffness matrix $i,j=1,\dots, 6$
E_i	Modulus of Elasticity in i direction, $i=1,2,3$
E_{hc}	Modulus of Elasticity of the honeycomb core material
ν_{ij}	Poisson's Ratio in ij , $i,j=1,2,3$
ν_{hc}	Poisson's Ratio of the honeycomb core material

G_{ij}	Shear Modulus of Elasticity in i direction, $i=1,2,3$
G_{hc}	Shear Modulus of Elasticity of the honeycomb core material
A_{hc}	Area of the honeycomb in 1-2 plane
ε_{hc}	Strain of the honeycomb
K	Plate Stiffness
$w_{,\bar{x}}$	Partial derivative of w in \bar{x}
$w_{,\bar{x}\bar{x}}$	Second partial derivative of w in \bar{x}
$w_{,\bar{x}\bar{x}\bar{x}}$	Third partial derivative of w in \bar{x}
$w_{,\bar{x}\bar{x}\bar{x}\bar{x}}$	Fourth partial derivative of w in \bar{x}
δ	Displacement
MPC	Multi Point Constraint
APDL	ANSYS Parametric Design Language

CHAPTER 1

INTRODUCTION

Composite materials are widely used in today's modern world. With the advent of new materials, production techniques and new application areas, etc., composite materials have become one of the most attractive areas in engineering. As in many areas of engineering, generic applications are based on analytical methods and with the increasing complexity of the geometries, boundary conditions and material, in almost every case, the use of analytical methods become very tedious if not impossible. At this point, the use of computational methods comes into picture. With the help of computational methods, namely finite element method (FEM) for structural analyses, highly complicated problems can be handled with great accuracy. The disadvantage of using computational methods is that, in order to get accurate results, too much computational time is needed, and this increases when the problem becomes more complex. In addition, FEM models require a detailed study before the model is sent to the solver.

In this thesis, honeycomb structures (HC), which is a specific type of composite structure are investigated. HC structures are mostly used in sandwich structures. Because of the web-type structure of the HC's, the sandwich structure made from HC's is relatively complex from the modeling and analysis point of view. The goal in this post-graduate study is to generate an orthotropic equivalent model that can be used instead of the honeycomb structure itself. Thus, a great decrease in the preprocessor time and computation time can be achieved. The generated equivalent model can be used mostly in the preliminary design stage of the design process. Because of the nature of the preliminary design stage, the

requirements, the geometries, and the loads of any kind, change very often, which resolves the problem to get the results for the updated design. In addition to these, there are many different HC's with different cell sizes, wall thicknesses and material that can be readily found on the market. Hence, instead of using a finite element model that fully models the details, an equivalent model can be used to reduce the time spent for the analysis of the HC structure. In the following chapters, it will be seen that the equivalent model gives macro scale results, which means that in order to get the results for the micro scale, i.e. the stresses on the cell walls and local displacements, a more detailed 3-D model should be used.

In the FEM analyses, the ANSYS commercial program is used. ANSYS is a very powerful FEM solver with sophisticated pre- and post- processor capabilities. Although during the analyses, version 7.0 and 10.0 are used, the analyses are finalized with the release of the latest version, v11.0. In the modeling of HC's, the popular computer aided design programs NX 3.0 and later on NX 4.0 are used together with the preprocessor module of ANSYS. The advantages in using NX are the ease of parametric modeling and array creation, alongside the capability of exporting the model in various file types, like parasolid and IGES. Lastly, another very significant advantage of NX is the direct import capability of the NX file to ANSYS without of additional operations is also a very significant advantage of NX. [1]

In the following sections of this chapter, general information on the composites and specifically on honeycomb structures will be presented. In chapter 2, sandwich theory will be introduced and the material properties of the honeycombs will be investigated. In chapter 3, geometric and finite element modeling of the honeycomb structures will be explained and the different approaches in modeling will also be discussed. In addition, honeycomb cores that are subjected to analyses are introduced here. In chapter 4, information on

equivalent modeling, candidate equivalent models, meshing, loading and boundary conditions is given.

In chapter 5, results of the analyses performed for the determination of the study will be supplied, alongside the problems encountered and solutions proposed, and finally the “best” equivalent model will be chosen. In the 6th chapter, a case study is performed in order to demonstrate the application of equivalent model; subsequently, the results are supplied. Finally, in the last chapter, conclusion of the studies is given and researchers interested in the subject matter are encouraged to do further work.

1.1 COMPOSITE MATERIALS

A composite material is made by combining two or more materials to give a unique combination of the properties of the constituent materials [2]. The advantage of the composites is that they usually exhibit the best qualities of the constituents and some qualities that neither constituent possesses. The properties that can be improved include [3]:

- Strength
- Stiffness
- Corrosion resistance
- Wear resistance
- Attractiveness
- Weight
- Fatigue life
- Thermal insulation
- Thermal conductivity
- Acoustical Insulation

The composite materials are not "new". Since ancient times mankind has used composite materials in different areas. Straw was used to strengthen mud bricks. Medieval swords and armor were constructed with layers of different materials [3]. In the Mongolian arcs, compressed parts that are made of corn, and stretched parts that are made of wood and cow tendons were glued together [4]. Although the use of composite materials is not new, the history of modern composites probably began in 1937 when salesmen from the Owens Corning Fiberglass Company began to sell fiberglass to interested parties around the United States. In 1930, fiberglass had been made, almost by accident in 1930, when an engineer became intrigued by a fiber that was formed during the process of applying lettering to a glass milk bottle [5]. Since then, many different types of composite materials have been invented and numerous studies performed on the mechanics of composite structures.

The range of application of composite materials is very large; some of the main application areas are listed below: [4]

- Electronics
- Buildings
- Road transportation
- Rail transportation
- Marine Transportation
- Air & Space Transportation

In general, composite materials can be classified as follows:

1. Fibrous composites
2. Laminated composites
3. Particulate composites

The reader may refer to any book on composite materials (for instance, [2], [3], [4] etc.) in order to find much more detailed information.

1.2 SANDWICH STRUCTURES

Sandwich structures are a special kind of laminated composite. Laminated composites consist of layers of at least two different materials that are bonded together. A structural sandwich consists of three elements, as shown in Fig 1.1:

1. Face sheets;
- 2) Core
- 3) Adhesive

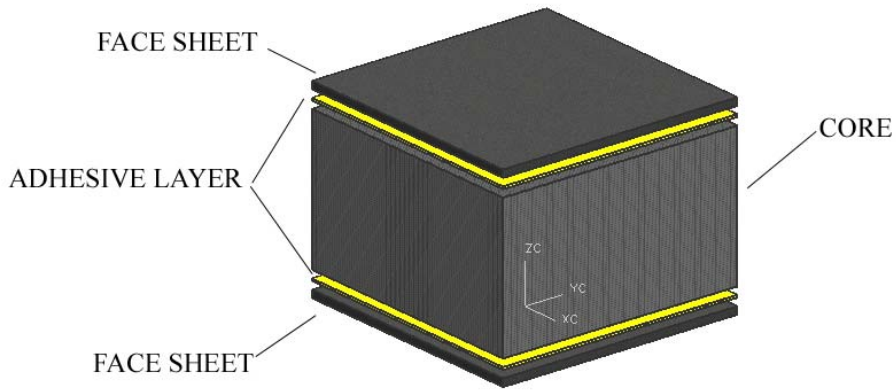


Figure 1.1 Sandwich Panel

Structural sandwich construction is one of the first forms of composite structures that have attained broad acceptance and usage. Virtually all commercial airliners and helicopters, and nearly all military air and space vehicles make extensive usage of sandwich construction. In addition to air and space vehicles, this system is commonly used in the manufacture of cargo containers, movable shelters and airfield surfacing, navy ship interiors, small boats and yachts, die models and production parts in the automobile and recreational vehicle industry,

snow skis, display cases, residential construction materials, interior partitions, doors, cabinets, and a great many of other everyday items. [6]

The idea of using two cooperating faces with a distance between them was introduced by Delau in about 1820. The first extensive use of sandwich panels was during WW II. First theoretical writings appeared also during WW II. In the “Mosquito” aircraft, shown in Fig. 1.2, the sandwich structure was used, mainly because of the shortage of other materials, in England during the war. The faces were made of veneer while the core consisted of balsa wood. One of the early uses of sandwich structures in an aerospace application was in 1937, where balsa wood core and cedar plywood face sheets were used in the construction of De Havilland Albatross airplane.

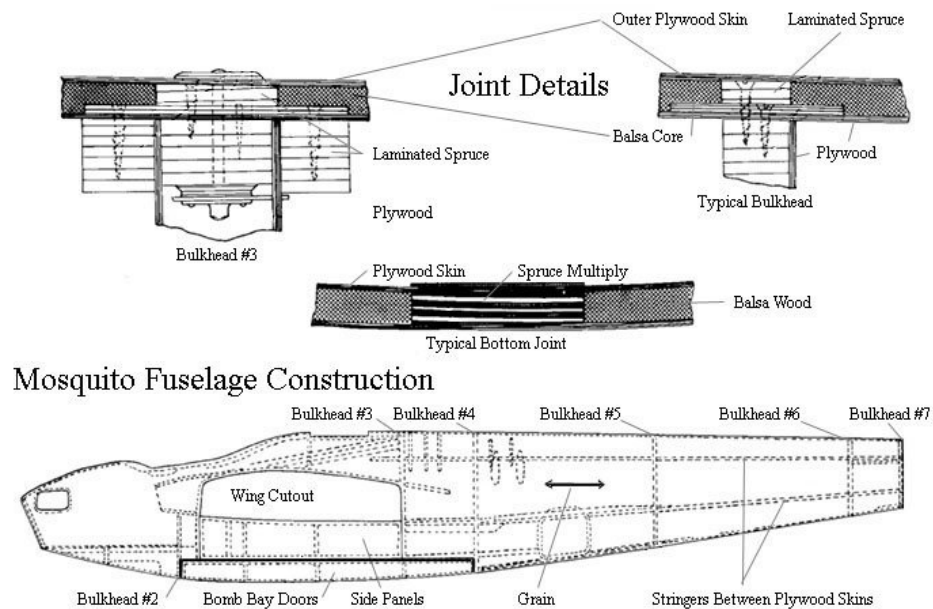


Figure 1.2 Mosquito Aircraft [7]

After the 50's, with the advent of new materials and new production techniques, most of the severe problems of sandwich panels were solved. [8]

Natural sandwich structures also exist, in Fig. 1.3, the upper figure is a section of a human skull, showing two layers of dense compact bone separated by a layer of spongy trabecular bone and the lower one is a section from a bird's wing. [9]

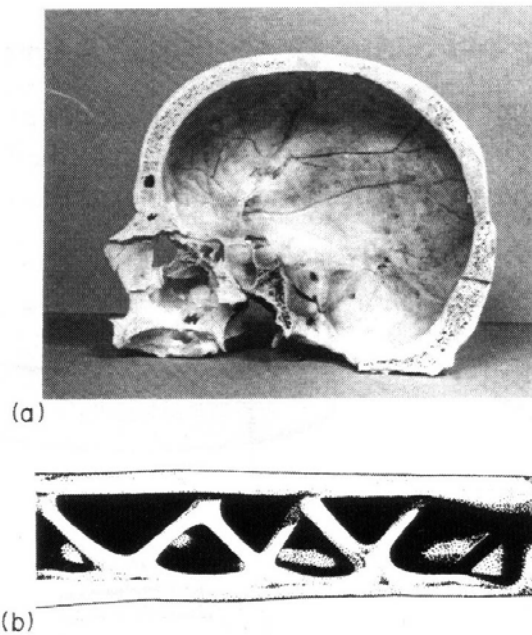


Figure 1.3 Natural Sandwich Structures

1.2.1 FACE SHEET MATERIALS

The primary functions of the face sheets are to provide the required bending and in-plane shear stiffness alongside to carry the axial, bending, and in-plane shear

loading [6]. There are various materials that can be used as face sheets. Some examples are given below:

- Aluminum
- Steel/Stainless Steel
- Carbon/Epoxy
- Fiberglass/Epoxy
- Aramid/Epoxy
- Plywood

In a panel, it is generally desirable to use the same materials on each side of the HC structure. In cases where dissimilar face sheets are required, caution is needed to eliminate face sheet distortion due to unequal thermal expansion coefficients. [10]

1.2.2 CORE MATERIALS

The core has several vital functions. It must be stiff enough to resist loads acting in perpendicular direction to the panels, so the distance between the upper and lower face sheet remains fixed. Also, it must be stiff enough in shear to prevent the sliding of the face sheets over each other. If this condition is not fulfilled, the face sheets act as two independent panels and the sandwich effect is lost [11]. In addition, the core should be stiff enough to stabilize the thin face sheets, otherwise wrinkling (local buckling) of the face sheets may occur [11], [6]. The most commonly used core materials can be classified in three main groups: cellular cores, corrugated cores and honeycomb cores. [12]

1.2.3 ADHESIVES

Adhesives' (or the bounding layer) role in the sandwich structures is to keep the faces and the core co-operating with each other. The adhesive between the faces and the core must be able to transfer the shear forces between the faces and the

core. The adhesive must be able to carry shear and tensile stresses. It is hard to specify the demands on the joints; a simple rule is that the adhesive should be able to take up the same shear stress as the core [13]. Some adhesive types, such as phenolic, give out vapor during curing reaction. The vapor can cause several problems if this vapor is trapped; it may cause little or no bond in some areas, the pressure may damage the core material or it may cause the core to move to an undesired position. Common adhesives in current use are [6]:

1. Nitrile Phenolic
2. Vinyl Phenolic
3. Epoxy
4. Urethane
5. Polyimide
6. Polyamide

1.3 MAIN APPLICATION AREAS OF HONEYCOMB SANDWICH STRUCTURES

1.3.1 COMMERCIAL AEROSPACE

Figures 1.4, 1.5, and 1.6 show typical applications of sandwich structures in commercial aerospace vehicles. These examples show the extent to which sandwich composite structures are utilized in the structural parts.



Figure 1.4 A Commercial Aircraft [14]

1. Radome: Specialized glass Prepregs. Flexcore® honeycomb
2. Landing Gear Doors and Leg Fairings: Glass/carbon Prepregs, honeycomb and Redux® bonded assembly. Special process honeycomb.
3. Galley, Wardrobes, Toilets: Fabricated Fibrelam® panels
4. Partitions: Fibrelam® panel materials
5. Wing to Body Fairing: Carbon/glass/aramid Prepregs. Honeycombs. Redux® adhesive.
6. Wing Assembly: (Trailing Edge Shroud Box) Carbon/glass Prepregs. Nomex® honeycomb. Redux® bonded assembly
7. Flying Control Surfaces - Ailerons, Spoilers, Vanes, and Flaps: Glass/carbon/aramid Prepregs. Honeycomb. Redux® adhesive
8. Passenger Flooring: Fibrelam® panels
9. Engine Nacelles and Thrust Reversers: Carbon/glass Prepregs. Nomex® honeycomb. Special process parts.
10. Cargo Flooring: Fibrelam® panels
11. Overhead Storage Bins: Prepregs/fabricated Fibrelam panels
12. Airstairs: Fabricated Fibrelam® panels

13. Rudder: Carbon/glass Prepregs. Honeycomb bonded assembly
14. Elevator: Carbon/glass Prepregs. Honeycomb bonded assembly

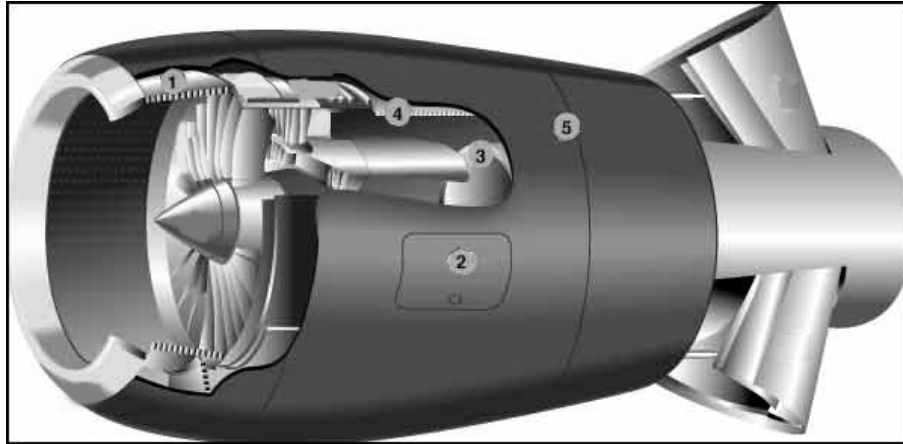


Figure 1.5 A Jet Engine [14]

1. Acoustic Lining Panels: Carbon/glass Prepregs, high temperature adhesives, aluminum honeycomb
2. Engine Access Doors: Woven and UD carbon/glass Prepregs, honeycomb and adhesives
3. Compressor Fairing: BMI/epoxy carbon Prepreg. Honeycomb and adhesives
4. Bypass Duct: Epoxy carbon Prepreg, non-metallic honeycomb and adhesives
5. Nacelle Cowling: Carbon/glass Prepregs and honeycomb



Figure 1.6 A Helicopter [14]

1. Rotor Blades: Prepregs/carbon/glass honeycombs. Machined Nomex® cores. Redux® adhesives
2. Flooring: Fibrelam® panels
3. Fuselage: Carbon and glass Prepregs. Honeycomb
4. Main and Cargo Doors: Epoxy carbon/glass Prepreg, honeycomb and Redux® adhesive
5. Boom and Tail Section: Epoxy carbon/glass Prepreg, honeycomb and Redux® adhesive
6. Fuselage Panels: Epoxy carbon/glass Prepreg, Nomex® honeycomb and Redux® adhesives

1.3.2 SPACE & DEFENCE

Figures 1.7, 1.8, and 1.9 show typical applications of sandwich structures in the military aircraft and spacecraft structures. These examples show the extent to which sandwich composite structures are utilized in the structural parts.



Figure 1.7 A Fighter Aircraft [14]

1. Fuselage Panel Sections: Epoxy carbon Prepregs. Non-metallic honeycomb core and Redux® adhesives
2. Flying Control Surfaces: Epoxy carbon and glass Prepregs. Honeycomb core material and Redux® adhesives

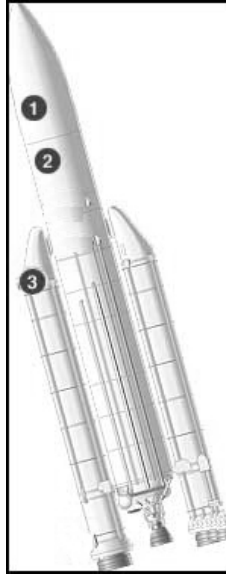


Figure 1.8 A Launcher [14]

1. Fairings: Carbon Prepregs. Aluminum honeycomb and adhesives.
2. External Payload Carrier Assembly (SPELTRA): Carbon prepregs, aluminum honeycombs and adhesives.
3. Booster Capotage: Epoxy glass/non-metallic honeycomb.

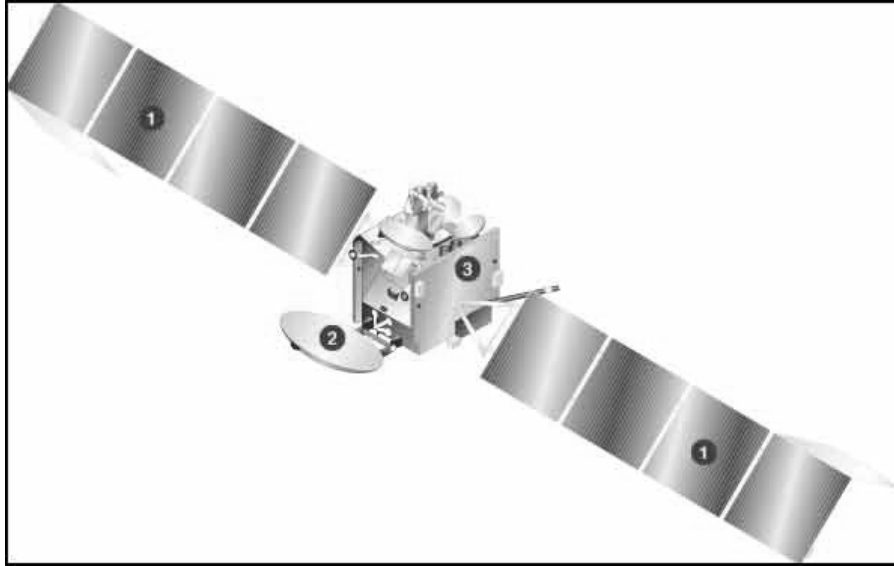


Figure 1.9 A Satellite [14]

1. Solar Panels : Epoxy carbon preregs, aluminum honeycomb, film adhesive
2. Reflectors Antennae : Epoxy/aramid prepreg, cyanate carbon prepreg, aramid/aluminum honeycomb
3. Satellite Structures : Carbon prepreg, aluminum honeycomb, film adhesive

1.3.3 MARINE & RAIL

In Figures 1.10 and 1.11, application areas of sandwich composite structures in marine and rail structures can be seen.

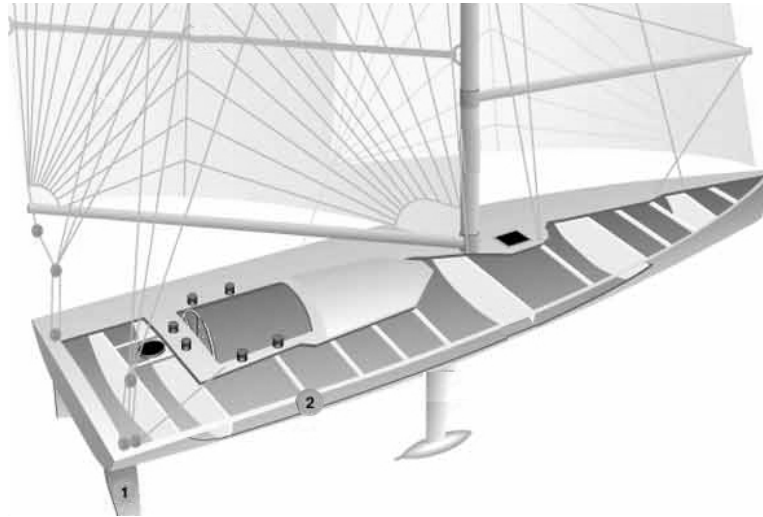


Figure 1.10 Sail [14]

1. Rudders: Carbon Glass, Woven/UD. Nomex honeycomb.
2. Hull & Deck: Carbon/glass Prepreg. Nomex honeycomb. Redux® adhesive.

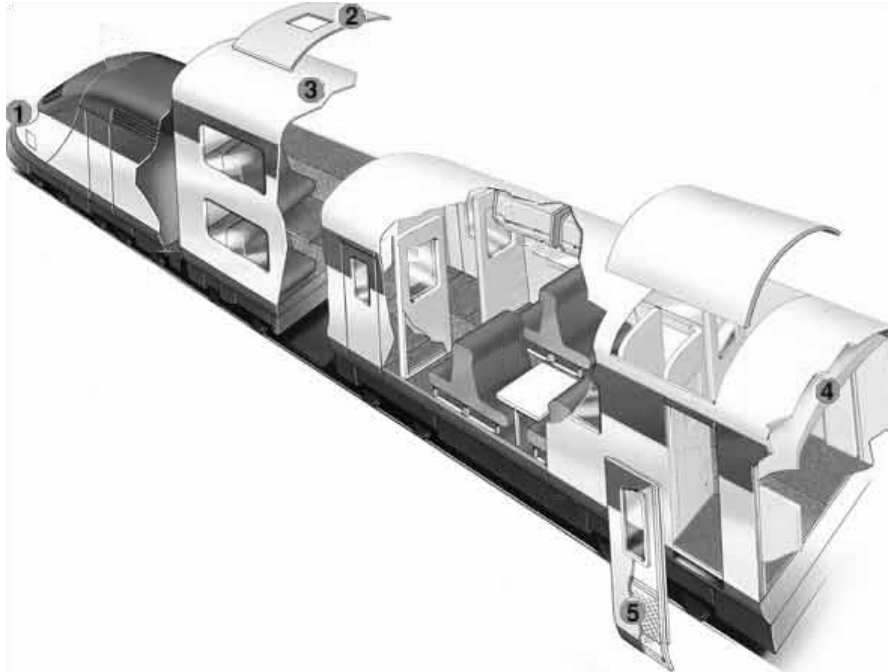


Figure 1.11 Train Wagon [14]

1. Energy Absorbers, Driver Protection: Pre-crushed metallic honeycomb assemblies and carbon preregs.
2. Ceiling panels: Molded with prepreg or honeycomb sandwich.
3. Upper Deck and Lower Flooring: Molded with prepreg or honeycomb sandwich
4. Connecting Archway: Molded component with honeycomb and prepreg materials.
5. External Doors: Bonded honeycomb sandwich construction.

1.3.4 AUTOMOTIVE

Figures 1.12 and 1.13 show the main application areas of sandwich structures in automotive industry. The sandwich structures are used not only directly in automobiles but also indirectly as crash test barriers due to their high shock absorbance capacity.

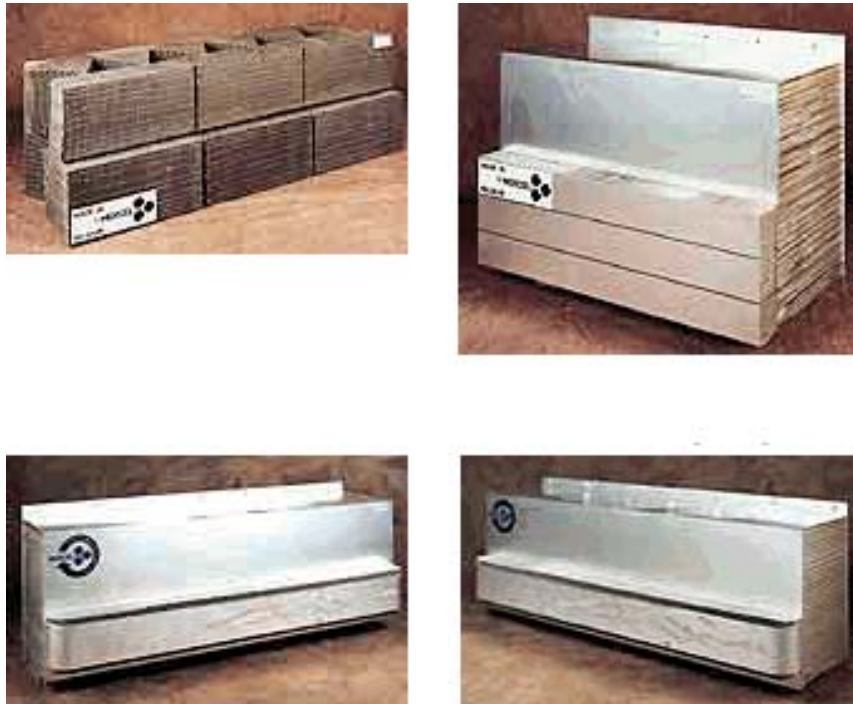


Figure 1.12 Crash Test Barriers [14]

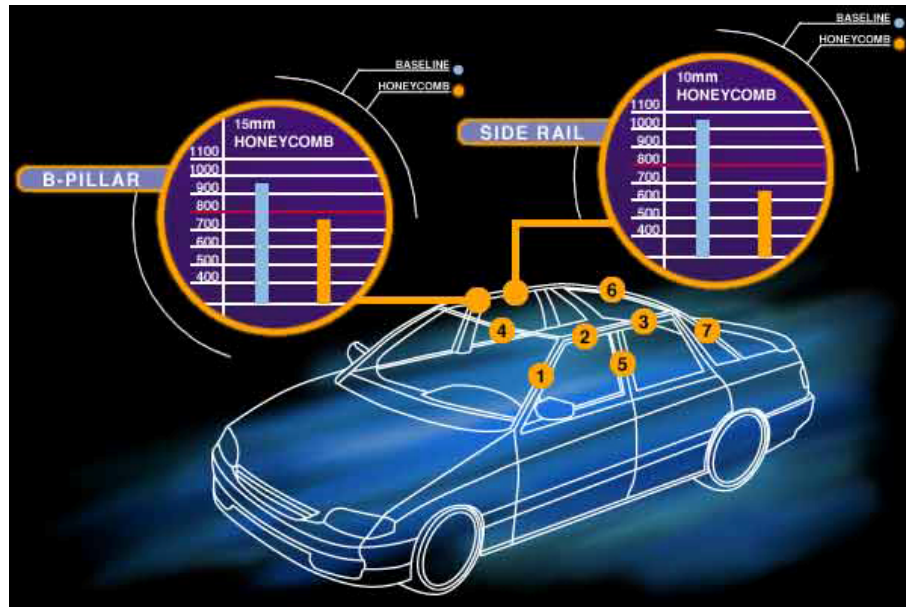


Figure 1.13 Car [14]

1. A-Pillar
2. Front Side Rail
3. Other Side Rail
4. Front Header
5. B-Pillar
6. Rear Header
7. Rearmost Pillar
8. Upper Roof: (Not Shown)

1.3.5 ELECTROMAGNETIC INTERFERENCE (EMI) FILTERING

Honeycombs may also be used as non-structural elements. Fig. 1.14 shows a honeycomb ventilation panel. In this application the honeycomb panel is used as a shield for electromagnetic waves, and it also provides space for proper ventilation.

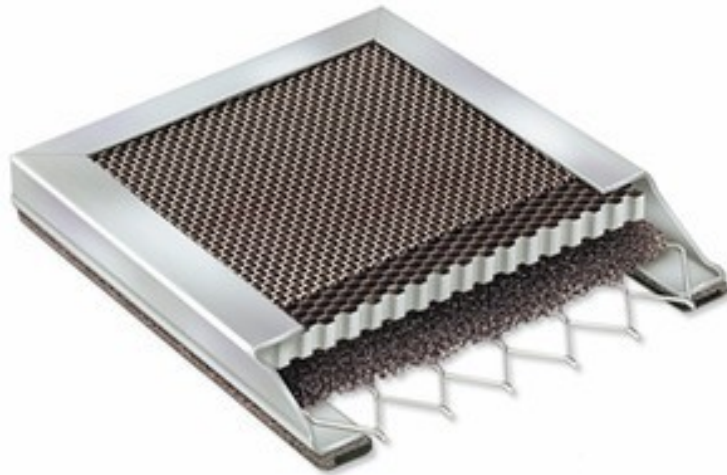


Figure 1.14 Ventilation panel with EMI shielding [15]

1.4 MANUFACTURING OF HONEYCOMB CORES

Honeycomb in common usage includes products made from uncoated and resin-impregnated Kraft paper, various aluminum alloys, aramid paper, and glass-reinforced plastics in a number of cloth weaves and resin systems. Titanium, stainless steel, and many others are used in lesser quantities. [6]

There are two major methods for the manufacture of honeycomb cores:

- Expansion
- Corrugation

The expansion method is more common and is used for making aluminum and aramid honeycombs. In the expansion process, sheets of material are stacked together in a block form. Before stacking, adhesive node lines are printed on the sheets to obtain interrupted adhesive bonding. The stacks of sheet are then cured. Slices of appropriate thickness are cut from the block and then expanded to obtain the desired shape. Fig. 1.16 shows the schematic drawing of the expansion method of honeycomb manufacturing.

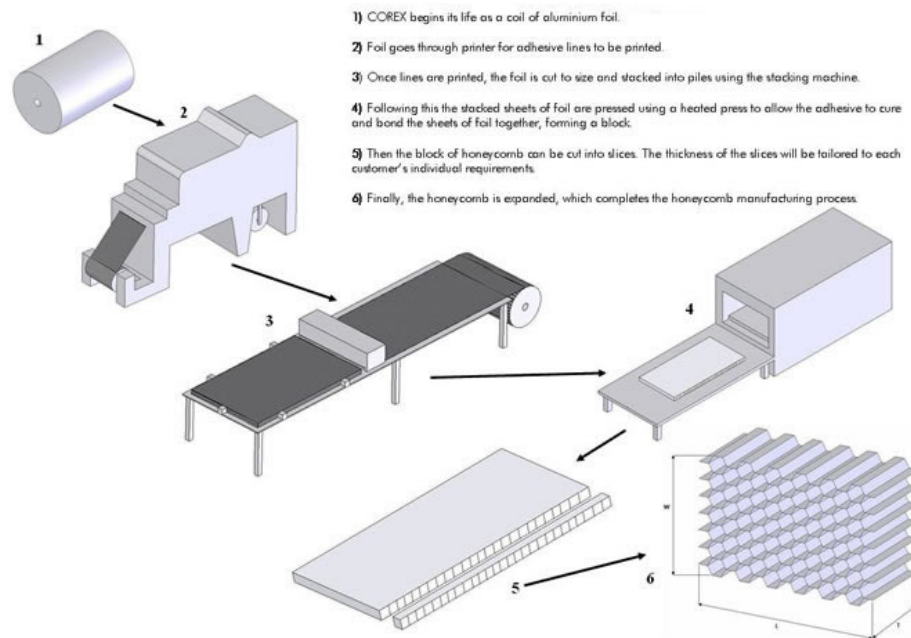


Figure 1.15 Expansion Method [16]

In the corrugation method, the sheet of material is transformed into corrugation form using corrugation rolls. The corrugated sheets are stacked together, bonded and cured. Honeycomb panels are cut from block into desired shape without any expansion [2]. Fig. 1.17 shows the schematic drawing of the corrugation method of honeycomb manufacturing.

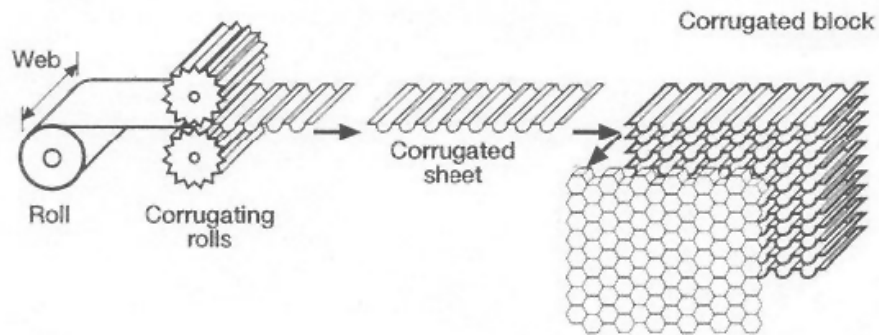


Figure 1.16 Corrugation Method [17]

When core materials must be cut, trimmed, carved, or shaped many special purpose tools are available. Sawing is the most common machining method in which either a conventional blade tooth pattern is used, or for some trimming operations, a special “honeycomb band” is used. In the honeycomb band, the blade appears to be running backwards with the teeth sharpened on the backside so that each tooth acts as a slicing knife blade. A different type of saw is also used as a mandrel mounted router bit. Such tools, shown in Fig.1.18 are very common, and with such tools, sculpturing of HC or foam can be accomplished. Router speeds vary from 1.200-30.000 rpm for blade diameters 1.8-10 cm. Roll forming can be accomplished on metal cores, while non-metal cores must usually be heat-formed. In either case, forming can be much easier if an inherently formable cell configuration is used. [6]

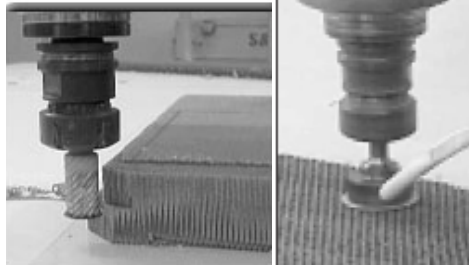


Figure 1.17 Router Bit Type Cutting Tools [18]

Physical and mechanical properties of the honeycomb core materials are strongly influenced by the properties of the material from which they are manufactured. However, several significant properties of honeycomb cores are peculiar to the honeycomb geometry rather than the basic materials, and should be separately noted [6]. The main material and geometric properties which affect the final mechanical property of the honeycomb core are listed below:

- Density
- Cell Shape
- Cell Size
- Thickness
- Specimen geometry and test method.

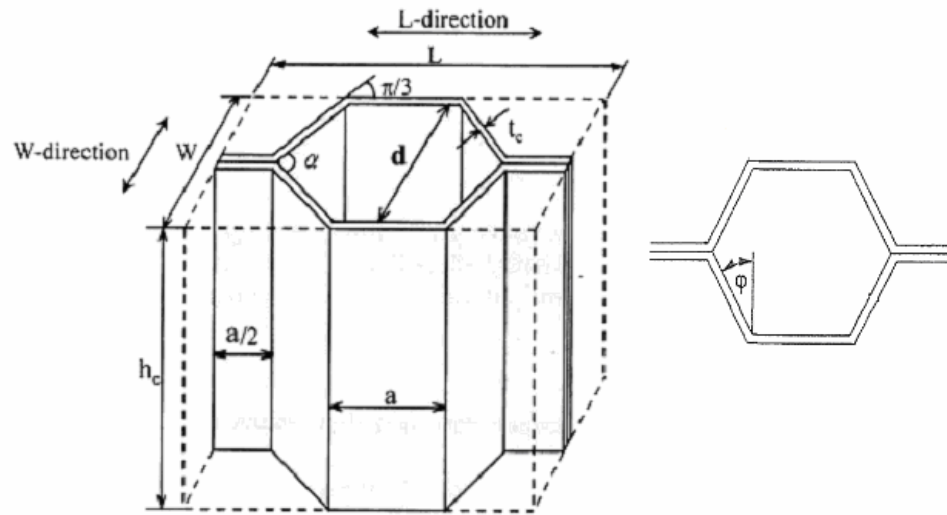


Figure 1.18 Unit HC Cell [19]

In Fig. 1.19 the basic parameters of a honeycomb are shown; d is the cell size, a is the edge length, t_c is the foil thickness, L is the length and W is the width and h_c is the height of the unit cell. If the cell forms a regular hexagon then it is called “regular cell”. It is the most common cell type, although irregular HC’s can also be found. For a regular HC cell the following relations hold (See Fig 2.9):

$$\varphi = \frac{\alpha}{4}$$

or,

$$\varphi = \frac{\pi}{6}$$

$$a = d \cdot \tan(\varphi)$$

$$L = 2 \cdot (a + a \cdot \sin(\varphi))$$

$$W = d + 2 \cdot t_c$$

1.5 FAILURE MODES OF HONEYCOMB SANDWICH STRUCTURES

Depending on the loading conditions, honeycomb sandwich structures may fail in the following ways:

1. Facing Failure
2. Transverse Shear Failure
3. Local Crushing of Core
4. General Buckling
5. Shear Crimping
6. Face Wrinkling
7. Intracell Buckling (Dimpling)

Figure 1.18 gives the pictorial explanations of these failure modes. [6]

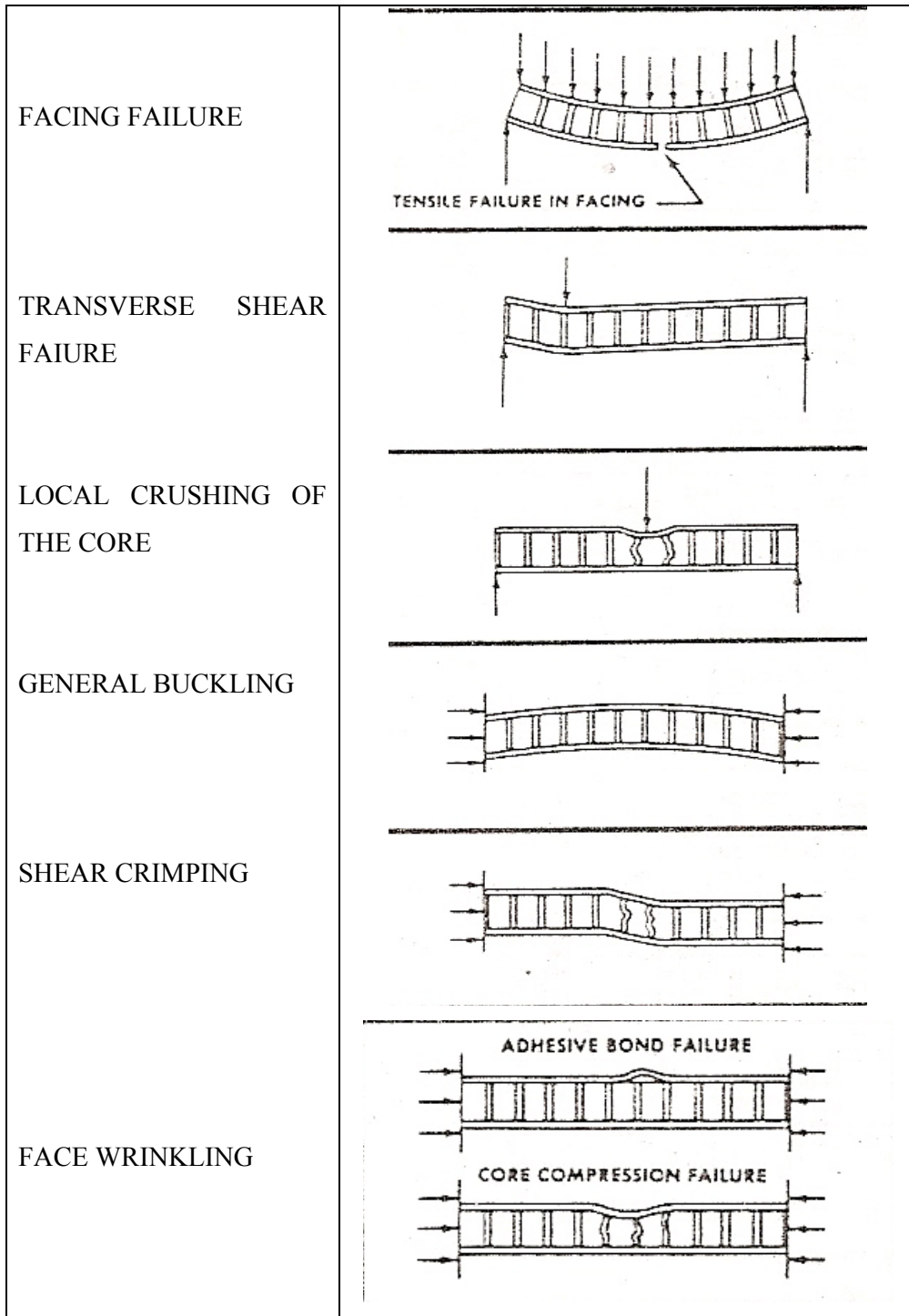


Figure 1.19 Failure Modes of HC Structures [6]

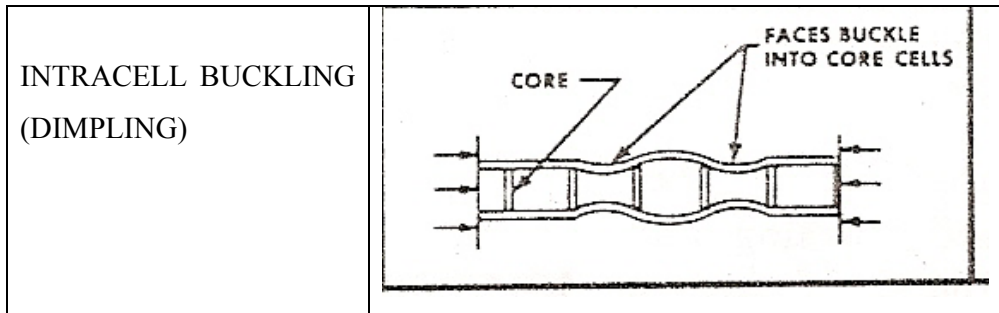


Figure 1.19 (Con't) Failure Modes of HC Structures [6]

1.6 ADVANTAGES OF USING HONEYCOMB STRUCTURES

There are many advantages of proper use of honeycomb structures. As can be seen in Fig. 1.20, with only a small penalty in weight, the overall performance of the system may be enhanced. Visa versa is also true; great weight savings can be achieved without losing too much from the stiffness and/or strength of the system. These results will be explained in detail in the “Theory” chapter. Besides, unlike the I-beams, the face sheets are stabilized across their whole length. Rigidity is accomplished in several directions. In addition to these advantages, honeycomb structures also offer advantages like the other types of composites do. For instance, they can be used as a thermal and/or acoustical insulator while acting as a structural element.

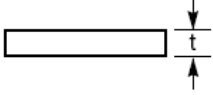
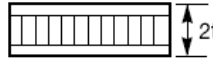
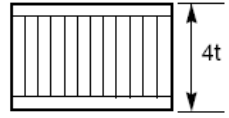
	Solid Metal Sheet	Sandwich Construction	Thicker Sandwich
			
Relative Stiffness	100	700 7 times more rigid	3700 37 times more rigid!
Relative Strength	100	350 3.5 times as strong	925 9.25 times as strong!
Relative Weight	100	103 3% increase in weight	106 6% increase in weight

Figure 1.20 Advantages of Sandwich Structures [20]

CHAPTER 2

THEORY

2.1 FUNDAMENTALS OF SANDWICH THEORY

The fundamentals of sandwich theory can be investigated by the help of the beam illustrated in Fig. 2.1. The beam is composed of two face skins and the core. The materials are assumed to be isotropic. The bond between the core and the face skins is assumed to be perfect. As a first approximation, the ordinary theory of bending can be used for a beam of this kind. The ordinary theory of bending assumes that cross-sections, which are plane and perpendicular to the longitudinal axis of unloaded beam, remain in this state when the bending takes place. This assumption leads to the relationship between the bending moment and the curvature, as given in Eq. 2.1 [11]

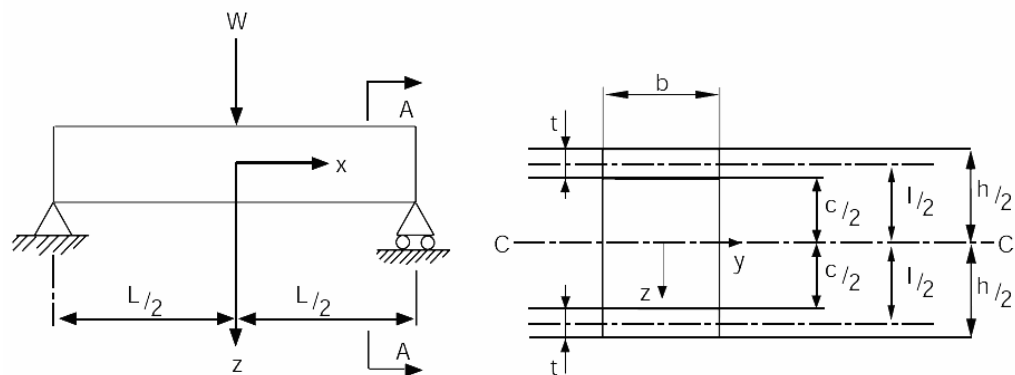


Figure 2.1 Dimensions of A Sandwich Beam

$$\frac{M}{EI} = -\frac{1}{R} \quad (2.1)$$

In Eq. 2.1, E.I is the flexural rigidity for an ordinary beam, where “E” is the modulus of elasticity and "I" is the moment of inertia. But for a sandwich beam flexural rigidity is the sum of the flexural rigidities of separate parts, faces and core. If we denote flexural rigidity about y axis by D, the flexural rigidity of the beam measured about the centroidal axis in Fig. 2.1 is:

$$D = 2 \left(\frac{1}{12} \cdot b \cdot t^3 + b \cdot t \cdot \left(\frac{l}{2} \right)^2 \right) \cdot E_f + \frac{1}{12} \cdot b \cdot c^3 \cdot E_c \quad (2.2)$$

$$D = \frac{1}{6} \cdot b \cdot t^3 \cdot E_f + \frac{1}{2} \cdot b \cdot t \cdot l^2 \cdot E_f + \frac{1}{12} \cdot b \cdot c^3 \cdot E_c \quad (2.3)$$

In these equations, E_f and E_c are the moduli of elasticity of the face sheets and the core, respectively.

In practical, in sandwich structures, since “t” and E_c are very small with respect to “l” and E_f, respectively, the second term in Eq. 2.3 is dominant. The error introduced by neglecting the first term is less than 1% provided the l/t > 5.77 [11]. The third term may also be neglected with an error less than 1% if E_f/E_c > 55 and l/t ≥ 5.77.

Thus, flexural rigidity of a sandwich beam may be reduced to:

$$D = \frac{1}{2} \cdot b \cdot t \cdot l^2 \cdot E_f$$

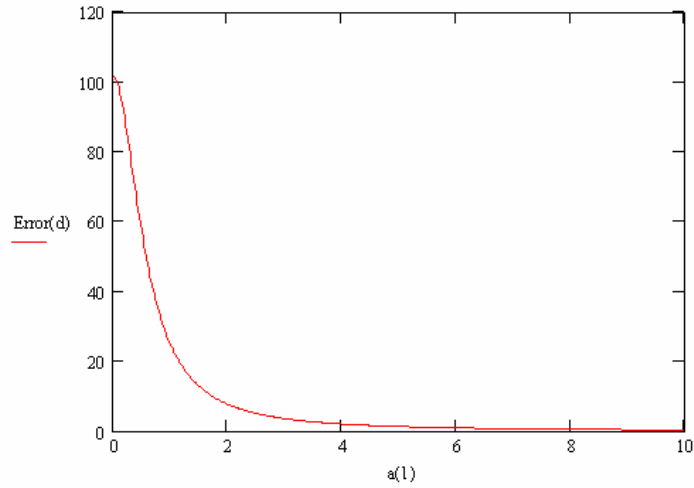


Figure 2.2 Error due to neglecting the first term in Eq. 2.2
($E_f/E_c = 55$, $a(l)$ is the l/t ratio)

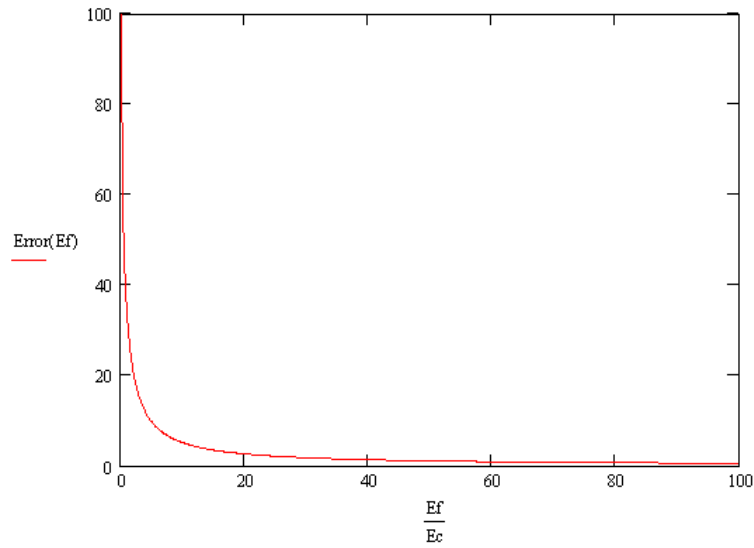


Figure 2.3 Error due to neglecting the first and third terms in Eq. 2.2
($l/t=5.77$)

In Fig. 2.2, the percent error due to neglecting the first term is plotted, and as can be seen, the error drops drastically with increasing l/t ratio. The error is 25% when l/t is 1, whereas it drops to 2.02% when the ratio is 4, and it drops below

1% if the ratio is above 5.7. The same trend is observed in Fig. 2.3. When neglecting the first and third terms in Eq. 2.2, results are less than a 1% error, as long as l/t ratio is greater than 5.77 and E_f/E_c is above 55.

The key point in sandwich theory is to increase the “ l ” distance by the core material. As the calculations above clearly state, the use of core material increases “ l ” distance, and this distance increases the flexural rigidity of the structure (See Sec. 2.2).

2.2 RELATIVE STIFFNESS & RELATIVE STRENGTH

As mentioned in section 1.6, relative stiffness and strength increases by the use of sandwich structures. In order to compare the stiffness of the 3 beams given in Fig. 1.20, we should compare their moments of inertia, I .

For Solid Metal Sheet:

$$I_s = \frac{1}{12} . b . t^3 \quad (2.4)$$

For Sandwich panel with thickness $2t$, (ignoring the core)

$$I_{2t} = 2 \cdot \left(\frac{1}{12} . b . \left(\frac{t}{2} \right)^3 + b . \frac{t}{2} . \left(\frac{3t}{4} \right)^2 \right) \quad (2.5)$$

$$I_{2t} = \frac{28}{48} . b . t^3$$

For the sandwich panel with thickness $4t$, (ignoring the core)

$$I_{4t} = 2 \cdot \left(\frac{1}{12} . b . \left(\frac{t}{2} \right)^3 + b . \frac{t}{2} . \left(\frac{7t}{4} \right)^2 \right) \quad (2.6)$$

$$I_{4t} = \frac{148}{48} . b . t^3$$

Comparing the results of Eq. 2.4, 2.5 and 2.6 reveals that

$$I_{2t} = 7 \times I_s \quad (2.7a)$$

$$I_{4t} = 37 \times I_s \quad (2.7b)$$

To compare the strength of these three beams, we have to go through the stress calculation for a beam in bending.

$$\sigma = \frac{M \cdot y}{I} \quad (2.8)$$

where M is the applied moment and y is the distance from the natural axis. To find the maximum moment that the beam can carry, Eq. 2.8 is rearranged and we get:

$$M_{\max.} = \left(\frac{I}{y_{\max}} \right) \cdot \sigma_{all.} \quad (2.9)$$

where, M_{\max} is the maximum moment, y_{\max} is the farthest distance from the natural axis, $\sigma_{all.}$ is the allowable stress that the material can resist. The sandwich beam face sheets' material is the same as the solid metal sheets', thus the allowable stress is the same for all three of them.

For the solid sheet metal

$$M_{s,\max} = \left(\frac{I_s}{(t/2)} \right) \cdot \sigma_{all.} \quad (2.10)$$

For the sandwich panel with 2t thickness;

$$M_{2t,\max} = \left(\frac{I_{2t}}{(t)} \right) \cdot \sigma_{all.} \quad (2.11)$$

If we plug in Eq. 2.7a to Eq. 2.11 we get,

$$M_{2t,\max} = \left(\frac{7 \times I_s}{(t)} \right) \cdot \sigma_{all.} \quad (2.12)$$

For the sandwich panel with 4t thickness;

$$M_{4t,\max} = \left(\frac{I_{4t}}{(2t)} \right) \cdot \sigma_{all.} \quad (2.13)$$

If we plug in Eq. 2.7b to Eq. 2.13 we get,

$$M_{4t,\max} = \left(\frac{37 \times I_s}{(2t)} \right) \cdot \sigma_{all}. \quad (2.14)$$

If we compare Eq's 2.10, 2.12 and 2.14 we see that;

$$M_{2t,\max} = 3.5 \times M_{s,\max} \quad (2.14a)$$

$$M_{4t,\max} = 9.25 \times M_{s,\max} \quad (2.14b)$$

As Eq. 2.7 and Eq. 2.14 clearly state, the relative stiffness and strength of the sandwich beams are much greater than the solid sheet metal. Depending on the density ratio of the face sheets' material and the core material, the weight penalty due to sandwich construction is almost negligible. As an example, consider the solid sheet beam and the "2t" sandwich. If we take the ratio of the core density to face sheet density as 1/27, then the weight increase is 3.7%.

As stated before, the vice versa is also true, i.e., using sandwich beams may result in great weight savings without a sacrifice from strength. For instance, consider the plot given in Fig. 2.4. The relative stiffness (I), strength (S), height (H) and weight (W) of the sandwich beam with respect to the solid metal sheet with thickness "t" is plotted. Relative values are obtained by dividing the I, S, H and W of the sandwich beams by the corresponding value of solid metal sheet. Core thickness is held constant at 0.5t. As shown, weight savings can be obtained as well as the increase in stiffness and strength. For example, when face sheet thickness is 0.3, relative weight is only 62% (38% reduction in weight) of the original weight, whereas relative I and relative S is 121% and 110%, respectively. When the only sacrifice is in relative height, there is a 10% increase in total height, which may be undesirable and/or inapplicable due to geometric limitations. If a limited height is in question, then consider Fig.2.5. This time the total height is kept constant and the variation of relative I, S, W and core thickness, with respect to face sheet thickness, are plotted. When face

sheet thickness is $0.4t$, relative I and S are 99% of the original I and S. On the other hand, relative W is 81% of the original weight, i.e., with only a one percent reduction in I and S, 19% weight saving can be achieved, while the total thickness is kept fixed.

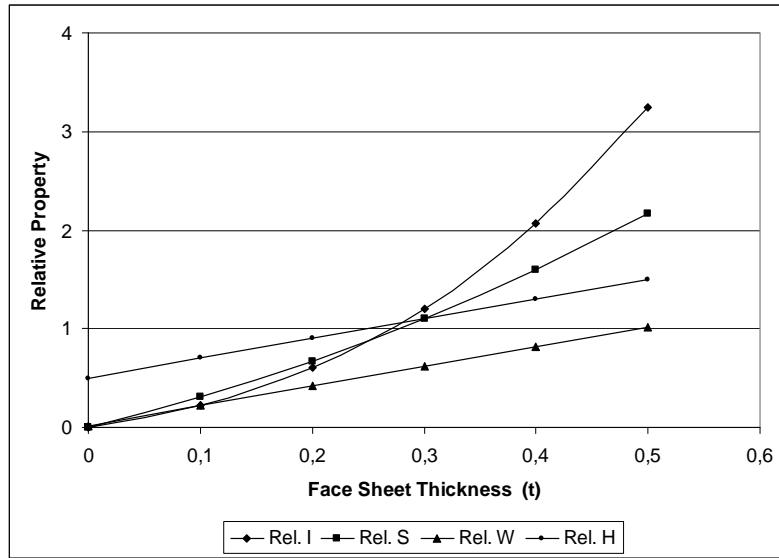


Figure 2.4 Relative I,S and W versus Face Sheet Thickness, Constant Core Thickness

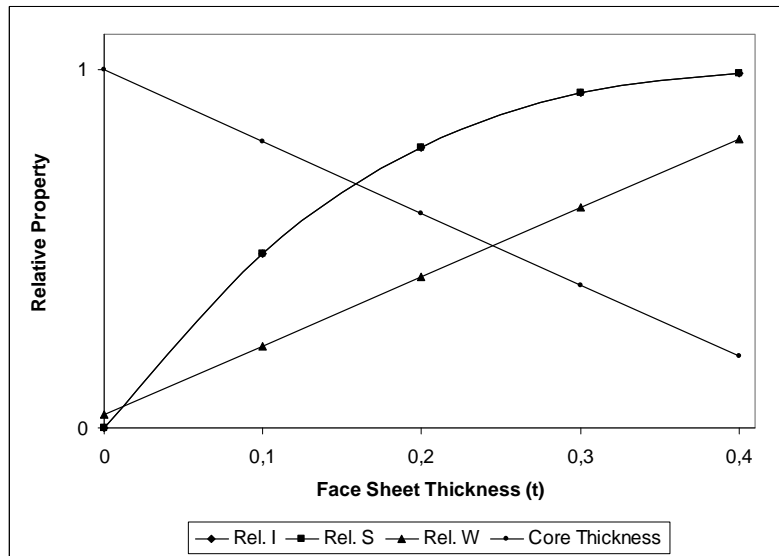


Figure 2.5 Relative I,S and W versus Face Sheet Thickness, Constant Total Height

2.3 ANISOTROPY – ORTHOTROPY

In this section, information on anisotropy-orthotropy will be given. Orthotropy is an important concept because not only the core material but also the face sheets may show orthotropic behavior. HC cores are highly orthotropic materials. Therefore a brief explanation on these topics is provided.

The generalized Hooke's law that relates the stresses to strains can be written as:

$$\sigma_i = C_{ij} \cdot \varepsilon_j \quad i,j=1,\dots,6$$

C_{ij} is the stiffness matrix and it has 36 constants. However, it can be easily shown that less than 36 of the constants are independent for elastic materials. In fact, the elastic stiffness matrix is symmetric and it has only 21 independent constants. [3]

$$\begin{Bmatrix} \sigma_1 \\ \sigma_2 \\ \sigma_3 \\ \tau_{23} \\ \tau_{31} \\ \tau_{12} \end{Bmatrix} = \begin{bmatrix} C_{11} & C_{12} & C_{13} & C_{14} & C_{15} & C_{16} \\ C_{12} & C_{22} & C_{23} & C_{24} & C_{25} & C_{26} \\ C_{13} & C_{23} & C_{33} & C_{34} & C_{35} & C_{36} \\ C_{14} & C_{24} & C_{34} & C_{44} & C_{45} & C_{46} \\ C_{15} & C_{25} & C_{35} & C_{45} & C_{55} & C_{56} \\ C_{16} & C_{26} & C_{36} & C_{46} & C_{56} & C_{66} \end{bmatrix} \times \begin{Bmatrix} \varepsilon_1 \\ \varepsilon_2 \\ \varepsilon_3 \\ \gamma_{23} \\ \gamma_{31} \\ \gamma_{12} \end{Bmatrix} \quad (2.15)$$

Eq.2.15 is the most general expression for linear elasticity. In fact, the Eq. 2.15 defines the stress-strain relationship of anisotropic materials. An anisotropic material is the one that exhibits material properties that are directionally independent, i.e., a given material property can have different values in different directions. [21]

Unlike anisotropic materials, orthotropic materials show symmetric material properties. If there are two orthogonal planes of material property symmetry for

a material, symmetry will exist relative to a third mutually orthogonal plane. This defines an orthotropic material [3]. The independent elastic coefficients reduce to 9 for an orthotropic material. The stress-strain relations for an orthotropic material are given by:

$$\begin{Bmatrix} \sigma_1 \\ \sigma_2 \\ \sigma_3 \\ \tau_{23} \\ \tau_{31} \\ \tau_{12} \end{Bmatrix} = \begin{bmatrix} C_{11} & C_{12} & C_{13} & 0 & 0 & 0 \\ C_{12} & C_{22} & C_{23} & 0 & 0 & 0 \\ C_{13} & C_{23} & C_{33} & 0 & 0 & 0 \\ 0 & 0 & 0 & C_{44} & 0 & 0 \\ 0 & 0 & 0 & 0 & C_{55} & 0 \\ 0 & 0 & 0 & 0 & 0 & C_{66} \end{bmatrix} \times \begin{Bmatrix} \varepsilon_1 \\ \varepsilon_2 \\ \varepsilon_3 \\ \gamma_{23} \\ \gamma_{31} \\ \gamma_{12} \end{Bmatrix} \quad (2.16)$$

The stiffness coefficients in Eq.2.16 C_{ij} for an orthotropic material may be expressed in terms of engineering constants by [21]:

$$C_{11} = \frac{1 - \nu_{23} \cdot \nu_{32}}{\Delta E_2 \cdot E_3} \quad (2.17)$$

$$C_{12} = \frac{\nu_{21} + \nu_{31} \cdot \nu_{23}}{\Delta E_2 \cdot E_3} = \frac{\nu_{12} + \nu_{13} \cdot \nu_{32}}{\Delta E_1 \cdot E_2} \quad (2.18)$$

$$C_{13} = \frac{\nu_{31} + \nu_{21} \cdot \nu_{32}}{\Delta E_2 \cdot E_3} = \frac{\nu_{13} + \nu_{12} \cdot \nu_{23}}{\Delta E_1 \cdot E_2} \quad (2.19)$$

$$C_{22} = \frac{1 - \nu_{13} \cdot \nu_{31}}{\Delta E_1 \cdot E_3} \quad (2.20)$$

$$C_{23} = \frac{\nu_{32} + \nu_{12} \cdot \nu_{31}}{\Delta E_1 \cdot E_3} = \frac{\nu_{23} + \nu_{21} \cdot \nu_{13}}{\Delta E_1 \cdot E_2} \quad (2.21)$$

$$C_{33} = \frac{1 - \nu_{12} \cdot \nu_{21}}{\Delta E_1 \cdot E_2} \quad (2.22)$$

$$C_{44} = G_{23} \quad (2.23)$$

$$C_{55} = G_{13} \quad (2.24)$$

$$C_{66} = G_{12} \quad (2.25)$$

$$\Delta = \frac{1 - \nu_{12} \cdot \nu_{21} - \nu_{23} \cdot \nu_{32} - \nu_{31} \cdot \nu_{13} - 2 \cdot \nu_{21} \cdot \nu_{32} \cdot \nu_{13}}{E_1 \cdot E_2 \cdot E_3}$$

2.4 ESTIMATION / CALCULATION OF THE ELASTIC CONSTANTS OF ORTHOTROPIC MATERIALS

As figured out in the previous section, there are 9 constants to be determined in order to construct the stiffness matrix of an orthotropic material. Since the HC core will be modeled as an orthotropic material, the calculation of these constants is very crucial. (See Section 4.1) The coefficients are functions of engineering constants, and they are given in Eq. 2.17 through Eq. 2.25. Therefore, to determine these coefficients, the following 9 engineering constants are needed. These engineering constants are:

- E_1, E_2, E_3
- $\nu_{12}, \nu_{13}, \nu_{23}$
- G_{12}, G_{13}, G_{23}

The suffixes of the constants represent the axis system that is given in Figure 2.6 for a honeycomb core throughout this thesis.

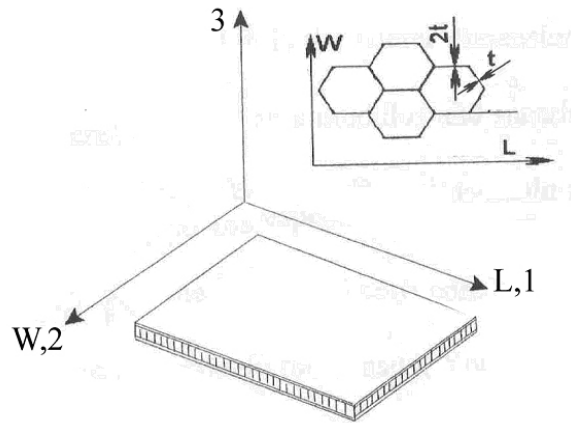


Figure 2.6 HC Axis System

There has been various studies investigating one or more of these constants, but it is hard to find a study which gives the complete set of nine elastic constants for a honeycomb core material.

Masters & Evans [22] developed a theoretical model for predicting E_1 , E_2 , ν_{12} , G_{12} in 2D. They studied flexing, hinging and stretching mechanisms. They considered both regular HC cells and re-entrant HC cells. After separately investigating the three mechanisms they combined the results to get a general model that includes the three models.

Qunli Liu [23] gave the calculations for E_3 , G_{13} and G_{23} . Abd-el Sayed, Jones and Burgess [24] concentrated on E_1 , E_2 , ν_{12} in 2D. In their work, they also considered the effect of filling the HC cell with a low modulus infill. Prior to that, they solved the mechanical properties of unfilled HC. When F_1 and F_2 in-plane forces are applied to the cell, the double thickness members (where the two strips are glued / bonded) remain straight and parallel to each other whereas the single thickness members deform elastically with points of contra flexure at their mid-lengths. Displacements in both directions are calculated and then Poisson's ratio and Young's moduli are calculated.

Grediac [25] and Shi & Tong [26] separately worked on the calculation of the G_{13} , G_{23} . They both continued on the studies of Kelsey et al. [27]. Grediac used a quarter portion of a cell and, using the symmetries of the HC, calculated the shear moduli using FEM. Shi & Tong used the two scale method of homogenization of periodic media and later also performed FEM studies.

Becker [28] formulated the E_1, E_2 , ν_{12} , ν_{32} , G_{12} while considering the core thickness effect.

Zhang & Ashby [29] gave the formulas for E_3 , ν_{32} , ν_{13} , G_{13} , G_{23} . They analyzed the collapse behavior in the out of plane direction. Buckling, debonding, and fracturing are identified as possible failure mechanisms.

E.Nast [30] performed a study similar to those of Abd-el Sayed, Jones and Burgess. Nast applied different boundary conditions in order to get the constants and finally managed to get a set of all 9 elastic constants.

In the following sub-sections, sample derivations of the equivalent elastic constants for a HC core will be described to give insight to the typical procedures used in the literature.

2.4.1 CALCULATION OF E_3

Of all the constants, E_3 calculation is the most straight forward one. This is a generally accepted calculation and there is no other approach that conflicts with this one. The calculation of E_3 basically depends on the equivalent area, equal displacement concept.

Re-consider the unit HC cell given in Fig. 1.18; a honeycomb cell is a thin walled structure and therefore its cross section area can be calculated by:

$$A_{hc} = 8 \times a \times t_c$$

From Fig. 1.18, the corresponding area for the rectangular prism is

$$A_3 = L \times W$$

where

$$L = 2.a + 2a \cos \theta$$

$$W = 2.a \sin \theta$$

and

$$\theta = \frac{\alpha}{2}$$

$$A_3 = (2.d + 2d \cos \theta) \times 2.d \sin \theta$$

$$A_3 = 4.d^2 . \sin \theta . (1 + \cos \theta)$$

$$\frac{A_{hc}}{A_3} = \frac{2.t_c}{d.(1 + \cos \theta). \sin \theta} \quad (2.26)$$

Now, we can calculate the equivalent modulus of elasticity. Let's assume that both of the two blocks, i.e. the unit HC cell and equivalent prism, are loaded by F in transverse direction (i.e. in the 3 direction). For an equivalent model, the deflections must be the same. Utilizing the equivalence of the deflections, we can get the equivalent E , after the following steps.

$$\varepsilon_{hc} = \frac{\sigma_{hc}}{E_{hc}} = \frac{F}{A_{hc}.E_{hc}}$$

Similarly,

$$\varepsilon_3 = \frac{\sigma_3}{E_3} = \frac{F}{A_3.E_3}$$

It is important to note that the height of both is the same; hence, if we want to have equal deflections, we must have equal strains and therefore Eq.2.27 must be satisfied in order to have an equivalent modulus.

$$A_{hc}.E_{hc} = A_3.E_3 \quad (2.27)$$

From Eq.2.27 equivalent elastic modulus E_3 can be calculated easily as in Eq.2.28.

$$E_3 = \frac{A_{hc}}{A_3} E_{hc} \quad (2.28)$$

if we plug in the A_{hc}/A_3 ratio from Eq.2.26 to Eq.2.28, we get:

$$E_3 = \left[\frac{2.t_c}{d.(1 + \cos \theta). \sin \theta} \right] E_{hc}$$

or

$$E_3 = \left[\frac{2.E_{hc}}{(1 + \cos \theta). \sin \theta} \right] \left(\frac{t_c}{d} \right) \quad (2.29)$$

2.4.2 CALCULATION OF E_1 & E_2

The calculation of the in-plane equivalent moduli for a honeycomb core will be demonstrated based on the work of Nast [30].

According to the work of Nast [30], calculation of E_1 and E_2 depends on the fact that in plane loading, horizontal walls do not deform, whereas diagonal walls deform. Figure 2.7 shows the horizontal and diagonal walls of typical honeycomb cores. Thus, the deformation of the walls can be reduced to the problem of solving a plate equation [30].

$$w_{,xxxx} = 0 \tag{2.30}$$

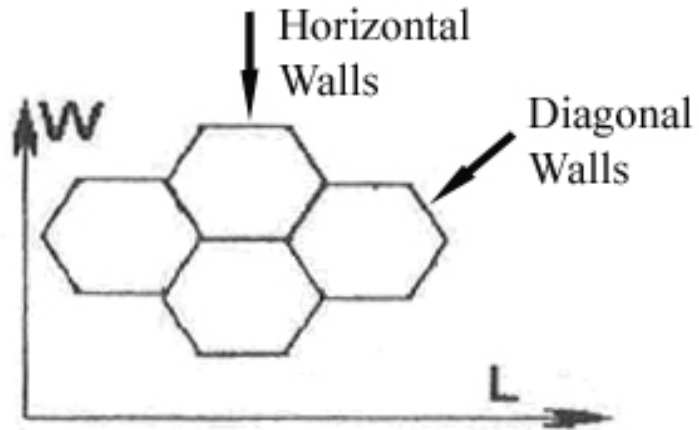


Figure 2.7 Walls of HC

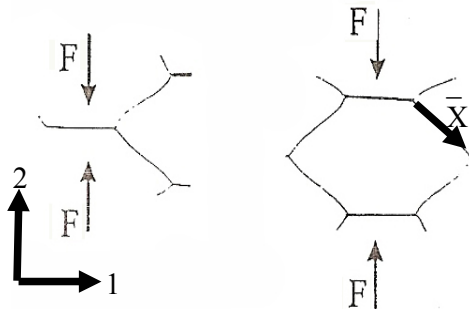


Figure 2.8 Deformation in 2 Direction [30]

In the first load case, an external stress σ_2 with respect to the whole projected cross section is applied in the 2 direction, and the central point is assumed to be clamped. The other end of the plate is assumed to have no rotation and the external stress is applied as a shear force boundary condition. Thus, the following boundary conditions are applied [30]:

$$w(\bar{x} = 0) = 0$$

(2.31)

$$w_{,\bar{x}}(\bar{x} = 0) = 0$$

(2.32)

$$w_{,\bar{x}}(\bar{x} = a) = 0$$

(2.33)

$$w_{,xxx}(\bar{x} = a) = -\frac{\sigma_2}{K} \cdot a \cdot (1 + \sin \varphi) \cdot \sin(\varphi)$$

(2.34)

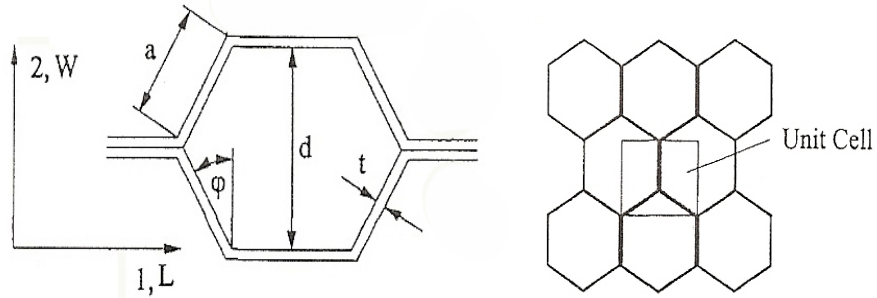


Figure 2.9 Idealized Unit Cell [30]

where K is the plate stiffness and it is equal to:

$$K = \frac{E_{hc} \cdot t^3}{12 \cdot (1 - \nu_{hc}^2)} \quad (2.35)$$

\bar{x} is the plate coordinate with its origin at the intersection point of diagonal walls. (See Fig.2.8)

Integrating the plate equation in Eq.2.30 four times gives;

$$w(\bar{x}) = c_1 \frac{x^3}{6} + c_2 \frac{x^2}{2} + c_3 \cdot x + c_4 \quad (2.36)$$

From the first boundary condition (Eq.2.31);

$$w(\bar{x} = 0) = 0 \Rightarrow c_4 = 0$$

From the second boundary condition (Eq.2.32);

$$w_{,\bar{x}}(\bar{x} = 0) = 0 \Rightarrow c_3 = 0$$

From the third boundary condition (Eq.2.33);

$$w_{,\bar{x}}(\bar{x} = a) = 0 \Rightarrow$$

$$w_{,\bar{x}}(\bar{x} = a) = c_1 \frac{a^2}{2} + c_2 \cdot a = 0$$

$$c_1 = -2 \frac{c_2}{a} \quad (2.37)$$

From the fourth boundary condition (Eq.2.34);

$$w_{,\bar{x}\bar{x}\bar{x}}(\bar{x} = a) = -\frac{\sigma_2}{K} \cdot a \cdot (1 + \sin \varphi) \cdot \sin(\varphi) \Rightarrow$$

$$w_{,\bar{x}\bar{x}\bar{x}}(\bar{x} = a) = c_1 = -\frac{\sigma_2}{K} \cdot a \cdot (1 + \sin \varphi) \cdot \sin(\varphi)$$

$$c_1 = -\frac{\sigma_2}{K} \cdot a \cdot (1 + \sin \varphi) \cdot \sin(\varphi) \quad (2.38)$$

From Eq. 2.37 and 2.38

$$c_2 = \frac{\sigma_2}{2 \cdot K} \cdot a \cdot (1 + \sin \varphi) \cdot \sin(\varphi)$$

Then Eq. 2.35 becomes;

$$w(\bar{x}) = -\frac{\sigma_2}{K} \cdot a \cdot (1 + \sin \varphi) \cdot \sin(\varphi) \frac{x^3}{6} + \frac{\sigma_2}{2 \cdot K} \cdot a \cdot (1 + \sin \varphi) \cdot \sin(\varphi) \frac{x^2}{2} \quad (2.39)$$

$$\varepsilon_2 = \frac{\text{Displacement}_{\text{in 2 direction}}}{\text{Original Length}}$$

$w(\bar{x})$ gives the displacement in \bar{x} coordinate, therefore we need to find its component in 2 direction. Since we are dealing only with the upper section of the cell, original length is half of the cell size.

Hence;

$$\varepsilon_2 = \frac{\sigma_2}{E_2} = \frac{w(\bar{x} = a) \cdot \sin(\varphi)}{a \cdot \cos(\varphi)} \Rightarrow$$

$$E_2 = \frac{\sigma_2 \cdot a \cdot \cos(\varphi)}{w(\bar{x} = a) \cdot \sin(\varphi)} \Rightarrow$$

if we plug in Eq. 2.39 with $\bar{x} = a$ we get;

$$E_2 = \frac{\sigma_2 \cdot a \cdot \cos(\varphi)}{\left(-\frac{\sigma_2}{K} \cdot a \cdot (1 + \sin \varphi) \cdot \sin(\varphi) \frac{a^3}{6} + \frac{\sigma_2}{2 \cdot K} \cdot a \cdot (1 + \sin \varphi) \cdot \sin(\varphi) \frac{a^2}{2}\right) \cdot \sin(\varphi)} \quad (2.40)$$

using Eq. 2.35, Eq. 2.40 becomes;

$$E_2 = \frac{t^3 \cdot \cos \varphi}{(1 + \sin \varphi) \cdot a^3 \sin^2 \varphi \cdot (1 - \nu^2)} E_{hc} \quad (2.41)$$

Thus, Eq. 2.41 gives the equivalent modulus of the honeycomb core in the 2 direction.

Similar procedure is followed for the calculation of E1. Based on the microscopic view of the deformation of the unit cell and the finite element modeling of the unit cell, Nast [30] proposed the boundary conditions, given by Eq's. 2.42-2.45, for calculation of E1. In the second load case, an external stress σ_1 with respect to the whole projected cross section is applied in the 1 direction.

$$w(\bar{x} = 0) = 0 \quad (2.42)$$

$$w_{,\bar{x}}(\bar{x} = 0) = 0 \quad (2.43)$$

$$w_{,\bar{x}\bar{x}}(\bar{x} = a) = -\frac{\sigma_1}{K} \cdot a \cdot \cos^2(\varphi) \quad (2.44)$$

$$w_{,\bar{x}\bar{x}}(\bar{x} = a) = -\frac{\sigma_1}{K} \cdot a^2 \cdot \frac{\cos(\varphi)}{4} \cdot (1 + \cos(\varphi)) \quad (2.45)$$

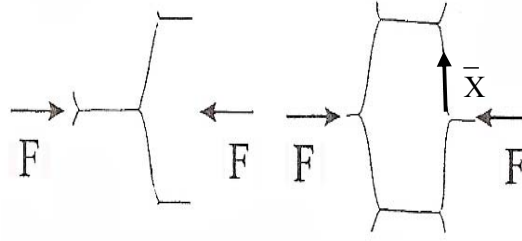


Figure 2.10 Deformation in 1 Direction

If we re-call Eq.2.36 and apply the first and second boundary conditions (Eq. 2.42 & 2.43) we again get ;

$$c_3 = 0$$

$$c_4 = 0$$

From the third boundary condition (Eq.2.44);

$$w_{,xxx}(\bar{x} = a) = -\frac{\sigma_1}{K}.a.\cos^2(\varphi) \Rightarrow$$

$$w_{,xxx}(\bar{x} = a) = c_1 = -\frac{\sigma_1}{K}.a.\cos^2(\varphi)$$

$$c_1 = -\frac{\sigma_1}{K}.a.\cos^2(\varphi) \tag{2.46}$$

From the fourth boundary condition (Eq.2.45);

$$w_{,xx}(\bar{x} = a) = -\frac{\sigma_1}{K}.a^2.\frac{\cos\varphi}{4}.(1 + \cos\varphi) \Rightarrow$$

$$w_{,xx}(\bar{x} = a) = c_1.a + c_2 = -\frac{\sigma_1}{K}.a^2.\frac{\cos\varphi}{4}.(1 + \cos\varphi) \Rightarrow$$

$$c_2 = -\frac{\sigma_1}{K}.a^2.\frac{\cos\varphi}{4}.(1 + \cos\varphi) - c_1.a$$

$$c_2 = -\frac{\sigma_1}{K}.a^2.\frac{\cos\varphi}{4}.(1 + \cos\varphi) + \frac{\sigma_1}{K}.a^2.\cos^2(\varphi)$$

$$c_2 = \frac{\sigma_1}{K} \cdot a^2 \cdot \left[-\frac{\cos \varphi}{4} \cdot (1 + \cos \varphi) + \cos^2(\varphi) \right]$$

$$c_2 = \frac{\sigma_1}{K} \cdot a^2 \cdot \left(\frac{-\cos(\varphi) + 3 \cdot \cos^2(\varphi)}{4} \right) \quad (2.47)$$

Hence Eq.2.36 for the second case becomes:

$$w(\bar{x}) = \frac{\sigma_1}{K} \cdot a \cdot \cos^2(\varphi) \cdot \frac{x^3}{6} + \frac{\sigma_1}{K} \cdot a^2 \cdot \left(\frac{-\cos(\varphi) + 3 \cdot \cos^2(\varphi)}{4} \right) \cdot \frac{x^2}{2} \quad (2.48)$$

$$\varepsilon_1 = \frac{\text{Displacement in 1 direction}}{\text{Original Length}}$$

Once again, $w(\bar{x})$ gives the displacement in \bar{x} coordinate, therefore we need to find its component in 1 direction.

Hence:

$$\varepsilon_1 = \frac{w(\bar{x} = a) \cdot \cos \varphi}{a \cdot (1 + \sin \varphi)} = \frac{\sigma_1}{E_1}$$

$$E_1 = \frac{\sigma_1 \cdot a \cdot (1 + \sin \varphi)}{\left[\frac{\sigma_1}{K} \cdot \cos^2(\varphi) \cdot \frac{a^4}{6} + \frac{\sigma_1}{K} \cdot \left(\frac{-\cos(\varphi) + 3 \cdot \cos^2(\varphi)}{4} \right) \cdot \frac{a^4}{2} \right] \cdot \cos(\varphi)}$$

re-arranging:

$$E_1 = \frac{t^3 \cdot (1 + \sin(\varphi))}{12 \cdot a^3 \cdot \cos^2(\varphi) \left(\frac{5 \cdot \cos(\varphi) - 3}{24} \right)} \cdot \left(\frac{E_{hc}}{1 - \nu_{hc}^2} \right) \quad (2.49)$$

2.4.3 CALCULATION of ν_{12} , ν_{13} , ν_{23}

Poisson's ratio is defined as:

$$\nu_{12} = -\frac{\varepsilon_2}{\varepsilon_1}$$

Thus, by using Eq.2.41 and Eq.2.49, we can calculate the ν_{12} :

$$v_{12} = \frac{\frac{\sigma_2}{E_2}}{\frac{\sigma_1}{E_1}} = \frac{\sigma_2}{\sigma_1} \cdot \frac{E_1}{E_2} \quad (2.50)$$

In order to obtain the Poisson's ratio v_{12} , we need to calculate the σ_2/σ_1 ratio. The applied force is the same for both cases. Therefore σ_2/σ_1 reduces to the ratio of the areas that the F force is applied. The cell height is the same for both cases therefore From Fig. 2.9 and Fig. 2.10 the area ratio is as follows:

$$\frac{\sigma_2}{\sigma_1} = \frac{\frac{F}{A_2}}{\frac{F}{A_1}} = \frac{A_1}{A_2} = \frac{\cos(\varphi)}{(1 + \sin(\varphi))} \quad (2.51)$$

If we recall Eq.2.50 and plug in the Eq. 2.41, Eq.2.49 and Eq.2.51 and make the simplifications we get:

$$v_{12} = \frac{(1 + \sin(\varphi)) \sin^2(\varphi)}{12 \cdot \cos^2(\varphi) \cdot \left[\frac{\cos(\varphi)}{3} - \frac{1 + \cos(\varphi)}{8} \right]} \quad (2.52)$$

There is also an upper limit for a positive definite stiffness matrix,

$$v_{12} \leq \sqrt{\frac{E_1}{E_2}} \quad (2.53)$$

If the value obtained from Eq.2.52 is bigger than the result of the Eq.2.53; then, the second one should be used.

Zhang & Ashby [29] stated that the Poisson's ratios v_{31} and v_{32} are simply equal to those for the solid core itself:

$$v_{31} = v_{32} = v_{hc}$$

The Poisson's ratios v_{13} , v_{23} can be found using reciprocal relations;

$$v_{13} = \frac{E_1}{E_3} v_{hc} \quad (2.54)$$

and,

$$v_{23} = \frac{E_2}{E_3} v_{hc} \quad (2.55)$$

since $E_3 \gg E_1$ and $E_3 \gg E_2$

Thus Ashby concluded that:

$$v_{13} \approx 0$$

$$v_{23} \approx 0$$

Nast [30] calculated the Poisson's ratios using Eq's. 2.41, 2.49, 2.54 and 2.55 in Eq. 2.28. In this calculation based on the unit cell definition defined Fig. 2.9 in Eq. 2.28.

$$v_{13} = \frac{t^2 (\sin \varphi + 1)^2}{24.a^2 \cos \varphi \left[\frac{\cos \varphi}{3} - \frac{1 + \cos \varphi}{8} \right]} \cdot \frac{v_{hc}}{(1 - v_{hc}^2)} \quad (2.56)$$

$$v_{23} = \frac{t^2 \cos^2 \varphi}{2.a^2 \sin^2 \varphi \cdot (1 - v_{hc}^2)} v_{hc} \quad (2.57)$$

2.4.4 CALCULATION of G_{12}, G_{13}, G_{23}

The calculation of shear moduli is a more complicated process. Because of the shear deformation, not only the vertical parts of the HC but also the diagonal parts of the HC are involved in the calculations. The details of the calculation of the shear moduli are given by in [30]. Based on Nast's analysis, the shear moduli of the honeycomb core are predicted by Eq's. 2.58, 2.59, and 2.60.

$$G_{12} = \frac{t^3 \cdot (1 + \sin(\varphi))}{a^3 \cdot \cos \varphi \cdot (6.25 - 6 \cdot \sin(\varphi))} \cdot \frac{E_{hc}}{(1 - v_{hc}^2)} \quad (2.58)$$

$$G_{13} = \frac{2.t}{a \cdot \cos(\varphi) \cdot (1 + \sin(\varphi))} G_{hc} \quad (2.59)$$

$$G_{23} = \frac{10.t}{9.a.\cos^3(\varphi)(1 + \sin(\varphi))} G_{hc} \quad (2.60)$$

2.5 DIFFERENT MODELS ON THE NINE ELASTIC CONSTANTS:

In this section, different models, which predict the nine equivalent elastic constants of the honeycomb core structure, will be introduced. Tables 2.1 - 2.9, summarize the different relations proposed by different researchers on each of the nine elastic constants of the equivalent orthotropic material model of the actual honeycomb structure. It should be noted that these models only constitute a fraction of the different orthotropic materials model studies performed in the literature. These models will be the basis for the generation of an equivalent orthotropic material model for the honeycomb structure. The material models will be combined together in an effort to come up with the most accurate equivalent material model. The generation of the equivalent model will be explained in detail in section 4.1. It should also be noted that all the models, given in Tables 2.1-2.9 use the same coordinate system given in Fig. 2.6.

Table 2.1 Formulas for E_1

Model Name	E_1
Masters & Evans [22]	$E_1 = \frac{E}{\frac{\cos \varphi}{(1 + \sin \varphi)} \left[\frac{\cos^2 \varphi . a^3}{t^3} + \frac{(2 + \sin^2 \varphi)t}{a} \right]}$
E.Nast [30]	$E_1 = \frac{t^3 . (1 + \sin(\varphi))}{12 . a^3 . \cos^2(\varphi) \left(\frac{1 - \cos(\varphi)}{8} - \frac{\cos(\varphi)}{12} \right)} \cdot \frac{E}{(1 - \nu^2)}$
Abd El-Sayed [24]	$E_1 = \frac{6 . \cos(\varphi) . \tan^2(\varphi)}{\left[\frac{a^2}{4 . \tan^2(\varphi) . h^2} + \sin(\varphi) + a . \frac{\cos(\varphi)}{2} \right]} \cdot \frac{t}{a} . E$

Table 2.2 Formulas for E₂

Model Name	E2
Masters & Evans [22]	$E_2 = \frac{E}{(1 + \sin \varphi) \cos \varphi} \left[\frac{\sin^2 \varphi \cdot a^3}{t^3} + \frac{\cos^2 \varphi \cdot t}{a} \right]$
E.Nast [30]	$E_2 = \frac{t^3 \cdot \cos \varphi}{(1 + \sin \varphi) \cdot a^3 \sin^2 \varphi \cdot (1 - \nu^2)} E$
Abd El-Sayed [24]	$E_2 = \frac{2}{3} \frac{\cos(\varphi)}{\left[\frac{a^2}{4 \cdot \tan^2(\varphi) \cdot h^2} + \cos^2(\varphi) \right]} \cdot \frac{t}{a} \cdot E$

Table 2.3 Formulas for E₃

Model Name	E3
E.Nast [30]	$E_3 = \frac{2 \cdot E}{(\cos \varphi \cdot (1 + \sin \varphi))} \cdot \frac{t}{a}$
Qunli Liu [23]	$E_3 = \frac{2 \cdot E}{(\cos \varphi \cdot (1 + \sin \varphi))} \cdot \frac{t}{a}$
Ashby [29]	$E_3 = \frac{2 \cdot E}{(\cos \varphi \cdot (1 + \sin \varphi))} \cdot \frac{t}{a}$

Table 2.4 Formulas for ν_{12}

Model Name	ν_{12}
Masters & Evans [22]	$\nu_{12} = \frac{\sin(\varphi)(1 + \sin(\varphi))}{\cos^2(\varphi)}$
E.Nast [30]	$\nu_{12} = \frac{(1 + \sin(\varphi)) \sin^2(\varphi)}{12 \cdot \cos^2(\varphi) \cdot \left[\frac{\cos(\varphi)}{3} - \frac{1 + \cos(\varphi)}{8} \right]}$
Abd El-Sayed [24]	$\nu_{12} = 3 \cdot \tan^2(\varphi)$

Table 2.5 Formulas for ν_{23}

Model Name	ν_{23}
E.Nast [30]	$\nu_{23} = \frac{t^2 \cos^2 \varphi}{2 \cdot a^2 \sin^2 \varphi \cdot (1 - \nu^2)} \nu$
Ashby [29]	0

Table 2.6 Formulas for ν_{13}

Model Name	ν_{13}
E.Nast [30]	$\nu_{13} = \frac{t^2 (\sin \varphi + 1)^2}{24 \cdot a^2 \cos \varphi \cdot \left[\frac{\cos \varphi}{3} - \frac{1 + \cos \varphi}{8} \right]} \cdot \frac{\nu}{(1 - \nu^2)}$
Ashby [29]	0

Table 2.7 Formulas for G_{12}

Model Name	G12
Masters & Evans [22]	$G_{12} = \frac{E}{\frac{3 \cdot \cos \varphi}{(1 + \sin \varphi)} \cdot \frac{a^3}{t^3} + [\cos \varphi + a \cdot \tan \varphi \cdot (1 + \sin \varphi)] \cdot \frac{a}{t}}$
E.Nast [30]	$G_{12} = \frac{t^3 \cdot (\sin \varphi + 1)}{a^3 \cdot (1 - \nu^2) \cos \varphi (6.25 - 6 \cdot \sin \varphi)} E$

Table 2.8 Formulas for G_{23}

Model Name	G23
E.Nast [30]	$G_{23} = \frac{10 \cdot t}{9 \cdot a \cdot \cos^3 \varphi \cdot (1 + \sin \varphi)} G$
Qunli Liu [23]	$G_{23} = \frac{\cos \varphi \cdot G}{1 + \sin \varphi} \cdot \frac{t}{a}$
Grediac [25]	$G_{23} = \frac{\cos \varphi}{1 + \sin \varphi} \cdot \frac{t}{a} \cdot G$
Shi [26]	$G_{23} = \frac{t \cdot \tan \varphi}{a} \cdot G$
Ashby [29]	$G_{23} = \frac{\cos \varphi}{(1 + \sin \varphi)} \cdot \frac{t}{a} G$

Table 2.9 Formulas for G_{13}

Model Name	G13
E.Nast [30]	$G_{13} = \frac{2t}{a \cdot \cos \varphi (1 + \sin \varphi)} G$
Qunli Liu [23]	$G_{13} = \frac{(1 + \sin \varphi) G}{2 \cdot \cos \varphi} \cdot \frac{t}{a}$
Grediac [25]	$\frac{1 + \sin \varphi}{2 \cdot \cos \varphi} \cdot \frac{t}{a} \cdot G \leq G_{13} \leq \frac{1 + \sin^2 \varphi}{(1 + \sin \varphi) \cos \varphi} \cdot \frac{t}{a} \cdot G$
Shi [26]	$G_{13} = \frac{3}{2} \cdot \frac{t \cdot \tan \varphi}{a} \cdot G$
Ashby [29]	$\frac{1 + \sin \varphi}{2 \cdot \cos \varphi} \cdot \frac{t}{a} \cdot G \leq G_{13} \leq \frac{1 + \sin^2 \varphi}{(1 + \sin \varphi) \cos \varphi} \cdot \frac{t}{a} \cdot G$

CHAPTER 3

MODELING

In this chapter, geometric modeling techniques of HC structures are introduced. As mentioned before, the aim in this thesis is to develop an equivalent model which will be a good substitute for actual HC geometry. “Modeling” is the first step in this process. As will be explained in the following sections, HC cores are first modeled detailed in geometry, and then equivalent models are generated. (see Sec 3.1.2, 3.1.3 and 4.1) The equivalent models have orthotropic material properties. These material properties are calculated through the equations that are given in Section 2.5. The use of equivalent model eases the analyses and design process to a great extent. The equivalent model is modeled and modified easily, it is fast to solve and requires less hardware. Therefore it is important and favorable to have an accurate equivalent model. Next step is the “Analyses” (See Chapter 4.) The generated models will be the input for the analyses. The equivalent models are compared with the detailed HC models to see whether or not they can be a good substitute for the real structure. Finally, the equivalent model is developed depending on the results of numerous analyses. (See Chapter 5) The developed equivalent model can be used in real structures’ analyses in macro-scale. Since the equivalent model is a simplified geometry, it does not have the details of the HC core. Therefore local stresses on the HC core can not be predicted by the use of equivalent model. On the other hand, in macro-scale, the level of stresses, the displacements can be predicted very accurately.

3.1 GEOMETRIC MODELING OF THE HONEYCOMB SANDWICH STRUCTURES

Geometric modeling of the honeycomb structures requires attention in order to have a good base for finite element procedures. In fact there is a two-way interaction between the geometric modeling and the FEM modeling. The geometry enforces the FEM model and the FEM modeling requirements affect the geometric model.

There are three ways to model a honeycomb sandwich structure:

1. Full 3D modeling
2. Shell modeling
3. Mixed modeling

3.1.1 Full 3D Modeling

Full 3D modeling term stands for the modeling of the face sheets plus the walls of the honeycomb in 3D. Plates and shells are a particular form of a three-dimensional solid, the treatment of which presents no theoretical difficulties, at least in the case of elasticity. However, the thickness of such structures is very small when compared with other dimensions. Moreover, the complete three dimensional numerical treatment is not only costly, but in addition often leads to serious numerical ill-conditioning problems [31]. Besides this, it requires a great preprocessing time in order to model the sandwich in a proper manner. Thus, 3D modeling is not considered in this thesis.

3.1.2 Shell Modeling

In shell modeling, both the face sheets and the honeycomb cells are modeled as shells. This approach reduces the amount of elements; also it is much easier to match the corresponding nodes. To solve the problem of mesh connectivity, the

face sheets are divided into sub-areas, as seen in Fig. 3.1 (See Section 3.2 for details). The problem arises from the nature of the shell modeling. In shell modeling, it is strongly suggested that the mid-plane (or mid-surface) of the structure be used. The use of these mid-planes causes problems in geometric modeling and meshing.

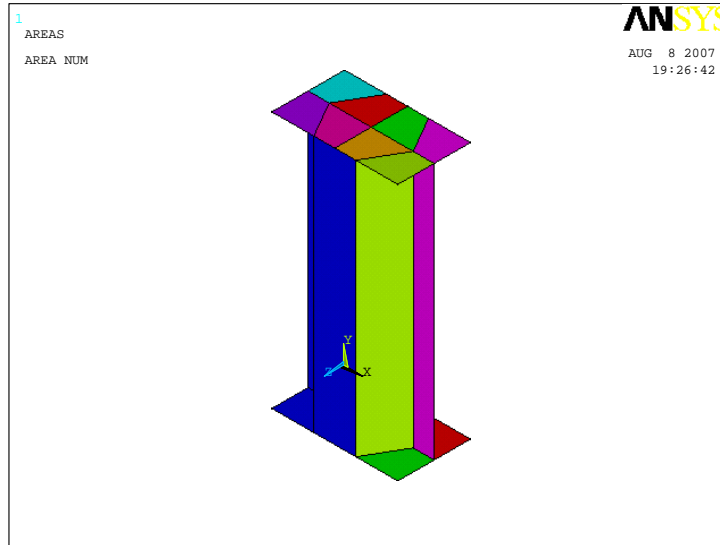


Figure 3.1 Divided Face Sheets Area

When mid-planes are used, as it can be see from the Fig. 3.2, there is an inevitable gap between the face sheet's mid-plane and the edge of the honeycomb. Because of this gap, it is not possible to make the corresponding nodes act as a whole. In order to solve this problem, two different methods are applied. Unfortunately, neither of these gives accurate and/or satisfactory results. The results of these two are given and discussed in the “Results and Discussion” chapter (See Section 5.2).

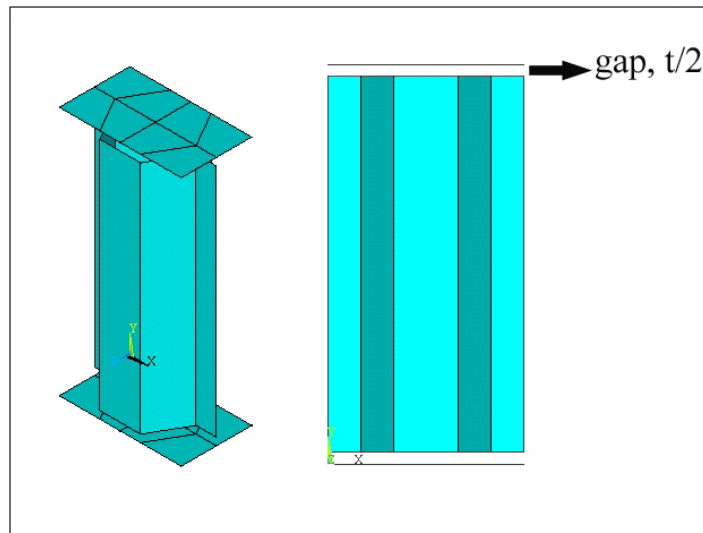


Figure 3.2 Sheet Modeling

3.1.3 Mixed Modeling

Mixed modeling is a mixture of 3D modeling and shell modeling. The face sheets are modeled in 3D and the HC core is modeled as shells. Mixed modeling stands in between the “Full 3D Modeling” and “Shell Modeling”. Mixed models are not as complicated and “heavy” as 3D models and they give better results than shell models. In Fig. 3.3 a unit cell with face sheets can be seen.

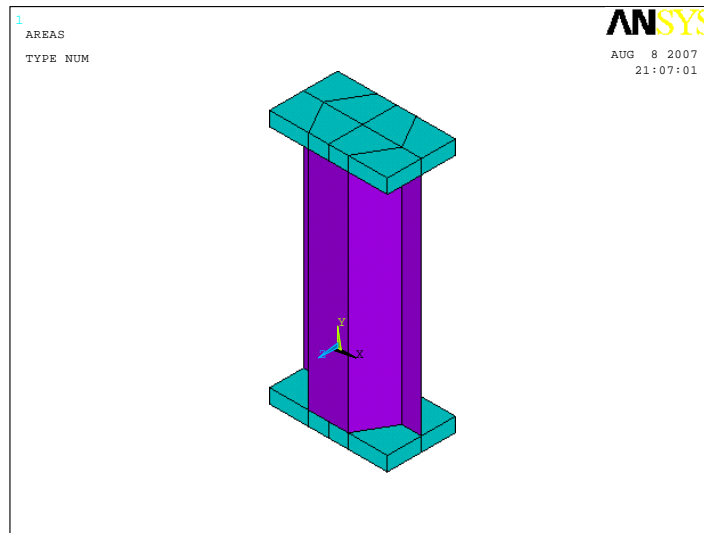


Figure 3.3 Mixed Modeling

3.2 FINITE ELEMENT MODELING OF THE HONEYCOMB STRUCTURES

Like in all other commercial finite element analysis programs, meshing is one of the most important preprocessor procedures that requires great attention in ANSYS. The FEM solver actually deals with the mesh structure, not the geometric structure. The geometric structure is a sub-step used in generating the desired mesh structure. Therefore, anything that is included in the mesh structure goes to the solver, and no matter, what if it is not included in the mesh, it is out of the solution. Meshing is relatively simpler for single types of entities (for example a single volume or surface). It is a little bit more complicated when the number of entities increases. In ANSYS, if someone likes to work with two different volumes together, they should have “common nodes”. In meshing, ANSYS treats the two volumes as separate volumes and meshes them separately, which results in non-common nodes. Since the finite element theory is based on node concept, if two volumes do not have common nodes, the individual volumes tend to behave independently. To clarify this, consider the

following example. In Fig. 3.4, two blocks of different sizes can be seen; the smaller block “physically” sits on the bigger one.

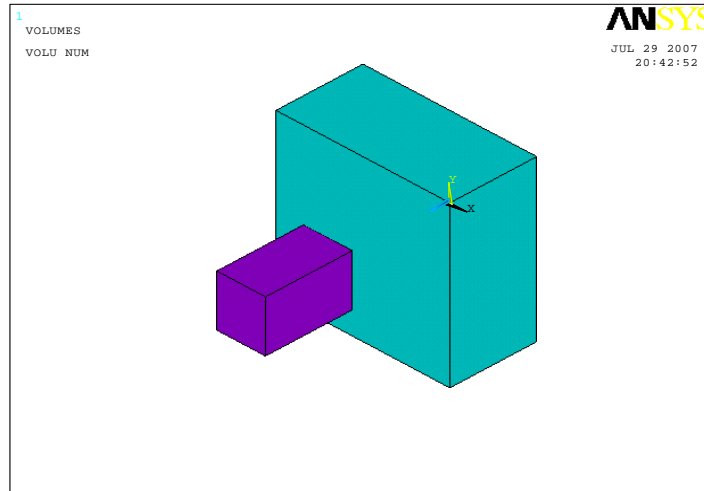


Figure 3.4 Two Blocks

When these two blocks are meshed in ANSYS, as seen in Fig. 3.5, they have independent meshes, which mean that there can be no load transfer in a linear or non-linear analysis. The only exception to this is the “contact” type problems. In contact problems, node connectivity is not essential.

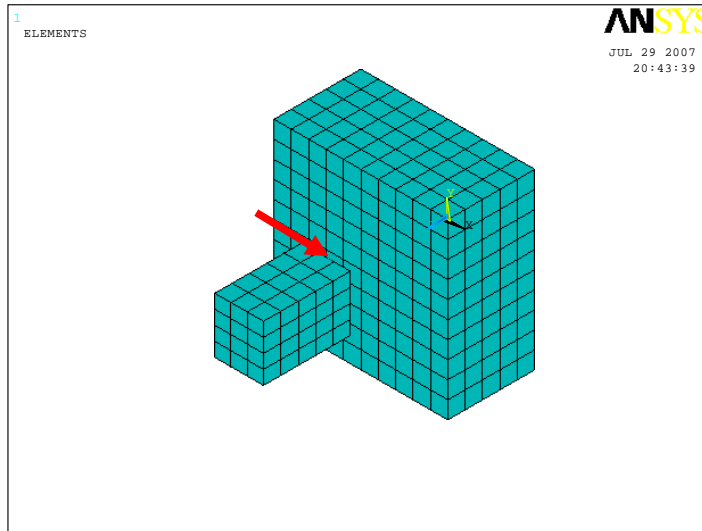


Figure 3.5 Meshed Two Blocks

To solve this problem, two different approaches can be followed. First, these two volumes can be added to result in one single volume, and then it can be meshed. The result of this procedure can be seen in Fig. 3.6.

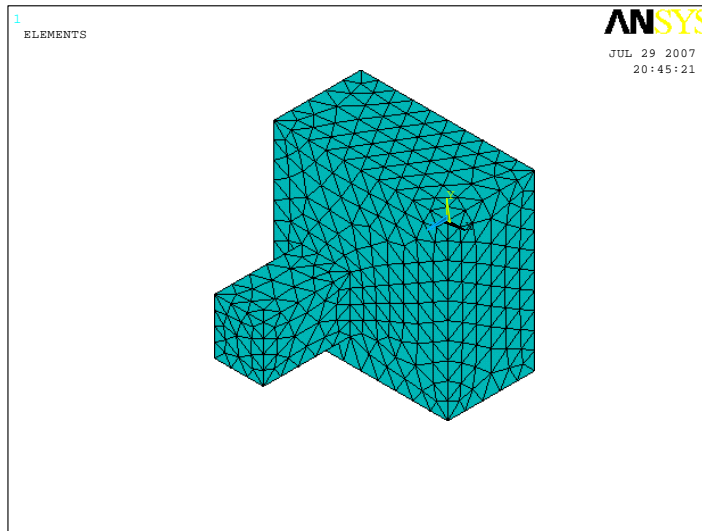


Figure 3.6 Mesh of Single Volume

This approach is feasible if both blocks are made of the same material. Since there is only one volume, only one material can be assigned to this volume. Another disadvantage of this method is that the structure can be meshed only with tetrahedral elements (free meshing), and this increases the number of elements (and nodes) used in meshing.

The second method solves the problem of mesh connectivity as well as the problems that may arise when the first method is applied. In the second method, the bigger volume is divided into sub-volumes, so that there are physical hard points at the corners of the smaller block. The divided volume can be seen in Fig. 3.7. The arrows in Fig. 3.7 show the physical corners that are generated to match the corners of the smaller block.

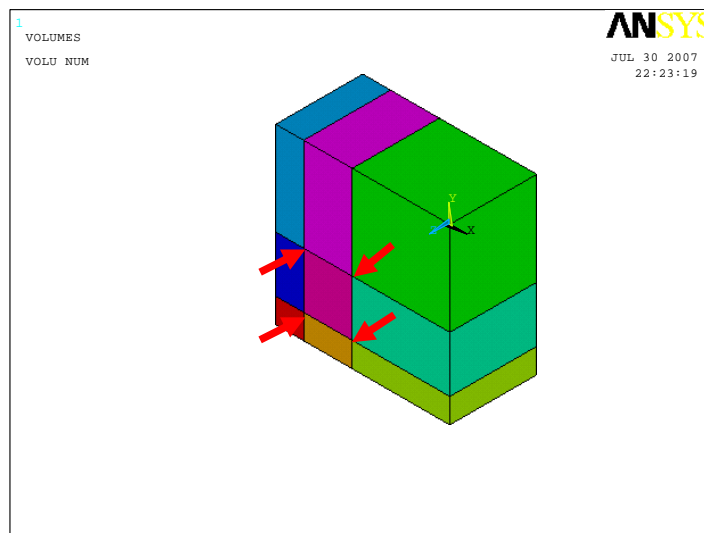


Figure 3.7 Divided Volume

After the proper division of the volume, merging of hard points should be performed. By this, the volumes are connected to each other via common points, lines and faces but not added to each other in a single volume. This gives the

chance of assigning one or two materials, which is not possible in the previous method. After merging, the volumes can be meshed readily. Mapped meshing or the sweep meshing technique can be applied to these re-worked volumes. A free mesh has no restrictions in terms of element shapes, and has no specified pattern applied to it. A mapped mesh is restricted in terms of the element shape and the pattern of the mesh. A mapped area mesh contains either only quadrilateral or only triangular elements, while a mapped volume mesh contains only hexahedron elements. In addition, a mapped mesh typically has a regular pattern, with obvious rows of elements [32]. The meshed volumes are depicted in Fig. 3.8

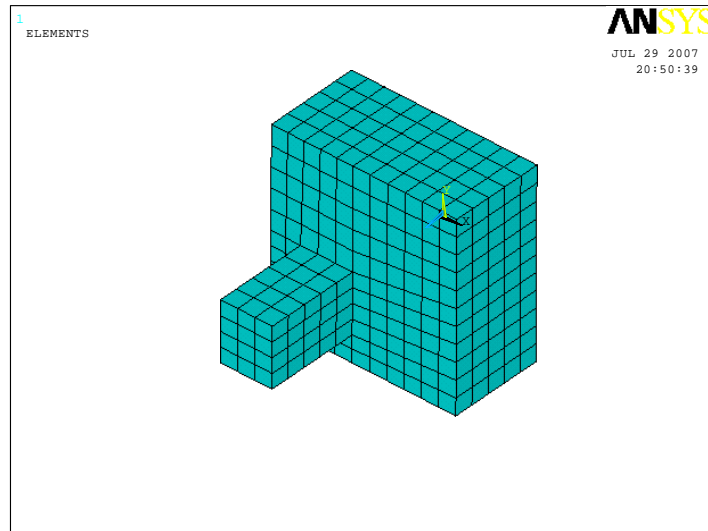


Figure 3.8 Mapped Meshed Volumes

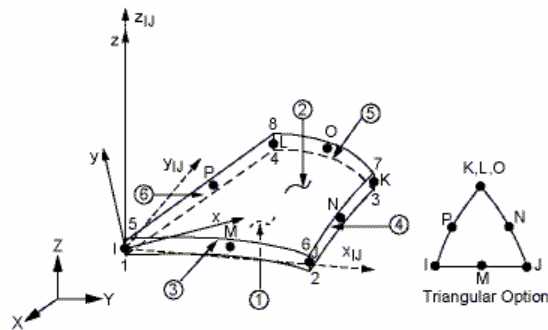
Although the characteristic element lengths of both cases are equal, there are 5859 elements and 9148 nodes in the volume(s) given in Fig. 3.6, whereas there are only 665 elements and 3523 nodes in the second one, Fig. 3.8. Even this simple example shows the importance of proper meshing. Although the number of elements is not as large for both cases, and they can be solved in a few

seconds with an ordinary PC, the time and hardware requirements may drastically increase with a bigger model.

3.2.1 ANSYS ELEMENTS USED IN ANALYSES

3.2.1.1 SHELL 93 ELEMENT:

SHELL93 is an 8 node structural shell element. It is particularly well suited to model curved shells. The element has six degrees of freedom at each node: translations in the nodal x, y, and z directions, as well as rotations about the nodal x, y, and z-axes. The deformation shapes are quadratic in both in-plane directions. The element has plasticity, stress stiffening, large deflection, and large strain capabilities. The geometry, node locations, and the coordinate system for this element are shown in Fig. 3.9 [32].



x_{IJ} = Element x-axis if ESYS is not supplied.

x = Element x-axis if ESYS is supplied.

Figure 3.9 SHELL93 ELEMENT

3.2.1.2 SOLID 186 ELEMENT

SOLID186 is a higher order 3-D 20-node solid element that exhibits quadratic displacement behavior. The element is defined by 20 nodes, each having three

degrees of freedom per node: translations in the nodal x, y, and z directions. The element supports plasticity, hyper-elasticity, creep, stress stiffening, large deflection, and large strain capabilities. It also has mixed formulation capability for simulating deformations of nearly incompressible elasto-plastic materials, and fully incompressible hyper-elastic materials.

SOLID186 is available in two forms:

Structural Solid (KEYOPT (3) = 0, the default)

Layered Solid (KEYOPT (3) = 1)

SOLID186 Structural Solid is well suited for modeling irregular meshes (such as those produced by various CAD/CAM systems). The element may have any spatial orientation. The geometry, node locations, and the element coordinate system for this element are shown in Fig. 3.10 [32].

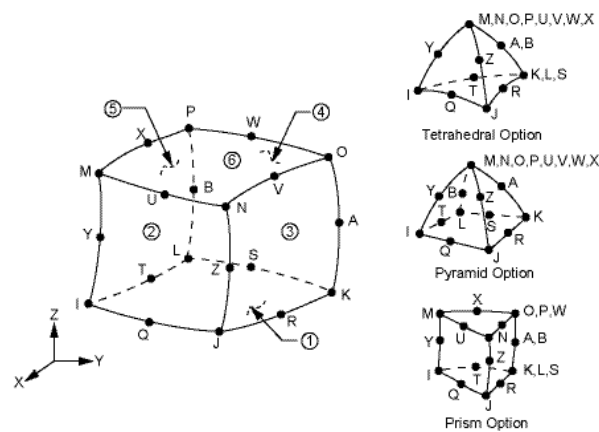


Figure 3.10 SOLID 186 ELEMENT

3.2.1.3 MPC 184 ELEMENT

Multi Point Constraint 184 (MPC184) element comprises a general class of multipoint constraint elements that apply kinematic constraints between nodes. The elements are loosely classified here as “constraint elements” (rigid link,

rigid beam, and slider) and “joint elements”. The constraint may be as simple as that of identical displacements between nodes. Constraints can also be more complicated, such as those modeling rigid parts, or those transmitting motion between flexible bodies in a particular way. The MPC184 rigid link/beam element can be used to model a rigid constraint between two deformable bodies or as a rigid component used to transmit forces and moments in engineering applications. This element is well suited for linear, large rotation, and/or large strain nonlinear applications. Fig. 3.11 shows the geometry, node locations, and the coordinate system for this element [32].

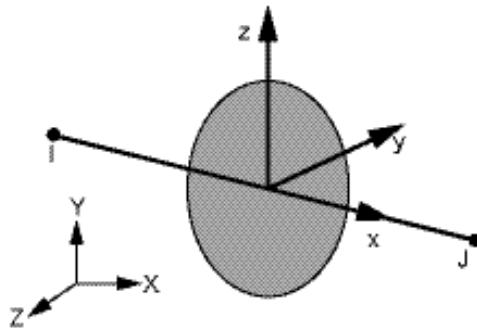
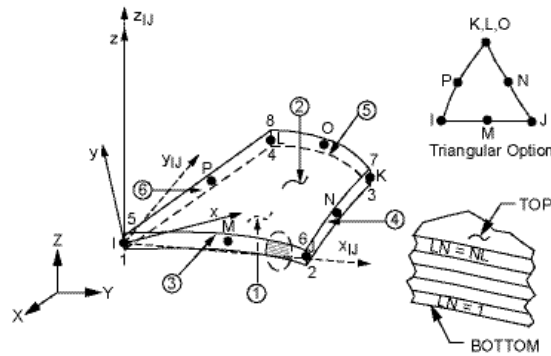


Figure 3.11 MPC 184 RIGID LINK/RIGID BEAM ELEMENT

3.2.1.4 SHELL99 ELEMENT

SHELL99 may be used for layered applications of a structural shell model and allows up to 250 layers. If more than 250 layers are required, a user-input constitutive matrix is available. The element has six degrees of freedom at each node: translations in the nodal x , y , and z directions, and rotations about the nodal x , y , and z -axes. The geometry, node locations, and the coordinate system for this element are shown in Fig. 3.12. The element is defined by eight nodes, average or corner layer thicknesses, layer material direction angles, and

orthotropic material properties [32]. Shell99 element has many element options, among them “Node offset option” deserves more attention. It is possible to locate the nodes of SHELL99 at mid-surface or bottom surface or top surface of the element. This property is used in the “Shell” modeling of HC, which will be explained Section 3.2.2.



x_{IJ} = Element x-axis if ESYS is not supplied.

x = Element x-axis if ESYS is supplied.

LN = Layer Number

NL = Total Number of Layers

Figure 3.12 SHELL99 ELEMENT

3.2.2 EFFECT OF NODE POSITIONS:

In shell modeling, to mesh the face sheets, the SHELL99 element is used. The reason for using this element is its capability of shifting its nodes to the bottom or top of the element; by default, the nodes are placed at mid surface of the shell element. In the early studies, it seemed wise to use node shifting property of SHELL99 element in shell modeling. As mentioned in Section 3.1.2 there is a gap between the face sheets and the core. To eliminate this gap, the face sheets moved $t/2$ inwards, towards the core. By this modification, the face sheets “touched” the core (Fig. 3.13). If the HC core and the face sheets are meshed

with an element with its nodes on the midplane of the element, interference occurs and the total height of the beam decreases (See Fig. 3.14-3.15).

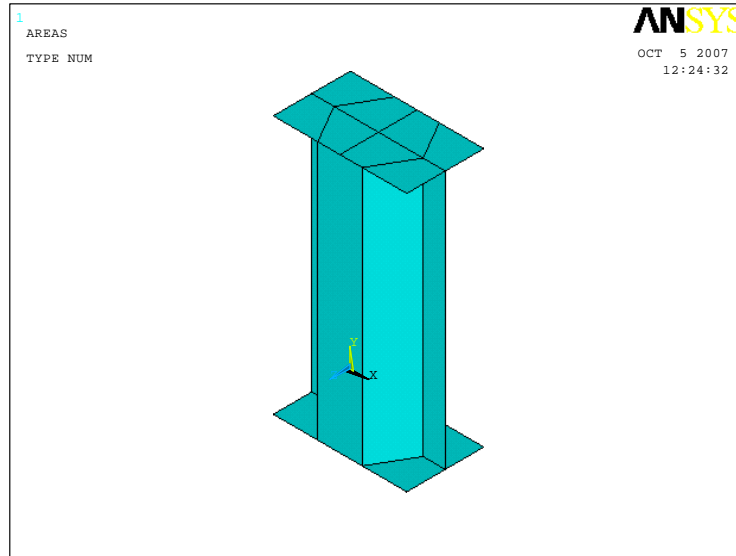


Figure 3.13 Modified Unit Cell

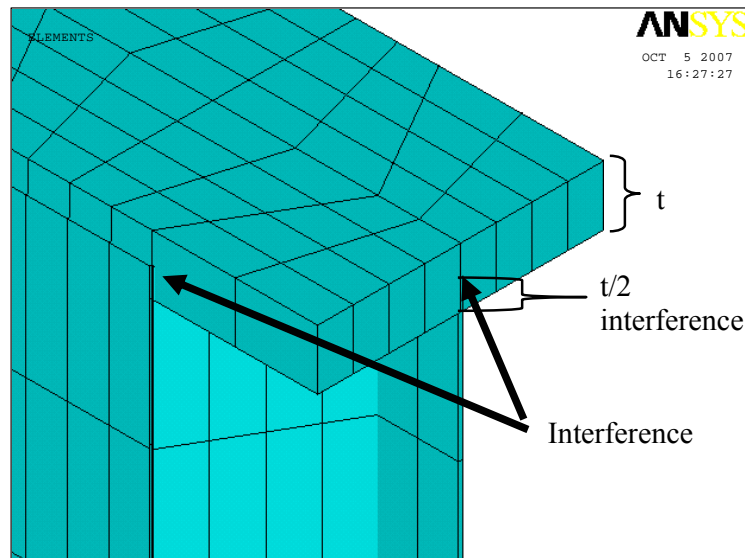


Figure 3.14 Interference of the HC Core and the Face Sheet

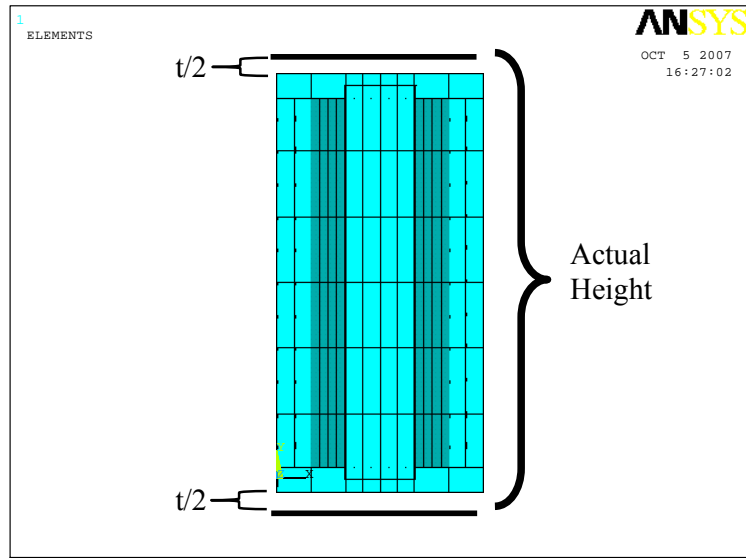


Figure 3.15 Reduced Height Due to the Interference

To solve this problem, SHELL99 element is used at the bottom face sheet with nodes at the top surface and at the top face sheet with nodes at the bottom face. Since the nodes are shifted either to the top surface or to the bottom surface, no interference occurs. (See Fig. 3.16) But, analyses ended in unexpected results.

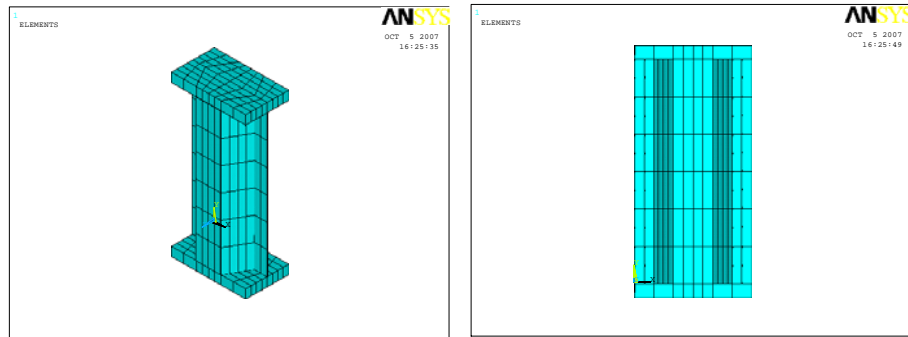


Figure 3.16 Unit Cell Meshed with SHELL99 (Nodes are shifted)

The reason for these erroneous results was node shifting. Due to this shift, an offset is generated between the neutral axis of the element and the node axis. This offset generates a moment which affected the results. To illustrate, consider the plates given in Fig. 3.17. The plates have the same dimensions and the material properties; the only difference is that they are meshed with 3 different SHELL99 elements. The left one is meshed with SHELL99 with the nodes at the bottom face, the middle one with nodes at the middle surface and the right one is meshed with the nodes at the top surface.

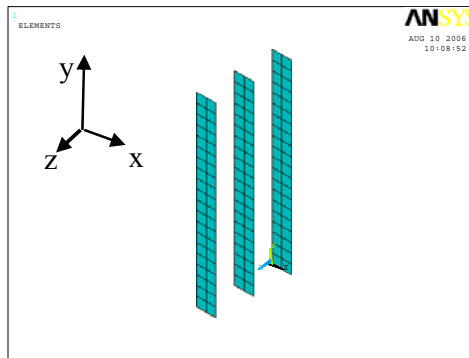


Figure 3.17 Beams with different node locations

All these plates are fixed at one of short edge, and uniform displacement is applied in $-y$ direction on the other short edge. Due to the shift effects, the plates with nodes either at the top or at the bottom of the element are bent, (See figure 3.18) which is not compatible with the linear elasticity theory.

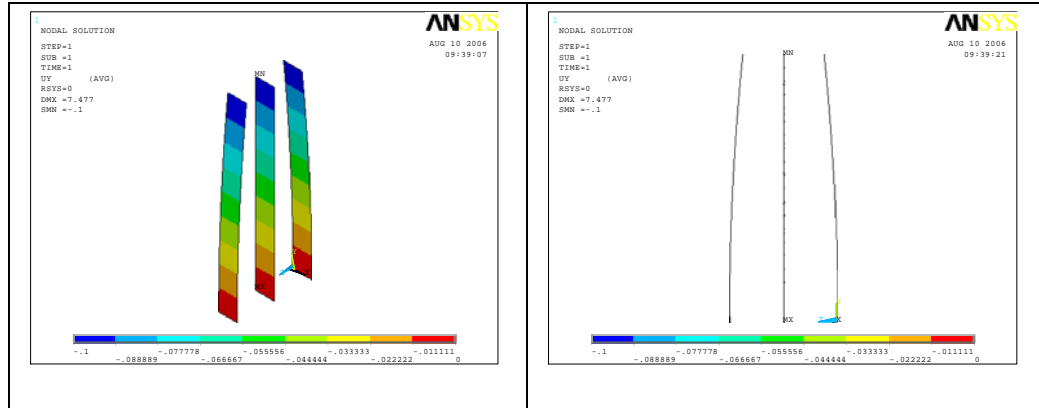


Figure 3.18 Effect of Node Locations

Due to the shift effect explained above, the nodes should be at the mid-surface. Thus, there is no need to use an element with a node shifting property. Therefore, instead of SHELL99 element, SHELL93 is used. When the nodes are the mid-surface, half thickness of the face sheets on both sides interferes with the core, so in order to keep the core thickness as desired, the core height is taken as $h' = h + t$, where h is the actual core height and t is the thickness of a face sheet. This solution, however, does not give satisfactory results. You will find the results in the “Results & Discussion” chapter. The problem of proper modeling of the HC and the face sheets solved by employing “Mixed Modeling” method. (See Section 3.1.3)

3.3 HONEYCOMBS USED IN THE ANALYSES:

In the analyses, 4 different HC’s are used. The geometric properties and the material are taken from HEXWEB Honeycomb Attributes and Properties Handbook [20]. All selected HC’s are regular hexagonal aluminum honeycombs. The selected HC’s are given in Table 3.1.

Table 3.1 The Selected Honeycombs
(See Fig.2.9)

CELL SIZE (d) (inch-mm)	ALLOY	FOIL GAUGE (t) (inch-mm)
3/16 – 4.76	5052	0.003 – 0.076
3/8 – 9.53	5052	0.003 - 0.076
1/4 – 6.35	5052	0.003 - 0.076
5/32 – 3.97	5052	0.0025 – 0.064

The mechanical properties of aluminum alloy AA-5052 are given in Table 3.2. Face sheet material is also AA-5052 alloy throughout this thesis except for Chapter 6. Aluminum alloys are widely used in aerospace industry, especially the wings and fins of missiles are usually made of aluminum. In addition to these, aluminum is one of the most popular materials for HC cores. That's why we choose aluminum as HC core and face sheet material.

Table 3.2 Mechanical Properties of AA-5052 [33]

Density	2.68 gr/kg ³
Poisson's Ratio	0.33
Young's Modulus	70-80 GPa
Tensile Strength	230 MPa
Yield Strength	195 MPa
Elongation	%12
Shear Strength	140 Mpa

4 different cell heights are used. The default cell height is taken as 0.625 inch (15.875 mm.) as suggested in AMS-C-7438 SAE Core Material, Aluminum, for Sandwich Construction standard [34]. The remaining three heights are calculated from this default height; 1/2 of the default size, 1.5 times and 2 times

of the default height. Hence, the cell heights are 15.875mm, 7.938, 21.813 and 31.750 mm's.

Therefore, using 4 different HC's and 4 different cell heights generate a 4 x 4 analyses matrix.

CHAPTER 4

ANALYSES

In order to achieve the goal of this thesis, an “equivalent model” needs to be generated. To figure out the best model, you obviously need a reference model with which you can compare the results. In this thesis study, first the HC’s are modeled in detail by preserving the actual geometry of the honeycomb structure. This is accomplished either by using “shell modeling” or “mixed modeling” technique, and the results of these models are accepted as reference models. As candidate equivalent models, a set of equivalent models is generated. Orthotropic material properties are calculated from the formulas given in Table 2.1 through Table 2.9. Model 1 is generated from Master’s [22] studies. Model 2 is based on E.Nast’s calculations [30]. Model 3 uses the formulas provided in Quin Liu [23]. Model 4 is based on Shi’s [26] studies. In model 5, Ashby’s [29] work is considered. Model 6 and 7 use the formulas of Grediac [25]. In model 6, the minimum value G_{12} is used whereas in model 7, the maximum value is used. The values of model 8 is taken from the HEXWEB [20]. Model 9 is generated from model 8, by adding the missing orthotropic constants from different models. Model 10 is a mixture of the other 9 models. The models and the related references are tabulated in Table 4.1.

Table 4.1 The Models and the Related References.

MODELS					
	1	2	3	4	5
E1	Master [22]	Nast [30]	-	-	-
E3	Universally Agreed On				
E2	Master [22]	Nast [30]	-	-	-
v_{13}	-	Nast [30]	-	-	Ashby [29]
v_{23}	-	Nast [30]	-	-	Ashby [29]
v_{12}	Master [22]	Nast [30]	-	-	-
G_{13}	-	Nast [30]	Quin Liu [23].	Shi [26]	Ashby [29]
G_{23}	-	Nast [30]	Quin Liu [23].	Shi [26]	Ashby [29]
G_{12}	Master [22]	Nast [30]	-	-	-
	6	7	8	9	10
E1	Grediac [25]	Grediac [25]	-	Nast [26]	Nast [26]
E3	Universally Agreed On	HEXCELL	HEXCELL	Un. Agr'ed on	
E2	Grediac [25]	Grediac [25]	-	Master [22]	Nast [26]
v_{13}	-	-	-	Nast [26]	Ashby [29]
v_{23}	-	-	-	Nast [26]	Ashby [29]
v_{12}	Grediac [25]	Grediac [25]	-	Nast [26]	-
G_{13}	Grediac [25]	Grediac [25]	HEXCELL	HEXCELL	Nast [26]
G_{23}	Grediac [25]	Grediac [25]	HEXCELL	HEXCELL	Nast [26]
G_{12}	-	-	-	Master [22]	Nast [26]

In the finite element analyses performed by ANSYS, elastic moduli can not be assigned as zero for any material. Therefore, in any model if elastic moduli, such as in-plane moduli or shear moduli, value is missing it is accepted taken as a very small number such as 0.1 or 0.01.

There is no predetermined way to figure out the best equivalent model. So trial & error method is employed. First, these models are analyzed under the same conditions. The results are tabulated and the relative difference with respect to the reference model is calculated. A detailed investigation of the errors shows the best performing models under different loading conditions. As will be seen in the “Results and Discussion” chapter, the results of the first runs are considered and then another set of equivalent models is generated to reduce the relative difference as much as possible. In Figure 4.1 flowchart of the overall process can be seen.

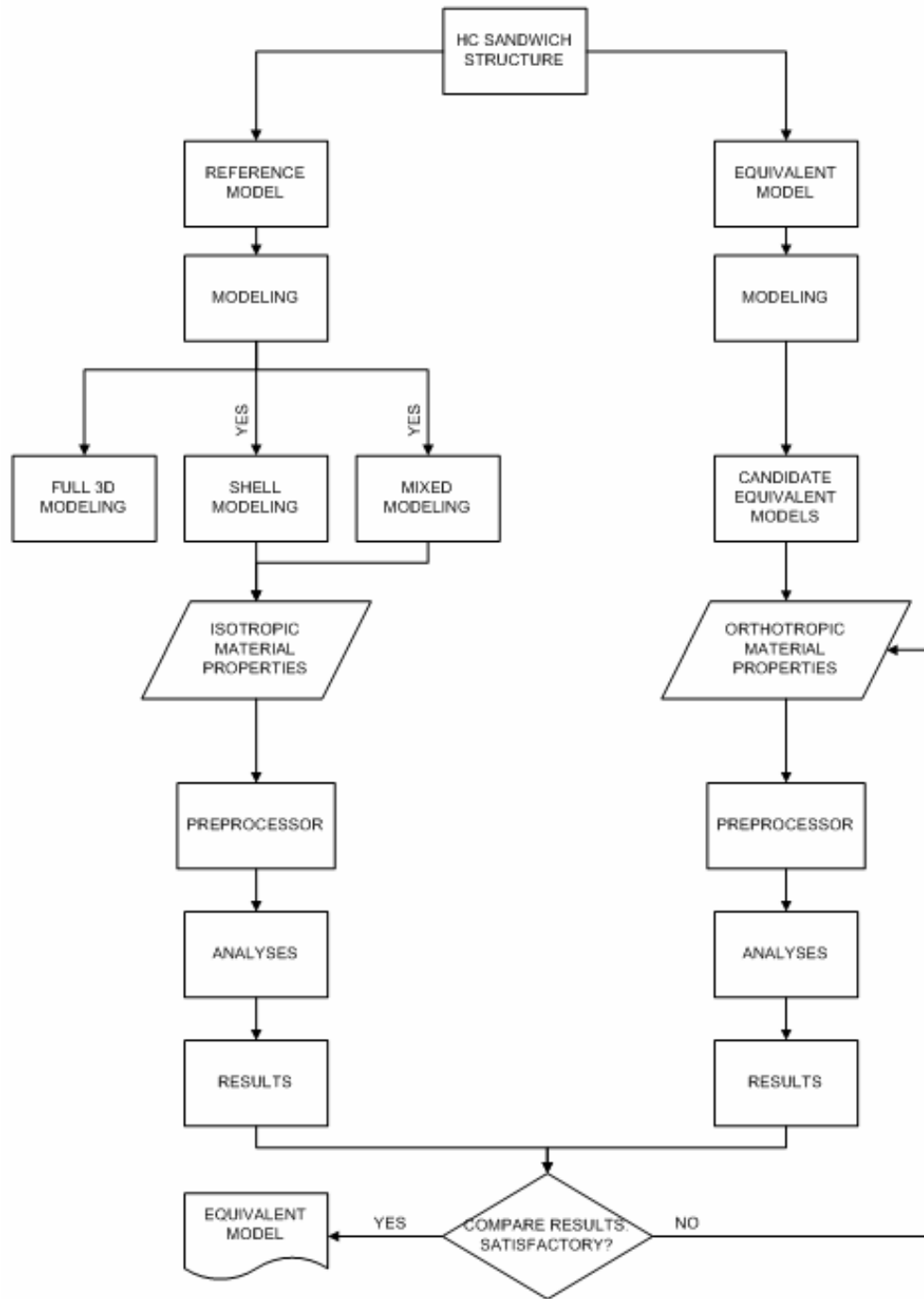


Figure 4.1 Flowchart of the Overall Process

4.1 EQUIVALENT MODELING:

In equivalent modeling, the goal is to replace HC cells with a bulk body that acts as the HC itself in a macroscopic view. In equivalent modeling instead of modeling the HC in detail, an orthotropic bulk material is used. In Fig. 4.2 HC beam model and its “equivalent” is seen.

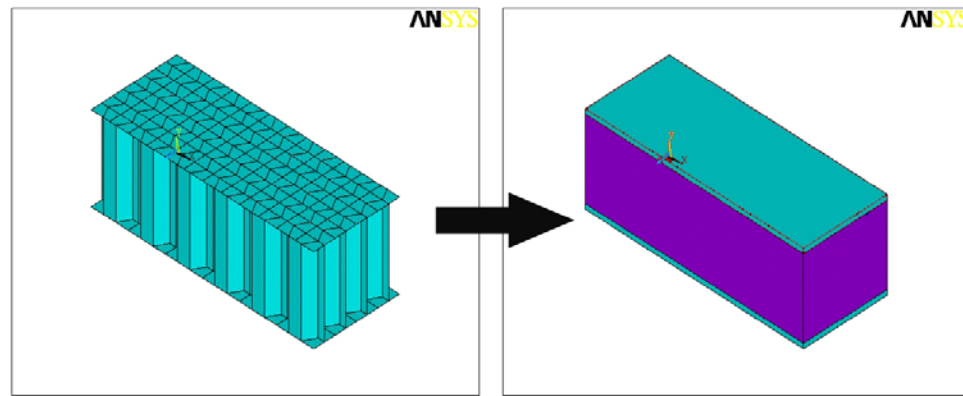


Figure 4.2 HC model and the Equivalent Model

4.2 CANDIDATE EQUIVALENT MODELS:

In this chapter, the material properties of the generated equivalent models can be found. Each column numbered from 1 to 10 represent a different candidate model. The models’ geometric and material properties are taken from the selected HC cores that are tabulated in Table 3.1. The orthotropic material constants are calculated by the help of the corresponding formulas that are given in Tables 2.1 through 2.9.

Table 4.2 Orthotropic Material Properties for 10 Equivalent Models for CS1

Cell Size 1 (CS1) (3/16 inches) (h=15.875 mm)					
	1	2	3	4	5
E1 (MPa)	3,53	5,06	0,1	0,1	0,1
E3 (MPa)	3072	3072	3072	3072	3072
E2 (MPa)	3,53	3,89	0,1	0,1	0,1
ν_{13}	0	0,0001	0	0	0
ν_{23}	0	0,0004	0	0	0
ν_{12}	1	1,128	0	0	0
G_{13} (MPa)	0,1	1181	665	738	665
G_{23} (MPa)	0,1	875,1	443	443	443
G_{12} (MPa)	0,883	0,897	0,01	0,01	0,01
Cell Size 1 (CS1) (3/16 inches) (h=15.875 mm)					
	6	7	8	9	10
E1 (MPa)	3,54	0,1	0,1	5,06	5,06
E3 (MPa)	3072	3072	2413,2	2413,2	3072
E2 (MPa)	3,53	0,1	0,1	3,53	3,89
ν_{13}	0	0	0	0,0001	0
ν_{23}	0	0	0	0,0004	0
ν_{12}	0,997	0	0	1,128	0
G_{13} (MPa)	665	738	931	931	1181
G_{23} (MPa)	443	443	372	372	875,1
G_{12} (MPa)	0,01	0,01	0,01	0,883	0,897

Table 4.3 Orthotropic Material Properties for 10 Equivalent Models for CS2

Cell Size 2 (CS2) (3/8 inches) (h=15.875 mm)					
	1	2	3	4	5
E1 (MPa)	0,442	0,633	0.1	0.1	0.1
E3 (MPa)	1536	1536	1536	1536	1536
E2 (MPa)	0,442	0,486	0.1	0.1	0.1
ν_{13}	0	2,52E-05	0	0	0
ν_{23}	0	9,50E-05	0	0	0
ν_{12}	0,997	1,128	0	0	0
G ₁₃ (MPa)	0.01	591	323,3	369,2	332,3
G ₂₃ (MPa)	0.01	438	221,5	221,5	221,5
G ₁₂ (MPa)	0,11	0,112	0.01	0.01	0.01
Cell Size 2 (CS2) (3/8 inches) (h=15.875 mm)					
	6	7	8	9	10
E1 (MPa)	0,442	0,1	0.1	0,633	0,633
E3 (MPa)	1536	1536	930	930	1536
E2 (MPa)	0,442	0,1	0.1	0,442	0,486
ν_{13}	0	0	0	2,52E-05	0
ν_{23}	0	0	0	9,50E-05	0
ν_{12}	0,997	0	0	1,128	0
G ₁₃ (MPa)	332,3	369,2	448	448	590,7
G ₂₃ (MPa)	221,5	221,5	200	200	437,6
G ₁₂ (MPa)	0.01	0,01	0.01	0,11	0,112

Table 4.4 Orthotropic Material Properties for 10 Equivalent Models for CS3

Cell Size 3 (CS3) (1/4 inches) (h=15.875 mm)					
	1	2	3	4	5
E1 (MPa)	1,491	2,136	0,1	0,1	0,1
E3 (MPa)	2304	2304	2304	2304	2304
E2 (MPa)	1,491	1,641	0,1	0,1	0,1
ν_{13}	0	5,67E-05	0	0	0
ν_{23}	0	2.1E-04	0	0	0
ν_{12}	0,998	1	0	0	0
G ₁₃ (MPa)	0,01	886	499,5	553,8	498,5
G ₂₃ (MPa)	0,01	656	332	332	332
G ₁₂ (MPa)	0,373	0,379	0,01	0,01	0,01
Cell Size 3 (CS3) (1/4 inches)					
	6	7	8	9	10
E1 (MPa)	1,491	0,1	0,1	2,136	2,136
E3 (MPa)	2304	2304	1620	1620	2304
E2 (MPa)	1,491	0,1	0,1	1,491	1,641
ν_{13}	0	0	0	5,67E-05	0
ν_{23}	0	0	0	2.1E-04	0
ν_{12}	0,997	0	0	1	0
G ₁₃ (MPa)	498,5	553,8	662	662	886
G ₂₃ (MPa)	332	332	279	279	656
G ₁₂ (MPa)	0,01	0,01	0,01	0,373	0,379

Table 4.5 Orthotropic Material Properties for 10 Equivalent Models for CS4

Cell Size 4 (CS4) (5/32 inches) (h=15.875 mm)					
	1	2	3	4	5
E1 (MPa)	3,532	5,066	0,1	0,1	0,1
E3 (MPa)	3074	3074	3074	3074	3074
E2 (MPa)	3,532	3,892	0,1	0,1	0,1
ν_{13}	0	1.0E -04	0	0	0
ν_{23}	0	3,8 E-04	0	0	0
ν_{12}	0,997	1	0	0	0
G ₁₃ (MPa)	0,01	1182	665	739	665
G ₂₃ (MPa)	0,01	875,7	443,3	443,4	443,4
G ₁₂ (MPa)	0,885	0,899	0,01	0,01	0,01
Cell Size 4 (CS4) (5/32 inches)					
	6	7	8	9	10
E1 (MPa)	3,532	0,1	0,1	5,066	5,066
E3 (MPa)	3074	3074	2551	2551	3074
E2 (MPa)	3,532	0,1	0,1	3,532	3,892
ν_{13}	0	0	0	1.0E-04	0
ν_{23}	0	0	0	3,8 E-04	0
ν_{12}	0,997	0	0	1	0
G ₁₃ (MPa)	665	739	965	965	1182
G ₂₃ (MPa)	443,4	443,3	386	386	875,7
G ₁₂ (MPa)	0,01	0,01	0,01	0,885	0,899

4.3 MODEL GENERATION:

In the analyses, beams with 6 cells in 1 direction and 4 cells in 2 direction are used. The face sheets' thickness is taken as 1 mm in all models. HC models are generated by the following procedure:

1. Model a unit cell with face sheets in NX.4.0
2. Import the geometry into ANSYS
3. Mesh the unit cell
4. Create an array of 4 x 6 cells
5. Merge the nodes

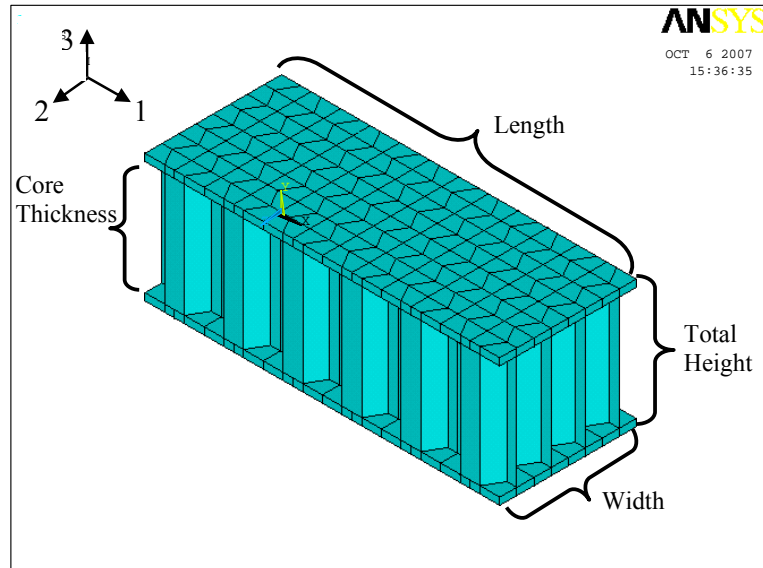


Figure 4.3 Sample Beam Geometry

The unit cell imported to ANSYS is first meshed and then the array is created, as it is easier to mesh the cell walls this way. The diagonal walls are single walls whereas the horizontal walls are doubled. Adhering two strips of aluminum form the horizontal walls so that the thickness is doubled.

Equivalent models are generated directly in ANSYS environment. They are basically composed of 3 single blocks and it is not a difficult task to build the model in ANSYS. The dimensions of the equivalent models for each cell size and height are equal to those of the corresponding HC models. The dimensions of the beams is summarized in Table 4.5. (See Fig. 4.3)

Table 4.6 Dimensions of the Analyzed Beams

Cell Size (inches- mm.)	Foil (mm.)	Width (mm.)	Length (mm.)	Core height (mm.)	Face thickness (mm.)	Total thickness (mm.)
3/16-4.76	0.076	19.05	49.5	15.875	1.0	17.875
3/16-4.76	0.076	19.05	49.5	7.938	1.0	9.938
3/16-4.76	0.076	19.05	49.5	21.813	1.0	23.813
3/16-4.76	0.076	19.05	49.5	31.750	1.0	33.750
3/8 - 9.53	0.076	38.10	99.0	15.875	1.0	17.875
3/8 - 9.53	0.076	38.10	99.0	7.938	1.0	9.938
3/8 - 9.53	0.076	38.10	99.0	21.813	1.0	23.813
3/8 - 9.53	0.076	38.10	99.0	31.750	1.0	33.750
1/4 - 6.35	0.076	25.40	66.0	15.875	1.0	17.875
1/4 - 6.35	0.076	25.40	66.0	7.938	1.0	9.938
1/4 - 6.35	0.076	25.40	66.0	21.813	1.0	23.813
1/4 - 6.35	0.076	25.40	66.0	31.750	1.0	33.750
5/32-3.97	0.064	15.86	41.2	15.875	1.0	17.875
5/32-3.97	0.064	15.86	41.2	7.938	1.0	9.938
5/32-3.97	0.064	15.86	41.2	21.813	1.0	23.813
5/32-3.97	0.064	15.86	41.2	31.750	1.0	33.750

4.4 ASSUMPTIONS:

The following assumptions are made through the all the analyses:

1. Cells have perfect geometry, no deviations from hexagonal shape
2. Corner radii of the cell walls are very small
3. There is perfect bonding between the strips of the HC, and the adhesive layer is very thin and can be neglected.
4. There is perfect bonding between the HC cells and the face sheets, and the adhesive layer is very thin and can be neglected.

4.5 LOADS AND BOUNDARY CONDITIONS:

All the analyses are performed under the same loading and boundary conditions. The 9 different loading cases are included in the analyses. In all 9 cases, as shown in Fig. 4.2, the model is kept fixed on one face and uniform displacement is applied on the opposite face. In Table 4.7 the loading cases and the BC's are tabulated. During the analyses, instead of applying force, displacement is applied; the reaction force on the fixed face is considered. When force is applied to the faces, it is not easy to examine the results because the face sheets of the HC model are not fully supported, whereas they are fully supported by the equivalent core. This difference causes waviness in the displacement field and it becomes hard to make an objective judgement. Therefore, displacement is used as input, and the reaction force is taken as the output for these models. To visualize this, a beam is analyzed. (See Fig. 4.4) The beam is kept fixed on one face (Face A in Fig 4.4) and distributed force is applied on the opposite face's upper edge (Edge B in Fig 4.4) The deformed beam is given in Fig.4.5. The "wavy" displacement field is not clear in Fig 4.5, therefore a closer view of the beam is given in Fig. 4.6. As it can be seen in Fig.4.6 because of the unsupported sections of the beam, the displacement field varies over the edge, which makes it hard to evaluate the results.

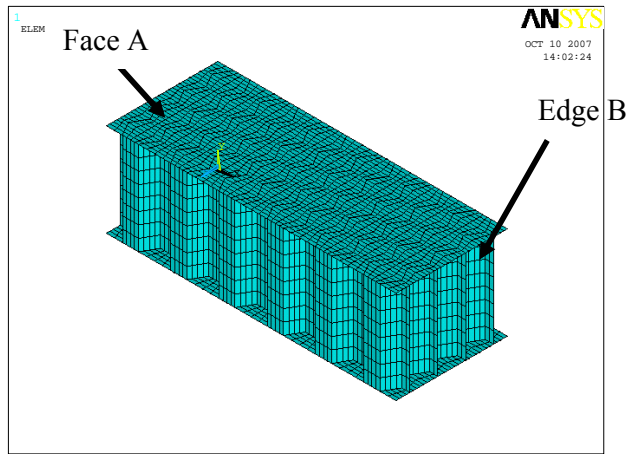


Figure 4.4 The Analyzed Beam to Visualize the Waviness

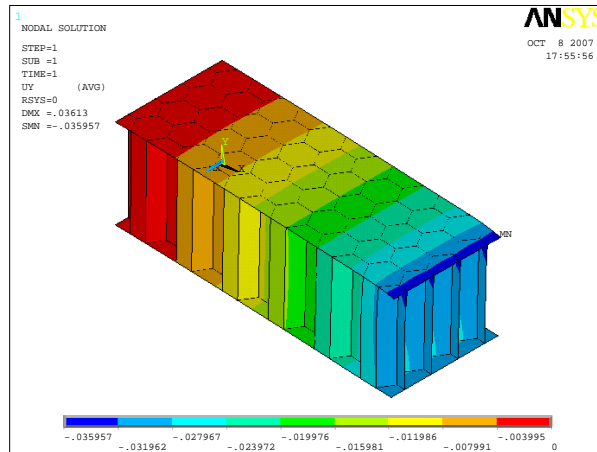


Figure 4.5 The Deflections of the Analyzed Beam

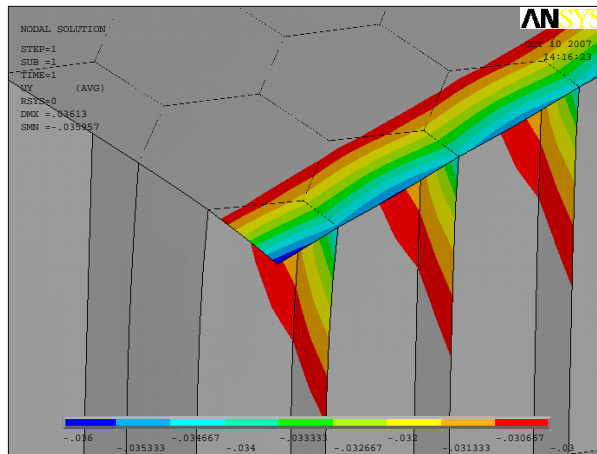


Figure 4.6 The Deflections of the Analyzed Beam (Closer View)

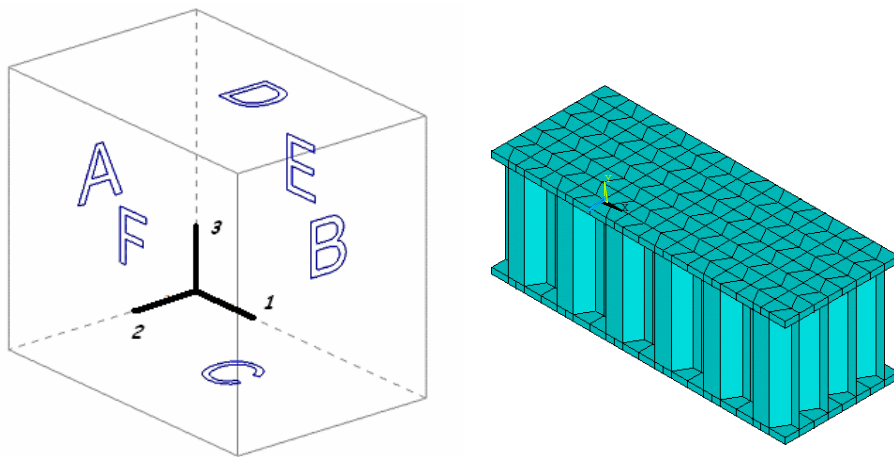


Figure 4.7 Faces of a Beam

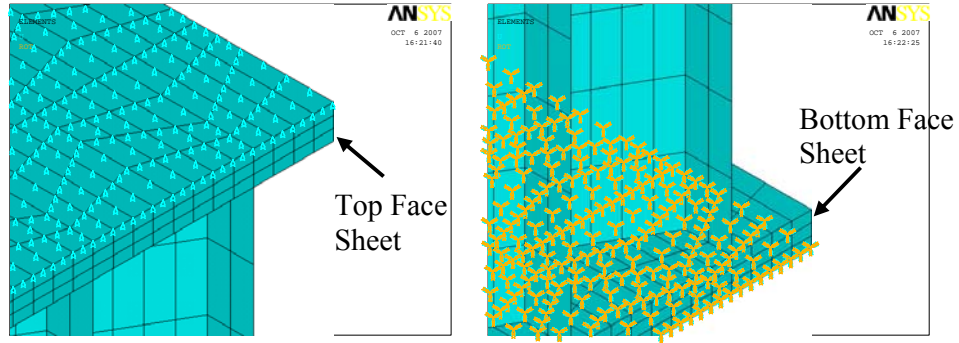


Figure 4.8 Boundary Conditions for Load Case 2

Table 4.7 Loads & Boundary Conditions

LOAD CASE	FIXED FACE	DISPLACEMENT APPLIED TO	DIRECTION OF APPLIED DISPLACEMENT	DISPLACEMENT IN mm.
1	A	B	1	-0.0001
2	C	D	3	-0.0001
3	E	F	2	-0.0001
4	A	B	3	-0.0001
5	A	B	2	-0.0001
6	C	D	1	-0.0001
7	C	D	2	-0.0001
8	E	F	1	-0.0001
9	E	F	3	-0.0001

4.6 MESHING:

4.6.1 Meshing of the HC Models:

In shell modeling, SHELL93 element is used. There are 16 different model geometries. (4 HC sizes X 4 Cell Heights). To keep the meshes as alike as possible, instead of defining the element edge length, element per edge is entered. In this way, the element number of each different HC model is the same as the other one. A mesh size study is performed and with the help of the results of this study, elements per edge along the cell height is chosen such that the aspect ratio of the elements on the cell walls is in-between 0.5 (for maximum cell height) and 2 (for minimum cell height). Quadrilateral elements are used in both the walls and the face sheets.

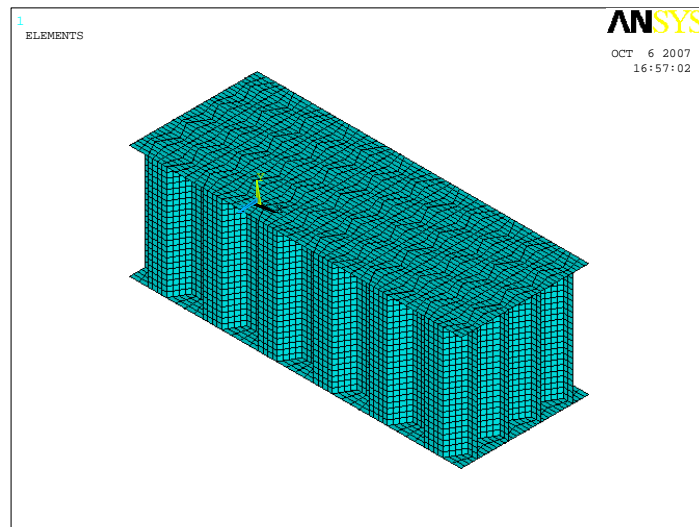


Figure 4.9 A sample Beam, Meshed with Shell Elements

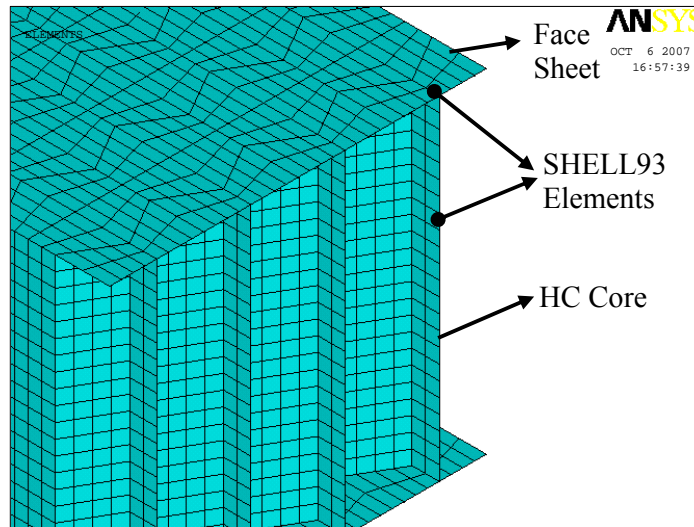


Figure 4.10 A sample Beam, Meshed with Shell Elements (Closer View)

In the mixed modeling, meshing of the cell walls is the same as the shell modeling. For face sheets, SOLID186 element is employed.

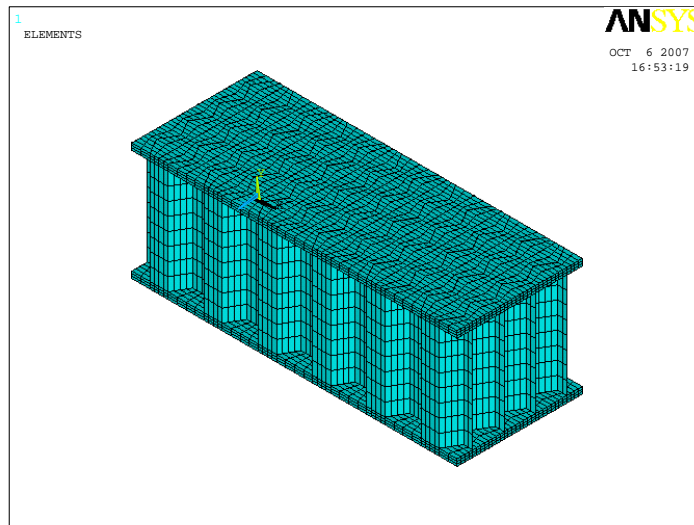


Figure 4.11 A sample Beam, Meshed with Shell and Solid Elements

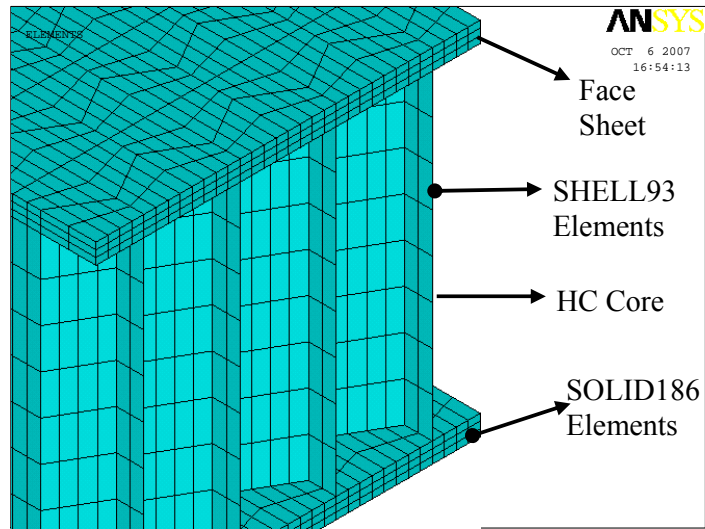


Figure 4.12 A sample Beam, Meshed with Shell and Solid Elements (Closer View)

4.6.2 Meshing of the equivalent models:

Equivalent models are meshed with SOLID186 element. In a similar manner when meshing of HC models, element per edge is defined.

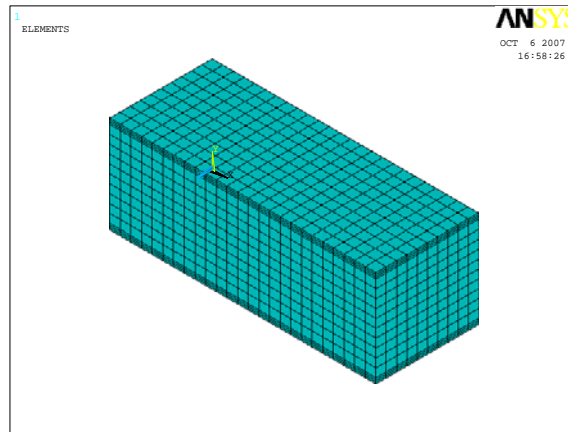


Figure 4.13 A sample Equivalent Beam, Meshed with Solid Elements

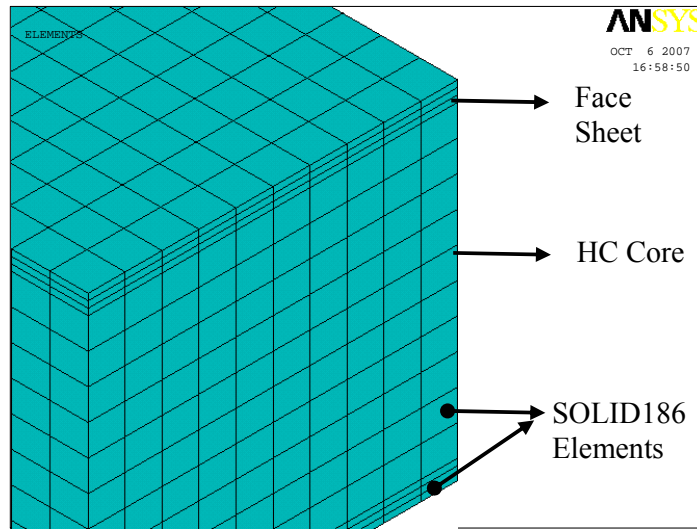


Figure 4.14 A sample Equivalent Beam, Meshed with Solid Elements (Closer View)

CHAPTER 5

RESULTS & DISCUSSION

In this chapter, the analyses results on the honeycomb model and the equivalent model will be presented and discussion on these analyses will be held. The analyses are performed in three parts.

In the first set of runs, 1584 runs are performed in total. In the second and third sets, 144 and 576 runs are performed respectively. The result of each run is examined and tabulated. Depending on the results of the first set, the second set is generated. Likewise the third set is generated depending of the results of the preceding set, i.e. the second set. After investigating the results of the first runs, a second set of runs is performed due to reasons that will be clarified through this chapter. Finally, the decision on the equivalent model will be made by the third runs.

5.1 RESULTS OF THE FIRST RUNS:

In the first runs, the reference HC models are modeled as shell models. As mentioned before, the judgment between the equivalent models are made by comparing their relative errors with respect to the reference honeycomb models. Tables 5.2 to 5.5 give the relative errors of 4 HC cells, with core height of 15.875 mm, for the ten equivalent models given in Section 4.2. For the other core heights the tables are given in Appendix A.

“FSUM” values in the tables are the total reaction forces on the nodes of the fixed face, in the direction of the applied deformation. The load cases, given in Table 4.6, corresponding to different FSUM values are tabulated in Table 5.1.

Table 5.1 The Load Cases and Corresponding FSUM Values

FSUM	LOAD CASE
F1SUM	1
F12SUM	5
F13SUM	4
F2SUM	2
F21SUM	8
F23SUM	9
F3SUM	3
F31SUM	6
F32SUM	7

Table 5.2 The Relative difference between Honeycomb and Equivalent Models of CS1-H1 in the First Runs

CS1 - H1 (Relative Difference, %) (See Table 4.1)					
Total Reaction Force	1	2	3	4	5
F1SUM	-2,35	-1,57	-2,54	-2,54	-2,54
F12SUM	-0,91	-0,50	-1,10	-1,09	-1,10
F13SUM	-99,40	22,40	-4,80	0,17	-4,87
F2SUM	-3,77	-3,05	-4,04	-4,04	-4,04
F21SUM	-0,41	-0,31	-0,47	-0,47	-0,47
F23SUM	-96,66	92,61	8,98	8,98	8,98
F3SUM	-17,61	-17,60	-17,61	-17,61	-17,61
F31SUM	-99,98	45,74	-10,76	-2,27	-10,88
F32SUM	-99,97	42,86	-5,63	-5,63	-5,63
Total Reaction Force	6	7	8	9	10
F1SUM	-1,45	-2,54	-2,54	-2,29	-2,49
F12SUM	-0,53	-1,09	-1,10	-0,91	-1,04
F13SUM	-4,58	0,17	11,16	11,21	22,14
F2SUM	-1,83	-4,04	-4,05	-3,85	-4,00
F21SUM	-0,23	-0,47	-0,48	-0,42	-0,45
F23SUM	9,04	8,98	-6,32	-6,31	92,51
F3SUM	-17,60	-17,61	-35,22	-35,21	-17,61
F31SUM	-10,65	-2,27	14,93	14,97	45,59
F32SUM	-5,38	-5,63	-22,31	-22,25	42,63

Table 5.3 The Relative difference between Honeycomb and Equivalent Models of CS2-H1 in the First Runs

CS2 - H1 (Relative Difference, %) (See Table 4.1)					
Total Reaction Force	1	2	3	4	5
F1SUM	-2,15	-2,13	-2,19	-2,19	-2,19
F12SUM	-0,97	-0,95	-1,01	-1,01	-1,01
F13SUM	-98,80	14,47	-3,28	0,98	-3,28
F2SUM	-2,22	-2,24	-2,28	-2,28	-2,28
F21SUM	-0,31	-0,31	-0,32	-0,32	-0,32
F23SUM	-95,05	87,89	13,59	13,60	13,59
F3SUM	-18,92	-18,91	-18,92	-18,92	-18,92
F31SUM	-100,0	50,02	-14,56	-3,19	-14,56
F32SUM	-99,99	77,16	0,47	0,47	0,47
Total Reaction Force	6	7	8	9	10
F1SUM	-1,85	-2,19	-2,19	-2,16	-2,19
F12SUM	-0,76	-1,01	-1,02	-0,98	-1,00
F13SUM	-3,21	0,98	6,81	6,82	14,45
F2SUM	-1,80	-2,28	-2,28	-2,26	-2,28
F21SUM	-0,24	-0,32	-0,32	-0,32	-0,32
F23SUM	13,61	13,60	4,74	4,74	87,77
F3SUM	-18,92	-18,92	-50,86	-50,86	-18,92
F31SUM	-14,54	-3,19	11,94	11,94	49,95
F32SUM	0,58	0,47	-14,17	-14,16	77,01

Table 5.4 The Relative difference between Honeycomb and Equivalent Models of CS3-H1 in the First Runs

CS3 - H1 (Relative Difference, %) (See Table 4.1)					
Total Reaction Force	1	2	3	4	5
F1SUM	-2,33	-2,40	-2,46	-2,46	-2,46
F12SUM	-0,94	-1,00	-1,05	-1,05	-1,05
F13SUM	-99,22	18,46	-4,05	0,33	-3,98
F2SUM	-3,05	-3,20	-3,24	-3,24	-3,24
F21SUM	-0,37	-0,39	-0,40	-0,41	-0,41
F23SUM	-96,25	90,89	-96,29	10,58	10,58
F3SUM	-18,14	-18,13	-18,14	-18,14	-18,14
F31SUM	-99,98	48,65	-11,29	-2,25	-11,16
F32SUM	-99,96	59,03	-100,0	-2,59	-2,59
Total Reaction Force	6	7	8	9	10
F1SUM	-1,58	-2,46	-2,46	-2,41	-2,43
F12SUM	-0,57	-1,05	-1,06	-1,02	-1,03
F13SUM	-3,80	0,33	7,43	7,44	18,45
F2SUM	-1,76	-3,24	-3,24	-3,21	-3,23
F21SUM	-0,21	-0,41	-0,41	-0,40	-0,40
F23SUM	10,62	10,58	-4,49	-4,49	90,89
F3SUM	-18,13	-18,14	-42,38	-42,38	-18,13
F31SUM	-11,08	-2,25	10,50	10,50	48,65
F32SUM	-2,35	-2,59	-21,25	-21,24	59,01

Table 5.5 The Relative difference between Honeycomb and Equivalent Models of CS4-H1 in the First Runs

CS4 - H1 (Relative Difference, %)					
Total Reaction Force	1	2	3	4	5
F1SUM	-1,92	-1,98	-2,12	-2,12	-2,12
F12SUM	-0,65	-0,71	-0,83	-0,83	-0,83
F13SUM	-99,44	27,71	-5,39	0,54	-5,39
F2SUM	-3,55	-3,69	-3,80	-3,80	-3,80
F21SUM	-0,29	-0,30	-0,35	-0,35	-0,35
F23SUM	-96,20	95,45	8,62	8,70	8,70
F3SUM	-17,21	-17,20	-17,21	-17,21	-17,21
F31SUM	-100,0	42,77	-10,67	-2,38	-10,67
F32SUM	-100,0	31,90	-7,81	-7,76	-7,76
Total Reaction Force	6	7	8	9	10
F1SUM	-0,99	-2,12	-2,12	-2,01	-2,06
F12SUM	-0,24	-0,83	-0,84	-0,74	-0,78
F13SUM	-5,17	0,54	15,86	15,88	27,69
F2SUM	-0,86	-3,80	-3,81	-3,73	-3,76
F21SUM	-0,07	-0,35	-0,35	-0,31	-0,32
F23SUM	8,78	8,70	-3,82	-3,81	95,44
F3SUM	-17,20	-17,21	-31,24	-31,24	-17,20
F31SUM	-10,53	-2,38	17,16	17,17	42,75
F32SUM	-7,47	-7,76	-21,13	-21,10	31,87

5.2 DISCUSSION ON THE FIRST RUNS:

A detailed investigation of the tabulated results of the first runs reveals that the errors of different equivalent models vary from 1% to 100%, which is an expected result as some of the coefficients are missing in some equivalent models. Therefore, the analyses depending on the missing coefficients ended up with very poor results. For instance, in Model 1 G_{13} , G_{23} values are missing. Therefore, relative difference of F13SUM, F31SUM, F23SUM and F32SUM are very high with respect to the reference model. (See Table 4.1) Of all the models, models 3, 4, 5, 6 and 7 seem to be most successful. What is surprising is that the error of F3SUM is unexpectedly high. This result depends on the modulus in the core height direction, E_3 . However, the derivation of E_3 is quite straightforward and almost universally agreed on (See Section 2.4.1). To find out the reason for the error on the total reaction force in the thickness direction of the honeycomb, material properties of the equivalent models are recalculated, and equivalent models are resolved but no change was found in the results. Since nothing wrong was found with the equivalent models, the reference models appear ambiguous because of this high rate of error. From sections 5.2.1 to 5.2.3 the reasons and the solutions for this problem will be explained.

5.2.1 CHECKING OF THE NUMERICAL RESULTS:

To check the validity of the numerical solutions, one of the equivalent beams is analyzed for the purpose of checking the accuracy of the calculation of the total reaction force in the thickness direction of the honeycomb structure. For the analysis the CS1-H1 beam is selected as the test case.

Finite element analysis performed by ANSYS gives that 18.16 Newton force is needed to displace the upper surface of the beam by -0.0001 mm. To check the validity of this result, the force needed is also calculated by using basic elasticity formulas.

$$\delta_{total} = 0.0001$$

Total displacement is the sum of the displacements of face sheets and the core:

$$\delta_{total} = \delta_{core} + 2.\delta_{face} \quad (5.1)$$

Using the basic formulas, the following calculations can be made as:

$$\delta_{core} = \varepsilon_{core} . h_{core}$$

$$\delta_{core} = \frac{F . h_{core}}{A . E_{core}} \quad (5.2)$$

$$\delta_{face} = \varepsilon_{face} . h_{face}$$

$$\delta_{face} = \frac{F . h_{face}}{A . E_{face}} \quad (5.3)$$

If we plug in Eq.5.2 and Eq.5.3 into Eq.5.1 we get;

$$F = \frac{\delta_{total}}{\left(\frac{h_{core}}{A . E_{core}} + 2 . \frac{h_{face}}{A . E_{face}} \right)} \quad (5.4)$$

where,

$$h_{core} = 15.875mm$$

$$h_{face} = 1mm$$

$$E_{core} = 3072MPa$$

$$E_{face} = 72000MPa$$

$$A = 942.85mm^2$$

When we plug in the necessary values into Eq. 5.4, the force needed to displace the upper surface of the beams is determined as 18.15 Newton. Table 5.6 gives the comparison of the finite element solution and solution by mechanics approach.

Table 5.6 Comparison of Calculations of ANSYS and Theory

	ANSYS	THEORY	DIFFERENCE	DIFFERENCE (%)
FORCE	18.16 N	18.15 N	0.01 N	% 0.055

This comparison shows that there is nothing wrong with the ANSYS solutions. It gives the same result with the theoretical calculation. Being sure about the calculation of the E_3 and the analyses, there is only one potential error source left; the reference model's itself! As mentioned in Section 3.2.2 in order to compensate the gap between the mid-plane of the face sheet and the HC core, the core height is increased as one face sheet thickness. However, the significant differences between the results of the total reaction force in the thickness direction of the honeycomb model and the equivalent models reveal that the shell-shell modeling approach of the facesheet and the honeycomb core walls may be the reason for the large discrepancy between the results.

5.2.2 RE-MODELING OF THE REFERENCE MODELS-1:

As an alternative approach, instead of filling the gap with the extended HC core, MPC184 rigid link element is used to join the corresponding nodes of face sheets to HC core. In Fig. 5.1 a unit cell with the MPC184 elements is shown.

The MPC184 element rigidly connects the two nodes, and with this element not only the displacements but also the rotations of the nodes are coupled. To check the effects of these changes, reference models are re-modeled and solved under the same conditions that are defined before. The core is at the exact height and the gap is $t/2$, i.e. the distance between the two nodes of the MPC184 element is half of the face sheet thickness. But the results obtained by the current modeling

approach also showed large differences in the total reaction force in the thickness direction (F3SUM) compared to the results of the equivalent models.

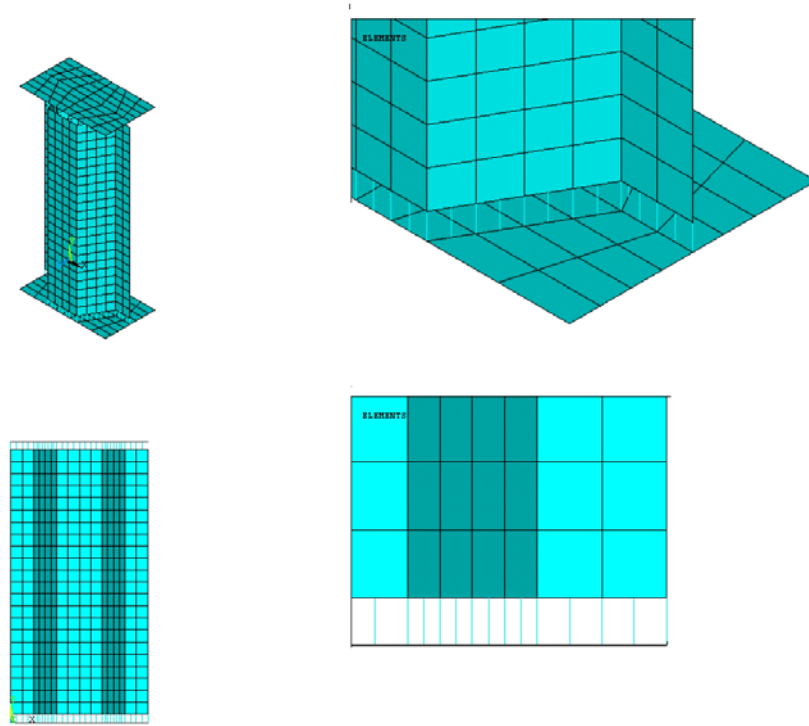


Figure 5.1 A unit cell with MPC184 elements

5.2.3 RE-MODELING THE REFERENCE MODELS - 2:

Having tried all the possible solutions to reduce the error in shell modeling, we have only one alternative left; re-modeling the reference models using mixed-modeling technique (See Section 3.1.3). All of the 16 reference models are re-modeled and analyzed. The results of these runs are accepted as the new reference values and they are compared to the results of the equivalent models.

5.3 DISCUSSION ON THE SECOND RUNS:

In this section, the relative differences of the equivalent models with respect to the second set of reference models are tabulated. But prior to that, the results of two different modeling techniques, namely shell modeling and mixed modeling are tabulated. In Table 5.7, comparison of the total reaction forces of the shell modeling and mixed modeling approaches are given. As the test case, CS1-H1 is selected as the beam used in the analyses. (See Appendix B for the other core heights)

Table 5.7 Comparison of the Total Reaction Forces- Shell Modeling and Mixed Modeling of the Honeycomb Structure for CS1-H1

CS1-H1 (h=15.875 mm)				
	Shell (N)	Solid (N)	Difference (N)	Difference (%)
F1SUM	5,72	5,69	0,03	-0,52
F12SUM	0,19	0,19	0	0,00
F13SUM	0,25	0,24	0,01	-4,00
F2SUM	40,48	40,34	0,14	-0,35
F21SUM	10,71	10,71	0	0,00
F23SUM	1,9	2,0	-0,1	5,26
F3SUM	22,04	18,21	3,83	-17,38
F31SUM	3,61	3,19	0,42	-11,63
F32SUM	1,72	1,63	0,09	-5,23

When comparing these two results, although there are only small variations in most of the values, F3SUM, F31SUM, F32SUM and F23SUM values changed to a great extent. The results of the revised reference models are much more

satisfactory. For instance, the result for the F3SUM of the mixed model is 18.21 N, and this result is very close to the result determined by the mechanics approach. Thus, the error in the F3SUM value drops to an acceptable limit. By this improvement, it can be claimed that the reference model has proved itself. Based on the studies that have been performed up to now, it can be concluded that the best way to model the HC core sandwich structures in detail is the “mixed modeling”. Thus, mixed model is accepted as the reference model to compare against the equivalent model. The comparison of the relative differences between the results of the mixed model and the equivalent models are tabulated in Table 5.8 through 5.11. The results given in Tables 5.8-5.11 are valid for a core height of 15.875mm. (See Appendix C for the other core heights)

Table 5.8 The Relative Difference between Mixed Honeycomb and Equivalent Models of CS1-H1 in the Second Runs

CS1 - H1 (h=15.875 mm)					
Total Reaction Force	1	2	3	4	5
F1SUM	-1,74	-0,95	-1,93	-1,93	-1,93
F12SUM	-0,47	-0,05	-0,65	-0,65	-0,65
F13SUM	-99,37	29,35	0,61	5,86	0,53
F2SUM	-3,43	-2,70	-3,70	-3,70	-3,70
F21SUM	-0,37	-0,27	-0,44	-0,44	-0,44
F23SUM	-96,80	84,60	4,45	4,45	4,45
F3SUM	-0,29	-0,27	-0,29	-0,29	-0,29
F31SUM	-99,98	64,67	0,83	10,42	0,70
F32SUM	-99,96	51,52	0,09	0,09	0,09
Total Reaction Force	6	7	8	9	10
F1SUM	-0,84	-1,93	-1,93	-1,68	-1,88
F12SUM	-0,08	-0,65	-0,66	-0,46	-0,60
F13SUM	0,84	5,86	17,46	17,52	29,07
F2SUM	-1,48	-3,70	-3,70	-3,51	-3,66
F21SUM	-0,19	-0,44	-0,44	-0,38	-0,41
F23SUM	4,50	4,45	-10,22	-10,21	84,51
F3SUM	-0,29	-0,29	-21,60	-21,60	-0,29
F31SUM	0,96	10,42	29,86	29,91	64,50
F32SUM	0,36	0,09	-17,60	-17,54	51,28

Table 5.9 The Difference between Mixed Honeycomb and Equivalent Models of CS2-H1 in the Second Runs

CS2 - H1 (h=15.875 mm)					
Total Reaction Force	1	2	3	4	5
F1SUM	-1,64	-1,63	-1,69	-1,69	-1,69
F12SUM	-0,58	-0,56	-0,61	-0,61	-0,61
F13SUM	-98,75	19,11	0,64	5,07	0,64
F2SUM	-2,04	-2,05	-2,10	-2,10	-2,10
F21SUM	-0,28	-0,27	-0,29	-0,29	-0,29
F23SUM	-95,25	80,38	9,05	9,05	9,05
F3SUM	-2,21	-2,20	-2,20	-2,20	-2,20
F31SUM	-100,0	71,80	-2,16	10,86	-2,16
F32SUM	-99,99	77,55	0,69	0,69	0,69
Total Reaction Force	6	7	8	9	10
F1SUM	-1,34	-1,69	-1,69	-1,65	-1,68
F12SUM	-0,36	-0,61	-0,62	-0,59	-0,61
F13SUM	0,71	5,07	11,14	11,15	19,08
F2SUM	-1,62	-2,10	-2,10	-2,07	-2,09
F21SUM	-0,20	-0,29	-0,29	-0,28	-0,28
F23SUM	9,07	9,05	0,55	0,55	80,26
F3SUM	-2,20	-2,20	-40,73	-40,73	-2,20
F31SUM	-2,13	10,86	28,19	28,19	71,71
F32SUM	0,80	0,69	-13,98	-13,98	77,40

Table 5.10 The Relative Difference between Mixed Honeycomb and Equivalent Models of CS3-H1 in the Second Runs

CS3-H1 (h=15.875 mm)					
Total Reaction Force	1	2	3	4	5
F1SUM	-1,77	-1,84	-1,90	-1,90	-1,90
F12SUM	-0,52	-0,58	-0,64	-0,64	-0,64
F13SUM	-99,19	24,41	0,78	5,37	0,84
F2SUM	-2,76	-2,91	-2,96	-2,96	-2,96
F21SUM	-0,34	-0,35	-0,37	-0,37	-0,37
F23SUM	-96,40	83,00	-96,44	6,01	6,01
F3SUM	-1,11	-1,10	-1,11	-1,11	-1,11
F31SUM	-99,98	68,40	0,49	10,74	0,64
F32SUM	-99,96	63,45	-100,00	0,12	0,12
Total Reaction Force	6	7	8	9	10
F1SUM	-1,01	-1,90	-1,90	-1,85	-1,88
F12SUM	-0,15	-0,64	-0,65	-0,60	-0,61
F13SUM	1,03	5,37	12,83	12,84	24,40
F2SUM	-1,47	-2,96	-2,96	-2,93	-2,94
F21SUM	-0,18	-0,37	-0,37	-0,36	-0,36
F23SUM	6,04	6,01	-8,44	-8,44	82,99
F3SUM	-1,11	-1,11	-30,39	-30,39	-1,11
F31SUM	0,73	10,74	25,17	25,18	68,39
F32SUM	0,37	0,12	-19,07	-19,05	63,43

Table 5.11 The Relative Difference between Mixed Honeycomb and Equivalent Models of CS4-H1 in the Second Runs

CS4 - H1 (h=15.875 mm)					
Total Reaction Force	1	2	3	4	5
F1SUM	-1,60	-1,66	-1,80	-1,80	-1,80
F12SUM	-0,32	-0,38	-0,50	-0,50	-0,50
F13SUM	-99,40	35,79	0,60	6,90	0,60
F2SUM	-4,40	-4,53	-4,65	-4,65	-4,65
F21SUM	-0,28	-0,29	-0,34	-0,34	-0,34
F23SUM	-96,37	86,86	3,84	3,92	3,92
F3SUM	3,27	3,27	3,27	3,27	3,27
F31SUM	-100,00	60,84	0,64	9,97	0,64
F32SUM	-100,00	42,80	-0,20	-0,14	-0,14
Total Reaction Force	6	7	8	9	10
F1SUM	-0,66	-1,80	-1,80	-1,69	-1,74
F12SUM	0,09	-0,50	-0,51	-0,41	-0,45
F13SUM	0,83	6,90	23,19	23,21	35,77
F2SUM	-1,72	-4,65	-4,65	-4,57	-4,60
F21SUM	-0,07	-0,34	-0,34	-0,30	-0,31
F23SUM	4,00	3,92	-8,05	-8,04	86,85
F3SUM	3,27	3,27	-14,2	-14,2	3,27
F31SUM	0,80	9,97	31,98	32,01	60,82
F32SUM	0,17	-0,14	-14,6	-14,5	42,77

5.4 DECISION ON THE EQUIVALENT MODEL:

Even though the results of the second runs seem to be satisfactory, there is still a need for the best model with the minimum relative difference between the results of the equivalent and the honeycomb model based on mixed modeling. For instance “Model 6” is very successful in F1SUM value but “Model 2” is better in F12SUM value, and so forth. In order to find a better equivalent model, four new models are generated based on the results of the ten models. The four new models are formed by picking the best performing values of the second set of runs based on mixed modeling of the honeycomb structure. The results of the second runs reveal that E_1 , E_3 , ν_{13} , ν_{23} and G_{23} can be picked easily from the existing models. On the other hand further investigation on the remaining constants is needed. Therefore, in generation of the new models, analyses are concentrated on these constants. The new models are numbered 11, 12, 13, and 14. In Table 5.12, the new models constants and where from they are taken is tabulated.

Table 5.12 New Candidate Models for the Third Runs

	11	12	13	14
E_1	Model 6			
E_2	Model 1	Model 2	Model 2	Model 2
E_3	Universally accepted			
ν_{13}	Model 5			
ν_{23}	Model 5			
ν_{12}	Model 1	Model 1	Model 1	0
G_{12}	0	Model 1	Model 1	Model 1
G_{23}	Model 7			
G_{13}	Model 7	Model 7	Model 6	Model 7

These four new models were also analyzed under the same boundary and loading conditions used in the previous analyses. The results are tabulated in Tables 5.12 to 5.15 for the core thickness of 15.875 mm. (See Appendix D for the remaining)

Table 5.13 The Relative Difference between the Honeycomb and Regenerated Equivalent Models of CS1-H1 in the Third Runs

CS1 - H1 (h=15.875 mm)				
Total Reaction Force	11	12	13	14
F1SUM	-0,57	-0,60	-0,61	-1,89
F12SUM	0,04	0,02	0,02	-0,61
F13SUM	6,22	6,23	0,93	5,87
F2SUM	-0,57	0,11	0,08	-3,66
F21SUM	-0,12	-0,05	-0,07	-0,41
F23SUM	4,52	4,53	4,53	4,45
F3SUM	-0,29	-0,29	-0,29	-0,29
F31SUM	10,58	10,58	0,98	10,43
F32SUM	0,41	0,44	0,44	0,10

Table 5.14 The Relative Difference between the Honeycomb and Regenerated Equivalent Models of CS2-H1 in the Third Runs

CS2 - H1 (h=15.875 mm)				
	11	12	13	14
F1SUM	-1,34	-1,42	-1,42	-1,68
F12SUM	-0,36	-0,41	-0,42	-0,61
F13SUM	7,43	5,13	1,59	5,07
F2SUM	-1,62	-1,67	-1,67	-2,09
F21SUM	-0,20	-0,21	-0,21	-0,28
F23SUM	9,07	9,07	9,07	9,05
F3SUM	-2,20	-2,20	-2,20	-2,20
F31SUM	18,48	10,89	0,34	10,86
F32SUM	0,80	0,78	0,78	0,69

Table 5.15 The Relative Difference between the Honeycomb and Regenerated Equivalent Models of CS3-H1 in the Third Runs

CS3 - H1 (h=15.875 mm)				
	11	12	13	14
F1SUM	-1,01	-1,13	-1,13	-1,88
F12SUM	-0,15	-0,21	-0,21	-0,62
F13SUM	5,57	5,55	1,00	5,37
F2SUM	-1,47	-1,45	-1,45	-2,94
F21SUM	-0,17	-0,16	-0,17	-0,36
F23SUM	6,04	6,04	6,04	6,01
F3SUM	-1,11	-1,11	-1,11	-1,11
F31SUM	10,83	10,82	0,73	10,74
F32SUM	0,37	0,36	0,36	0,12

Table 5.16 The Relative Difference between the Honeycomb and Regenerated Equivalent Models of CS4-H1 in the Third Runs

CS4 - H1 (h=15.875 mm)				
	11	12	13	14
F1SUM	-0,66	-0,70	-0,70	-1,76
F12SUM	0,09	0,08	0,08	-0,47
F13SUM	7,17	7,17	0,84	6,90
F2SUM	-1,70	-1,09	-1,12	-4,60
F21SUM	-0,06	0,00	0,00	-0,31
F23SUM	4,00	4,00	4,01	3,92
F3SUM	3,27	3,27	3,27	3,27
F31SUM	10,14	10,14	0,80	9,98
F32SUM	0,17	0,20	0,20	-0,13

Compared with the results of the final runs, Model 13 has the best overall performance. Still, in some values, other models are likely to give better results. On a whole, however, none perform as well as Model 13. Therefore, in this study model 13 has been selected as the equivalent model to be used in modeling the honeycomb core structure.

5.5 EQUIVALENT MODEL COEFFICIENTS:

In this section the relations for the elastic coefficients of the best performing equivalent model (Model 13) are tabulated. This model is the major output of this thesis study. In table 5.16 the material coefficients of the Model 13 and the related reference can be found.

Table 5.17 The Material Coefficients Of The Model 13

MATERIAL PROPERTY	
$E_1 = \frac{E}{\cos \varphi} \left[\frac{\cos^2 \varphi \cdot a^3}{t^3} + \frac{(2 + \sin^2 \varphi)t}{a} \right]$	Masters [22]
$E_2 = \frac{t^3 \cdot \cos \varphi}{(1 + \sin \varphi) \cdot a^3 \sin^2 \varphi \cdot (1 - \nu^2)} E$	Nast [30]
$E_3 = \frac{2 \cdot E}{(\cos \varphi \cdot (1 + \sin \varphi))} \cdot \frac{t}{a}$	Universally Agreed On
$\nu_{12} = 3 \cdot \tan^2(\varphi) \text{ or } \nu_{12} \leq \sqrt{\frac{E_1}{E_2}}$	Masters [22]
$\nu_{23} = 0$	Ashby [29]
$\nu_{13} = 0$	Ashby [29]
$G_{12} = \frac{E}{\frac{3 \cdot \cos \varphi}{(1 + \sin \varphi)} \cdot \frac{a^3}{t^3} + [\cos \varphi + a \cdot \tan \varphi \cdot (1 + \sin \varphi)]} \cdot \frac{a}{t}$	Masters [22]
$G_{13} = \frac{1 + \sin \varphi}{2 \cdot \cos \varphi} \cdot \frac{t}{a} \cdot G$	Grediac [25]
$G_{23} = \frac{\cos \varphi}{1 + \sin \varphi} \cdot \frac{t}{a} \cdot G$	Grediac [25]

5.6 COMPARISON OF REFERENCE AND EQUIVALENT MODELS:

As mentioned previously, the main goal in developing an equivalent model is to reduce the pre-processor time, computation time, and hardware requirements. In this section a comparison will be made between the models in this manner. In Table 5.17, reference and equivalent models for CS1-H1 are compared in terms of number of elements and nodes used, solution time, and hardware requirements. “Time to solve” is an approximate value estimated by ANSYS. These figures are for a single load case. The computer used for these analyses is an ordinary PC with AMD Athlon 2500XP+ processor and 512 MB DDR-RAM. Variations by a factor of about two in either direction are possible for the solution time. Experience shows that in general the real solving time is longer than the estimated one

Table 5.18 Comparison Of Reference and Equivalent Models

	Reference	Equivalent
Number of Elements	14016	4000
Number Of Nodes	60484	4862
Time to solve (sec)	147	2.67
Memory Requirement (MB)	1120	273
Output File Size (MB)	761	36

The importance and the success of equivalent modeling are apparent in Table 5.17. “Time to solve the model” can be reduced approximately 55 times. Memory requirement drops to quarter of the original requirement and also the out-files occupy about 20 times less space on hard disc than the reference model. It is important to note that the beam analyzed has only 24 cells. For a real case application, say a sandwich wing with HC core, there are about 5000 – 10.000 cells. For such a case, the equivalent model may reduce the time spent for a single analysis roughly speaking from 1 month to only 12 hours. In fact,

solving for a 5000-10.000 cell model is practically impossible on a regular PC. Neither a hard disk nor RAM will be sufficient for such analyses. A cluster of workstations, which is expensive and hard to maintain, will be needed.

Another important aspect of this simplified geometry is its suitability to ANSYS Parametric Design Language (APDL). APDL is a scripting language that you can use to automate common tasks or even build your model in terms of parameters (variables) [32]. It is much easier to reproduce the equivalent model in APDL. By using APDL it is possible to write down a batch file that makes ANSYS find solutions to successive analyses with different parameters (different orthotropic material properties for instance). Furthermore, the proper use of APDL with equivalent model will be bound to reduce the pre-processor time.

CHAPTER 6

TEST CASE

In this chapter, a test case study is performed. It is important to note that; the aim in this chapter is neither designing and optimizing a wing nor performing an aero-elastic analysis study. The purpose is just to demonstrate an application of an equivalent HC model.

The wing chosen for the analyses is Tomahawk cruise missile. Tomahawk is a long-range subsonic cruise missile for attacking land targets. It is 5.56 meters long and the wing span is 2.67 meters. Its speed is around 880 km/h and it is approximately 1190 kg. The wing data is taken from “Structural Optimization of a Composite Wing” study [35]. In her study, she investigated the structural optimization of a cruise missile wing for the aerodynamic loads for four different flight conditions. The flight conditions correspond to the corner points of the V-n diagram [35]. In this test case, the wing is subjected to the load case corresponding to the corner A in Fig. 6.1.

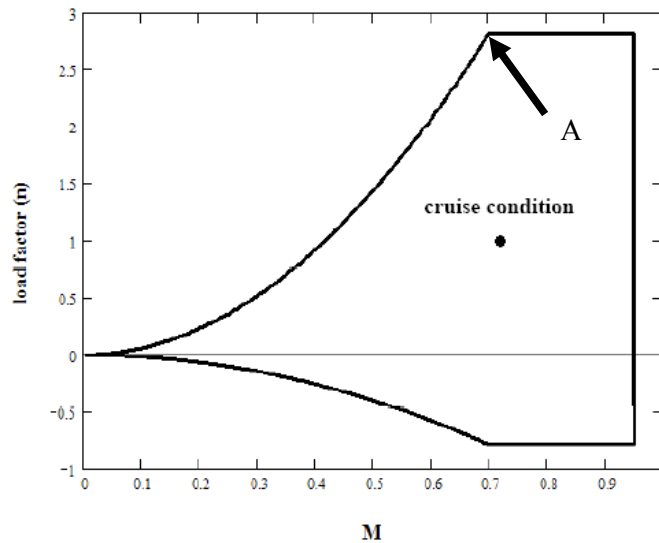


Figure 6.1 V-n Diagram for the Tomahawk Cruise Missile [35]

For this loading case, the forces and the moments acting on the wing is given in Table 6.1 [35]

Table 6.1 Forces and Moments Acting On the Wing

F_x (N)	F_y (N)	F_z (N)	M_x (N.mm)	M_y (N.mm)	M_z (N.mm)
-874	15680	-1420	-8918555	-147549	3123262

6.1 MODELING & ANALYSES OF THE WING:

The wing is modeled in NX 4.0. First, a single piece solid wing is modeled. This model is also used as a base for the sandwich wing. It is quite common to place solid supports on the leading edge, trailing edge, wing root, and the wing tip. The dimensions of these parts are selected randomly. The mid-section of the wing is surrounded by these four pieces, then divided into three; as the upper face sheet, the lower face sheet and the core. Upon this preparation, it is

imported to ANSYS. Fig. 6.2 is the exploded view of the wing; the green part is the core section and the dark grey parts are the aluminum parts.

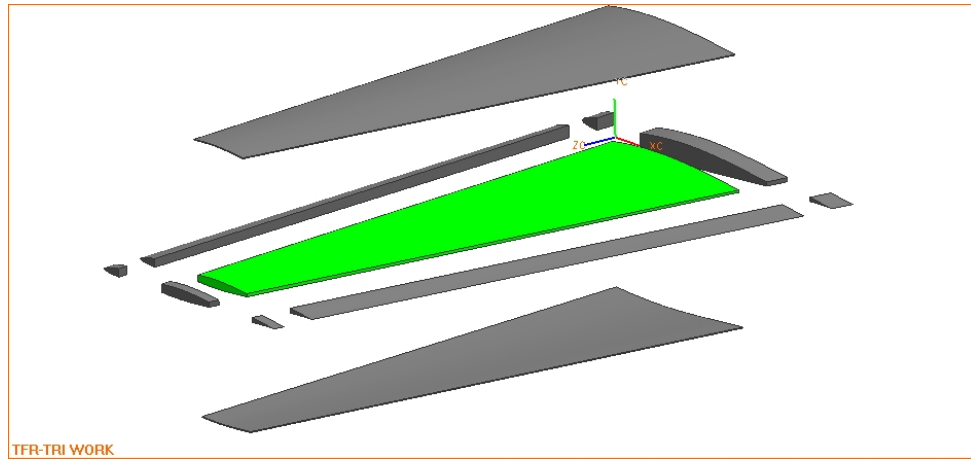


Figure 6.2 Exploded View of The Wing

The core is modeled as a bulk material. In the analyses, SOLID186 element is used. The face sheets and the support parts are added to each other to have a single volume, prior to meshing the core is merged to this structure. Then, just in the case of equivalent sandwich beam meshing, both volumes are meshed with SOLID186 element.

Flight at 0.7 Mach and at 7 degrees of positive angle of attack condition is considered. The aerodynamic loads are computed using “Fluent” commercial program and the loads are imported in the form of tables into ANSYS [35]. To import the pressure values into ANSYS following command is used:

```
“PARRES,CHANGE,'pressure_values'”
```

With PARRES command, ANSYS reads parameters from a file. “CHANGE” modifier, replaces any parameter set that already exists. The ‘pressure_values’ is the name of the file to read.

There are three pressure areas: the upper surface, the lower surface and the tip surface of the wing. The wing material is aluminum and for the core, 5/32 inch cell size and 0.0025 inch foil thickness HC is used, HC material is AA 5052 (See Table 3.1) The sandwich wing's material properties are calculated by the formulas given in Table 5.16. In Fig.6.3, the meshed wing and in Fig 6.4 a closer view of the pressure distribution can be seen.

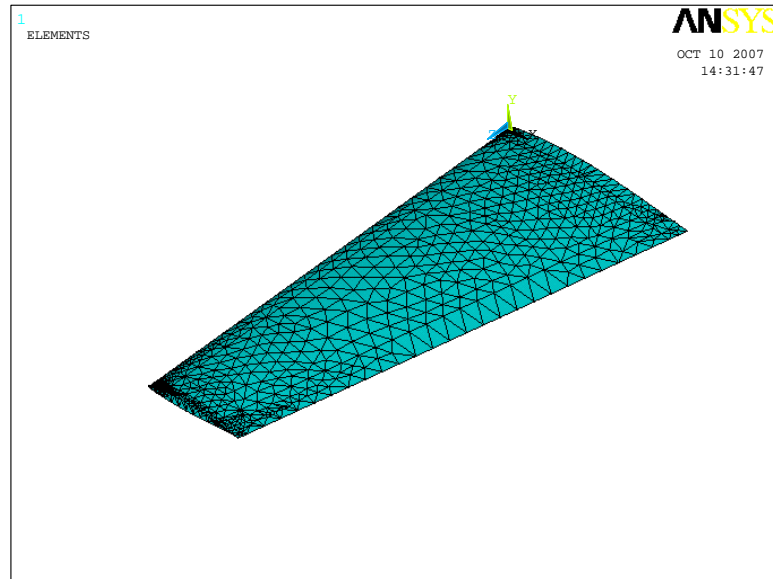


Figure 6.3 Meshed Wing

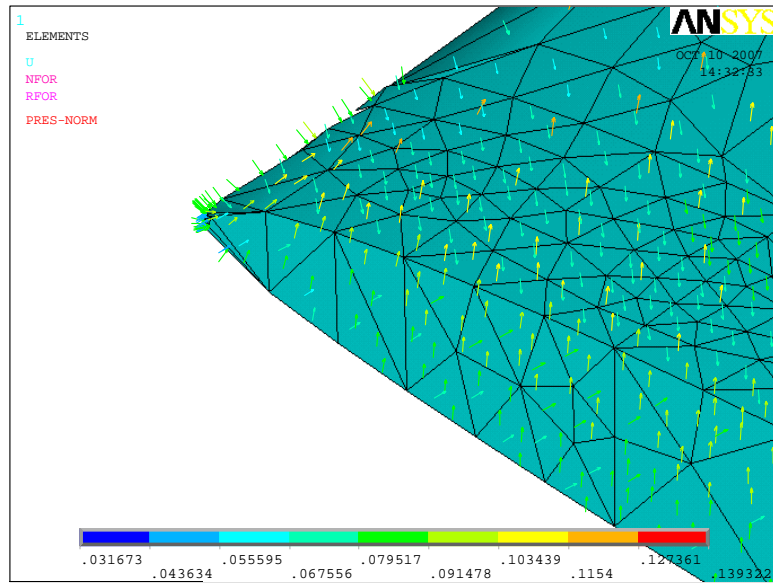


Figure 6.4 Pressure Distribution Over The Wing

6.2 RESULTS:

6.2.1 Weight:

Weight saving is one of the most important issues in sandwich beams; in our test case for comparison purposes two wings are considered. One is a solid wing made up of AA 7075 T6 (See Table 6.2 for material properties) . The other one is the sandwich wing made of honeycomb core as described above. The weight comparison of both wings is given below:

- i. 34.5 kg.; for the AA 7075 T6 solid wing
- ii. 13.6 kg.; for the sandwich wing

Table 6.2 Mechanical Properties of AA-7075 [36]

Density	2.8 gr/kg ³
Poisson's Ratio	0.33
Young's Modulus	72 GPa
Tensile Strength	570 MPa
Yield Strength	505 MPa
Elongation	%11
Shear Strength	330 MPa

The difference is approximately 21 kg. The sandwich wing is 39% of the aluminum wing. In other words, by using this sandwich wing 61% of the wing weight is saved. If we consider the whole missile; with a total of 42 kg. weight reduction, it results in 3.5% lighter missile.

6.2.2 Displacements & Stresses:

The displacement field of the wings can be seen in Fig. 6.2 and Fig. 6.3. and maximum deflections are compared in Table 6.3i As expected, the sandwich wing deforms almost twice as much as the aluminum one. The displacements (and the weight) may be reduced to a certain extent by performing these studies.

Table 6.3 Maximum Deflections for the Solid and the Sandwich Wing

	Maximum Deflection
SOLID WING	38 mm.
SANDWICH WING	80 mm.

It is the designers responsibility to decide whether or not the maximum deflection of the sandwich wing is acceptable. If the deflection is above the limits, there are various ways to reduce it. Changing the HC core, adding a spar

to the wing or increasing the skin thickness are three of the possible solutions. To see the effects of these modifications, three additional analyses are performed. In “Wing Alternative 1”, core is changed. Instead of the original core, a core with half cell size and triple foil thickness of the original one is used. This increased the core density 6 times. In “Wing Alternative 2” an aluminum spar with 10 mm thickness is added to the wing. The spar is located on the mid-chord-plane of the wing. Finally, in “Wing Alternative 3” the skin thickness is increased to 6 mm. The deflections and the weights of these together with the original solid wing and the original sandwich wing are given in Table 6.4 (See Appendix E). Results show that it is possible to reduce the deflections with a little weight penalty.

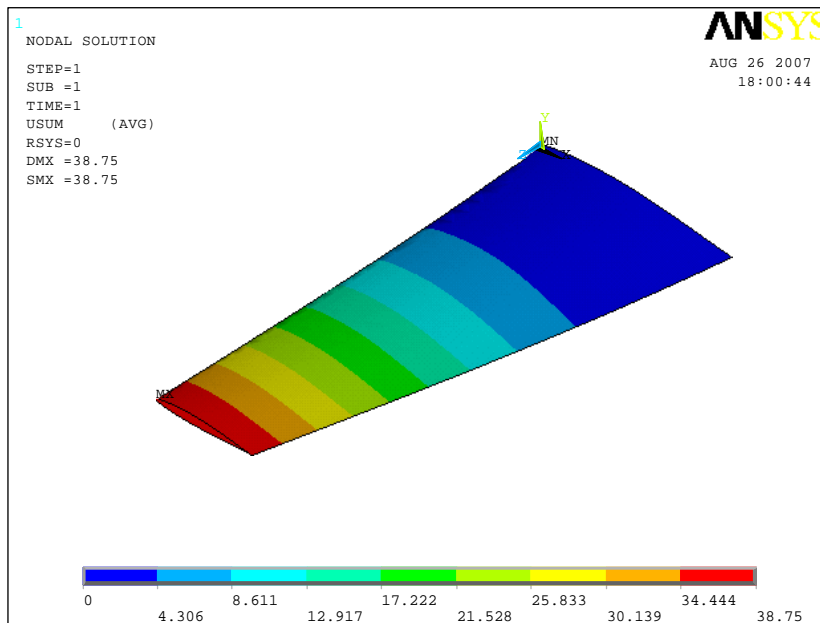


Figure 6.5 Displacement of Solid Wing

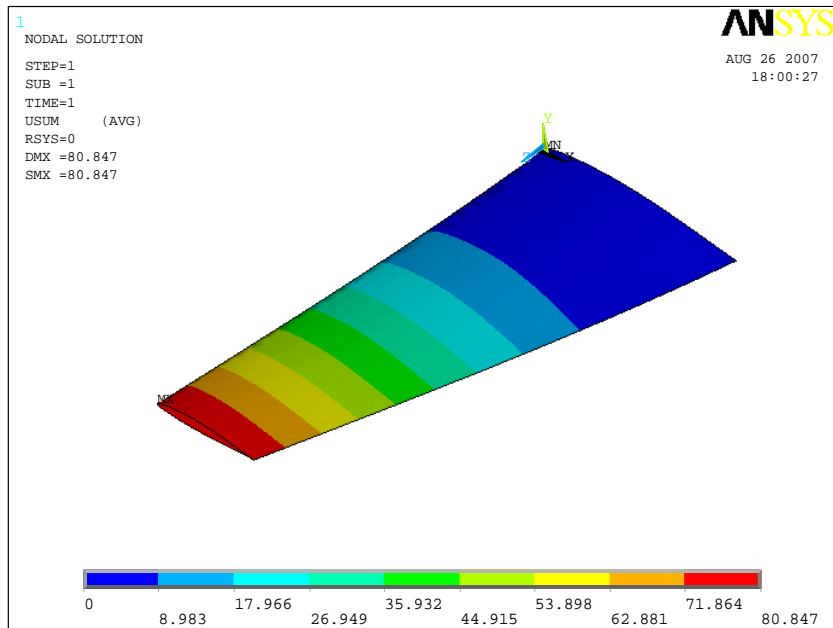


Figure 6.6 Displacement of Sandwich Wing

Table 6.4 Comparison of Wing Alternatives

	Maximum Deflection (mm.)	Weight (kg.)
Solid Wing	38	34.5
Sandwich Wing	80	13.6
Wing Alternative 1	68	18.8
Wing Alternative 2	65	14.2
Wing Alternative 3	43	21

From the stress point of view, the difference between these two structures is more obvious; from Fig. 6.7 to Fig. 6.12 different views of the von Misses stress distributions of the wings are given. If the stress distribution of the sandwich wing is considered (Fig 6.8), the stress contours are similar in fashion with the

solid one, but the order of magnitudes differ. This is the natural result of the sandwich construction; as seen in Fig 6.10 and Fig. 6.12, the core is almost stress free and the face sheets bear most of the load. Maximum von Misses Stresses for both wings are given in Table 6.5.

Table 6.5 Maximum Stress Values for the Solid and the Sandwich Wing

	Maximum Stress, Von Misses
SOLID WING	103 MPa
SANDWICH WING	236 MPa

Although the maximum stress in the sandwich wing is relatively high, it has still positive margin of safety. It is important to note that the stresses in sandwich wing are global, i.e, local stresses and any problems related to these local stresses can not be figured out by the equivalent model. In Table 6.6, margin of safety for both wings are tabulated. Obviously, the solid wing has a greater positive margin of safety but it is heavier, on the contrary the sandwich wing is less “safer” whereas it is lighter. This is another figure of merit that should be considered by the designer.

Table 6.6 Margin of Safety of the Solid and the Sandwich Wing

	Margin Of Safety
SOLID WING	3.9
SANDWICH WING	1.15

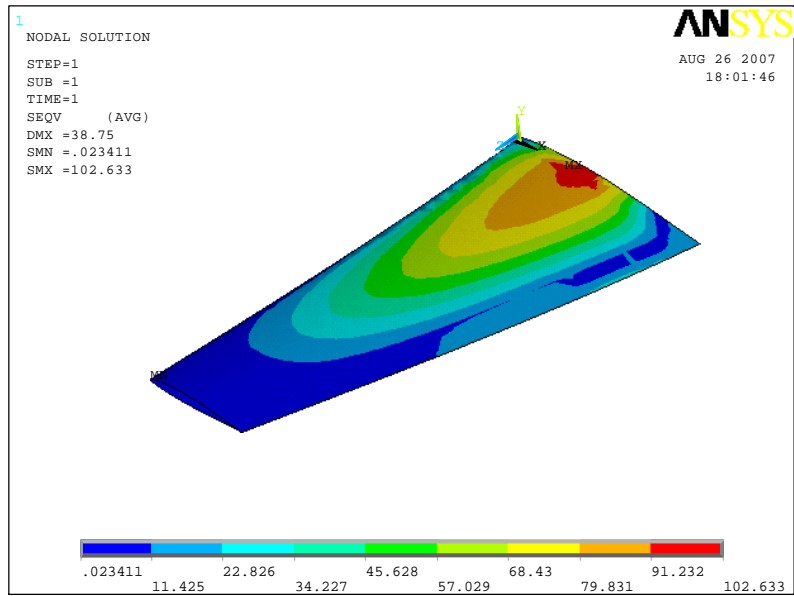


Figure 6.7 Solid Wing Stress Distribution

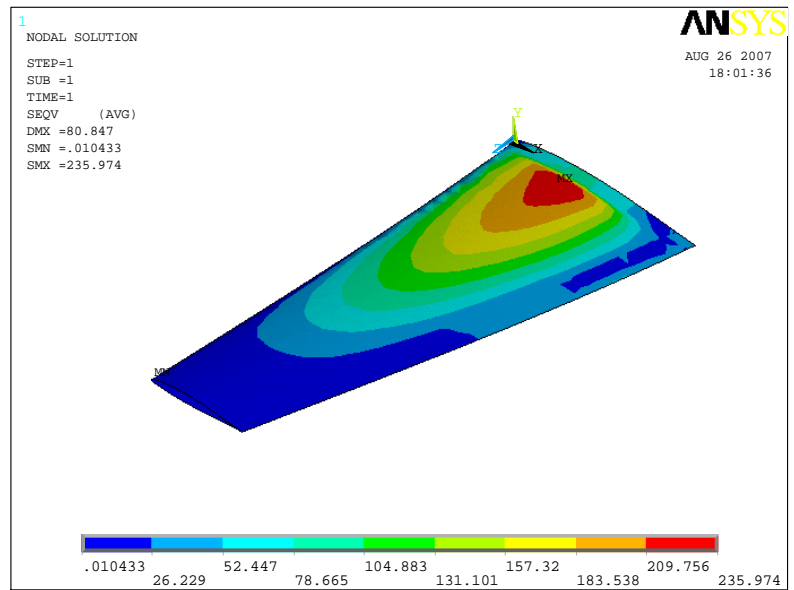


Figure 6.8 Sandwich Wing Stress Distribution

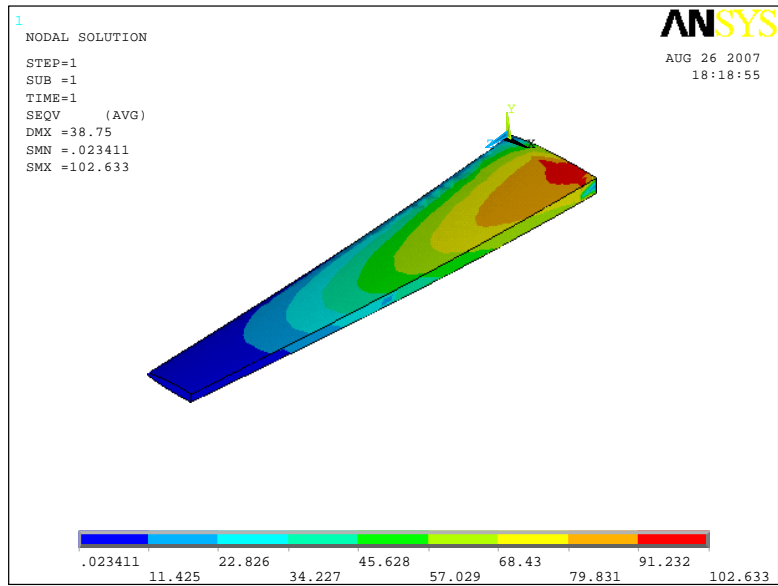


Figure 6.9 Solid Wing Stress Distribution, Longitudinal Cut

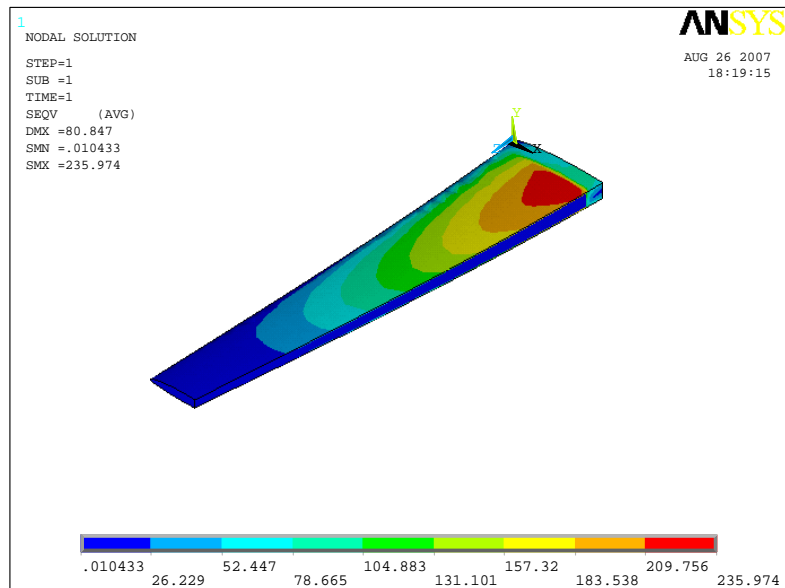


Figure 6.10 Sandwich Wing, Stress Distribution, Longitudinal Cut

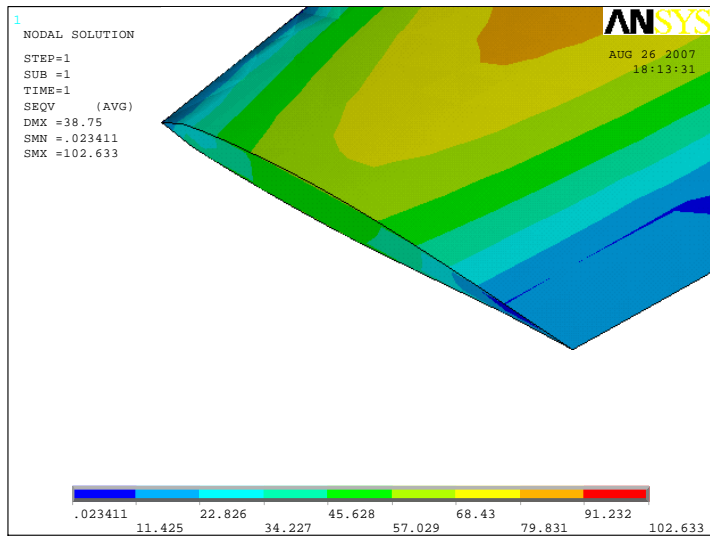


Figure 6.11 Solid Wing, Stress Distribution, Transverse Cut

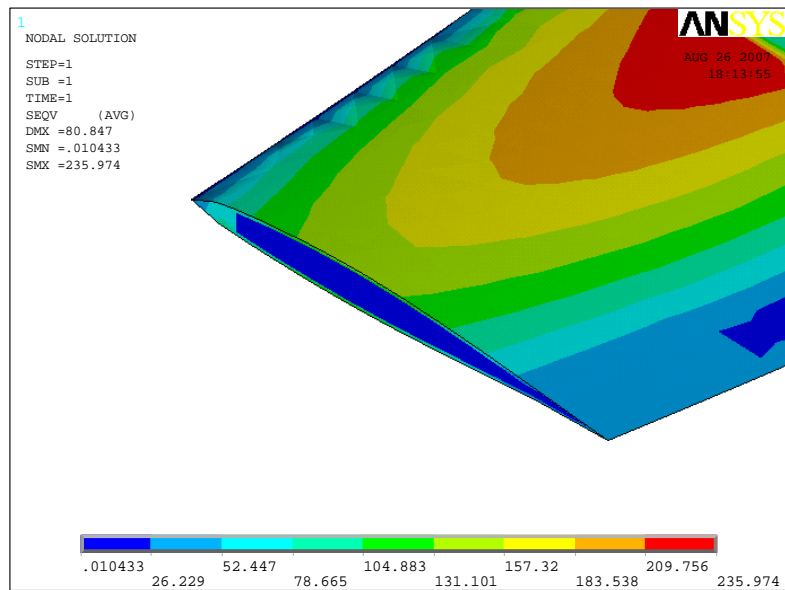


Figure 6.12 Sandwich Wing, Stress Distribution, Transverse Cut

First three modal frequencies of the wings also calculated, the frequencies are tabulated in Table 6.7. First two modes of the both models are first bending and

second bending, whereas the third modes are the torsion modes. In first two modes, the sandwich beam's frequencies are greater than the aluminum one, whereas in the third mode, the aluminum wing's frequency is greater. Again these frequencies also may be reduced / increased by changing the parameters of the sandwich wing. For instance, changing the skin thickness affects the natural frequencies. The first three natural frequencies of the "Wing Alternative 3" is 25.11 Hz., 106.86 Hz. and 175.80 Hz. These results show that by changing the parameters of the wing the natural frequencies can be modified.

The higher modal frequencies of the sandwich are mainly due to the weight / weight distribution of the two wings. Because, the sandwich model has lower weight which tends to increase the frequencies. To cross-check this, a hypothetical solid wing, weighting same as the sandwich wing, is put through modal analyses. The hypothetical solid wing's modal frequencies are higher than the sandwich wing, which supports the idea above. (The first three frequencies of the hypothetical wing is: 40.8 Hz., 171.3 Hz. and 291.1 Hz.) To decide the favorable frequencies of the wing(s), a flutter analyses should be performed. Without the flutter analyses it is not possible to eliminate on the wings from natural frequency point of view.

Table 6.7 First Three Modal Frequencies

Mode	Solid Model (Hz.)	Sandwich Model (Hz.)
1-Bending	24.86	25.35
2-Bending	104.28	114.16
3-Torsion	177.15	152.62

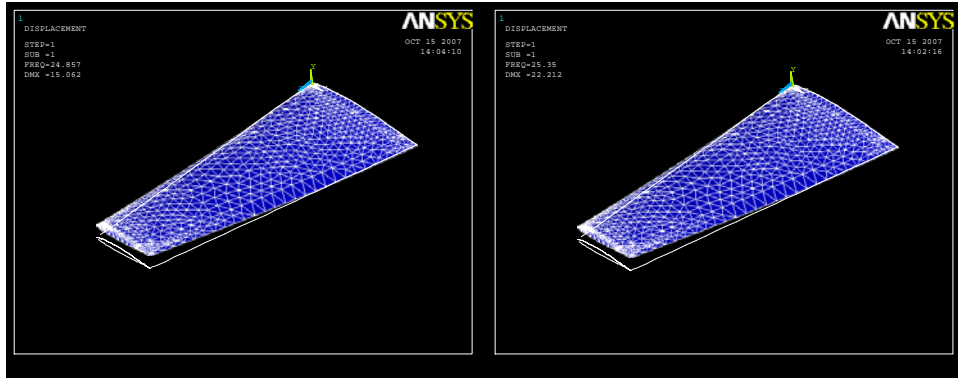


Figure 6.13 Deformation of The Solid and The Sandwich Wing, Mode 1, Bending

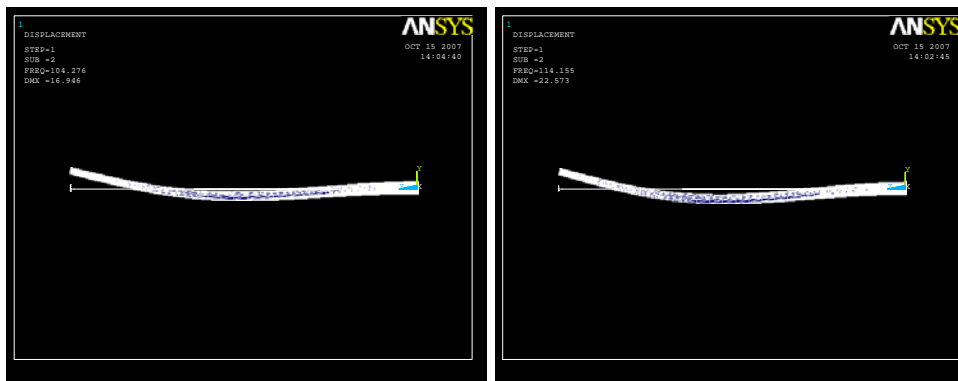


Figure 6.14 Deformation of The Solid and The Sandwich Wing, Mode 2, Bending

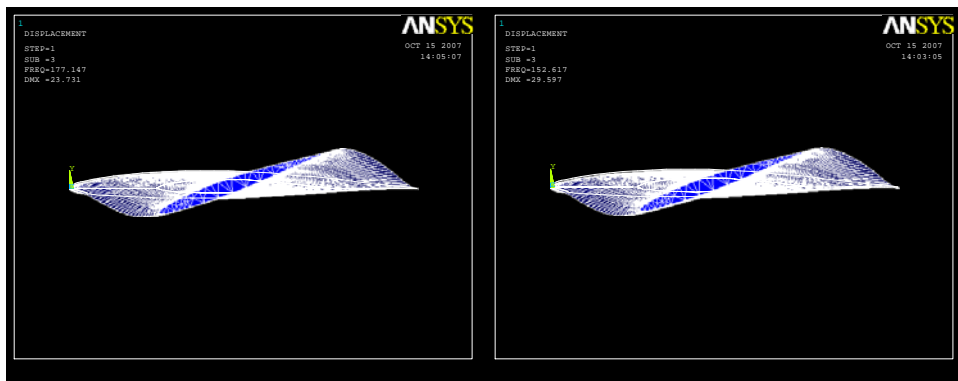


Figure 6.15 Deformation of The Solid and The Sandwich Wing, Mode 3, Torsion

To sum up, in this test case study, two wings are analyzed. The goal is to demonstrate that sandwich construction is capable of fulfilling the expectations. In addition to that, another goal is to show the ease of using the equivalent model in a real structure's analysis. The results obtained reveal that both goals are achieved.

CHAPTER 7

CONCLUDING REMARKS AND FUTURE WORK

In this thesis, the design and analyses of the HC sandwich structures are investigated. The main aim is to combine different equivalent models studied in the literature, thus coming up with a set of orthotropic material properties which will represent the actual honeycomb core material most accurately. The actual honeycomb structure is then analyzed by the finite element program “ANSYS”, which is used as a reference model to contrast with the equivalent model. The use of the equivalent model gives the following advantages in the design and analysis phase:

- A proper geometric substitution for the detailed model decreasing the effort in the computer aided design substantially
- Good overall performance in all loading cases
- Reduced pre-processor time
- Reduced solving time
- Fewer hardware requirements
- Easily modified

Beginning from the basics of the sandwich theory, different equivalent models on the HC material properties are investigated. The proposed material properties are tested under various loading conditions in the ANSYS environment. The load cases involve in-plane and out of plane loading including the shear loads. The results are analyzed, and based on the experience gained from the first analyses, second and third runs are performed to get the best performing equivalent model. Numerous analyses show that it is not a reliable method to

model the HC sandwiches using shell elements for the face sheets. Although in some loading cases, for instance in plane loading cases, shell modeling of the face sheets gives reasonable results. It is deemed that modeling the face sheets in 3D solid elements suits all loading cases well. The “Mixed modeling” approach, in which honeycomb core walls are meshed with shell elements and face sheets are modeled with solid elements, is used as the reference model of the HC sandwich structure. Thus, equivalent models are compared one by one with the corresponding solution of the reference model. Depending on these detailed analyses, an equivalent model is proposed. The proposed model combines the orthotropic elastic constants of various equivalent models in such a way that for all combinations of in-plane and out of plane loading of the honeycomb structure, the differences between the total reaction forces calculated by the equivalent model and the actual honeycomb model are all within 10%. The numerical examples also show that the use of equivalent model reduces significantly not only the solving time but also the hardware requirements.

The use of honeycomb structures in various engineering applications is rapidly increasing due to the excellent stiffness and weight advantages. In aerospace engineering, honeycomb structures are up to the increasing applications in various sub-structures of the air vehicles. Especially, in case of the missile systems the use of honeycomb structure in the fins is widespread. Chapter 6 presents a typical application on the use of the equivalent model on the structural analysis of a fin of a missile. It would be impossible to analyze such a fin structure with the actual honeycomb model based on mixed shell-solid modeling approach, on a normal workstation. A cluster of workstations, which is expensive and hard to maintain, would be needed to analyze the fin if the true geometry of the honeycomb structure is preserved. The advantage of using equivalent models becomes more eminent in such fin example.

Some caution is needed with regard to the use of equivalent models in analyzing the structures made of honeycomb material. Such equivalent models can be used with sufficient accuracy in representing the true stiffness of the structure. Thus, modal analyses, deflection analyses or aero-elastic analyses of honeycomb structures can be performed with reasonable accuracy by using the equivalent models. However, as for the stress analysis, the equivalent models can give information only about the global magnitude of the stress occurring in the honeycomb structure. Because the core geometry is destroyed in equivalent modeling, the actual stress levels in the core structure will be lost. However, stresses in the face sheets can be approximated with reasonable accuracy. Therefore, it is estimated that such equivalent models can be used for global stress analyses, and during the design phase the thicknesses of the core and the face sheets should be determined based on the analyses performed by the equivalent models. In addition, in case the face sheets are made of composite material, the structural analyses performed by the equivalent models may be used to decide on the fiber orientations of the layers in the face sheets.

It is concluded that the equivalent model proposed in this thesis is likely to be used as a fast, low cost, easily modified and adapted tool for preliminary design stages.

Like in any other scientific studies, the work is not finished yet. There is still a need for further studies. For future work the possible work items to be studied are as follows:

- Experimental validation of the equivalent model
- Expanding the analyses to different face sheet materials, such as e-glass/epoxy
- Investigating the effects of composite HC
- Validation of face sheet stresses based on equivalent and honeycomb modeling by using a small size honeycomb structure

- A thorough study of the modeling efforts on the equivalent modeling of the honeycomb structure in the literature, and search for other equivalent models which will perform better than the current model
- Theoretical study by the use of unit cell approach to come up with an equivalent model, and verification of the equivalent model by the finite element method performed on the unit cell
- Determination of the equivalent orthotropic constants of the honeycomb structure based on pure finite element analysis
- Aero-elastic analyzes of the wing geometry proposed in the Chapter 6.

The list of future works can be increased. However, of all the future work to be done, it is deemed that verification of the studied equivalent model by experiment seems to be the most urgent one to be accomplished

REFERENCES

- [1] UGS Corp. Web Site, [http://www.ugs.com /products/nx/](http://www.ugs.com/products/nx/), Last accessed date October 2007

- [2] Sanjay K.M., “Composites Manufacturing”, CRC Press, 2002

- [3] Robert M.J., “Mechanics of Composite Materials”, Hemisphere Publishing Corp., 1975

- [4] Tsai S.W., Hoa S.V., Gay D., “Composite Materials” CRC Press, 2003

- [5] Advanced Composites Web Site, www.advancedcomposites.com/technology, Last accessed date June 2007

- [6] Marshall A., “Sandwich Construction”, Handbook of Composites, Van Nostrand Reinhold Co., 1982, p. 557-601

- [7] VMC Web Site, <http://www.virtualmuseum.ca>, Last accessed date October 2007

- [8] Engin M.R., Rizkalla S.H., “Material Characteristics of 3-D FRP Sandwich Panels”

- [9] Cellular Solids Research Group Web Site, <http://web.mit.edu/dmse/csg>, Last accessed date October 2007

- [10] Niu M., “Airframe Stress Analysis and Sizing”, Adaso Adastr Engineering Center, 1998

- [11] Allen H.G., “Analysis and Design of Sandwich Panels”, Pergamon Press, 1969

- [12] Burton W.S., Noor A.K., “Assessment of Continuum Models for Sandwich Panel Honeycomb Cores”, *Comput. Methods Appl. Mech. Engrg.*, Vol. 145, 1997, pp 341 – 360
- [13] DIAB Group, “DIAB Sandwich Handbook”,
http://www.diabgroup.com/americas/u_literature/, Last accessed date October 2007
- [14] HEXCEL Corp. Web Site, <http://www.hexcel.com/Markets/>, Last accessed date October 2007
- [15] Global Spec Web Site, <http://www.globalspec.com>, Last accessed date October 2007
- [16] Corex Corp. Web Site, <http://www.corex-honeycomb.com>, Last accessed date October 2007
- [17] Paneltech Int. Corp. Web Site, <http://www.paneltech.biz>, Last accessed date October 2007
- [18] Piedmont Plastics Inc. Web Site,
<http://www.piedmontplastics.com>, Last accessed date October 2007
- [19] Paik J.K., Thayamballi A.K., Kim G.S., “The Strength Characteristics of Aluminum Honeycomb Sandwich Panels”, *Thin Walled Structures*, Vol. 35, 1999, pp 205-231
- [20] Hexcel Corp., “Honeycomb Attributes and Properties Handbook”
- [21] Ochoa O. O., Reddy J. N., “Finite Element Analysis of Composite Laminates”, Kluwer Academic Publishers, 1992
- [22] Masters I. G., Evans K. E., “Models for the Elastic Deformation of Honeycombs”, *Composite Structures*, Vol. 35, 1996, pp 403 – 422

- [23] Liu Q, Zhao Y., “Effect of Soft Honeycomb Core on Flexural Vibration of Sandwich Panel using Low Order and High Order Shear Deformation Models”, *Journal of Sandwich Structures and Materials*, Vol. 9, 2007, pp 95 - 108
- [24] Abd-el-Sayed F., Burgess I.W., Jones R., “A Theoretical Approach to the Deformation of Honeycomb-Based Composite Materials”, *Composites*, 1979, pp 209-214.
- [25] Grediac M., “A Finite Element Study of the Transverse Shear in Honeycomb Cores”, *Int. J. Solids Structures*, Vol. 30, 1993, pp 1777 – 1788
- [26] Shi G., Tong P., “Equivalent Transverse Shear Stiffness of Honeycomb Cores”, *Int. J. Solids Structures*, Vol. 32, 1995, pp 1383 – 1393
- [27] Kelsey S., Gellatly R. A., Clark B. W., “The Shear Modulus of Foil Honeycomb Cores”, *Aircraft Engng.*, Vol. 30, 1958, pp 294 – 302
- [28] Becker W., “Closed Form Analysis of the Thickness Effect of Regular Honeycomb Core Material”, *Composite Structures*, Vol. 48, 2000, pp 67 – 70
- [29] Zhang J., Ashby M. F., “The Out-of- Plane Properties of Honeycombs” *Int. J. Mech. Sci.*, Vol. 34, No. 6, 1992, pp 475 – 489
- [30] Nast E. “On Honeycomb-Type Core Moduli”, *AIAA/ASME/AHS Adaptive Structures Forum*, Kissimmee, FL, Apr. 7-10, 1997, Collection of Technical Papers, Pt. 2 (A97-24112 05-39)
- [31] Zienkiewicz O. C., “Finite Element Method”, 5th edition, Butterworth-Heinemann, 2000
- [32] ANSYS Online Help Documentation, ANSYS Inc.

- [33] eFUNDA Web Site,
<http://www.efunda.com/materials/alloys/aluminum> , Last accessed date
October 2007
- [34] SAE, AMS-C-7438, “Core Material, Aluminum, For Sandwich
Construction”, 1999
- [35] Sökmen Ö, “Structural Optimization of a Composite Wing”,
Middle East Technical University, 2006
- [36] MatWeb Web Site, <http://www.matweb.com/>, Last accessed date October
2007

APPENDIX A

Table A.1 The Relative Difference between the Honeycomb and
Regenerated Equivalent Models of CS1-H2 in the First Runs (h=7.938)

CS1 – H2 (Relative Difference, %) (See Table 4.1)					
Total Reaction Force	1	2	3	4	5
F1SUM	-2,21	-1,69	-2,31	-2,31	-2,31
F12SUM	-1,00	-0,63	-1,10	-1,10	-1,10
F13SUM	-98,43	15,37	-1,57	1,76	-1,62
F2SUM	-2,25	-1,87	-2,41	-2,41	-2,41
F21SUM	-0,36	-0,29	-0,39	-0,39	-0,39
F23SUM	-93,51	89,38	15,41	15,41	15,41
F3SUM	-14,62	-14,60	-14,62	-14,62	-14,62
F31SUM	-99,98	55,39	-8,42	0,90	-8,55
F32SUM	-99,97	81,56	4,74	4,74	4,74
Total Reaction Force	6	7	8	9	10
F1SUM	-1,48	-2,31	-2,31	-2,17	-2,28
F12SUM	-0,58	-1,10	-1,10	-0,98	-1,07
F13SUM	-1,42	1,76	8,73	8,75	15,23
F2SUM	-1,16	-2,41	-2,41	-2,31	-2,39
F21SUM	-0,21	-0,39	-0,39	-0,37	-0,38
F23SUM	15,44	15,41	0,83	0,84	89,33
F3SUM	-14,62	-14,62	-32,80	-32,80	-14,61
F31SUM	-8,36	0,90	22,82	22,84	55,32
F32SUM	4,94	4,74	-12,63	-12,60	81,35

Table A.2 The Relative Difference between the Honeycomb and Regenerated Equivalent Models of CS2-H2 in the First Runs (h=7.938)

CS2 – H2 (Relative Difference, %) (See Table 4.1)					
Total Reaction Force	1	2	3	4	5
F1SUM	-1,70	-1,69	-1,72	-1,72	-1,72
F12SUM	-0,89	-0,88	-0,91	-0,91	-0,91
F13SUM	-96,42	11,38	1,13	3,71	1,13
F2SUM	-1,21	-1,22	-1,25	-1,25	-1,25
F21SUM	-0,24	-0,23	-0,24	-0,24	-0,24
F23SUM	-89,67	81,96	22,07	22,08	22,07
F3SUM	-15,51	-15,50	-15,50	-15,50	-15,50
F31SUM	-100,0	52,31	-14,72	-3,04	-14,72
F32SUM	-99,99	103,55	8,92	8,92	8,92
Total Reaction Force	6	7	8	9	10
F1SUM	-1,53	-1,72	-1,72	-1,70	-1,71
F12SUM	-0,75	-0,91	-0,92	-0,90	-0,91
F13SUM	1,17	3,71	7,10	7,11	11,37
F2SUM	-1,00	-1,25	-1,25	-1,23	-1,24
F21SUM	-0,19	-0,24	-0,24	-0,24	-0,24
F23SUM	22,08	22,08	14,26	14,26	81,86
F3SUM	-15,50	-15,50	-48,75	-48,75	-15,50
F31SUM	-14,71	-3,04	14,71	14,71	52,24
F32SUM	8,97	8,92	-4,00	-3,99	103,38

Table A.3 The Relative Difference between the Honeycomb and Regenerated Equivalent Models of CS3-H2 in the First Runs (h=7.938)

CS3 – H2 (Relative Difference, %) (See Table 4.1)					
Total Reaction Force	1	2	3	4	5
F1SUM	-1,94	-1,98	-2,02	-2,01	-2,01
F12SUM	-0,96	-1,00	-1,03	-1,02	-1,02
F13SUM	-97,65	24,54	9,57	12,71	9,67
F2SUM	-1,62	-1,73	-1,75	-1,75	-1,75
F21SUM	-0,30	-0,31	-0,32	-0,32	-0,32
F23SUM	-92,02	98,97	-92,07	25,59	25,58
F3SUM	-19,87	-19,86	-19,87	-19,86	-19,86
F31SUM	-99,98	44,72	-15,95	-6,92	-15,76
F32SUM	-99,97	80,16	-100,0	-0,07	-0,07
Total Reaction Force	6	7	8	9	10
F1SUM	-1,44	-2,01	-2,02	-1,44	-2,00
F12SUM	-0,62	-1,02	-1,03	-0,62	-1,01
F13SUM	9,79	12,71	17,52	9,79	24,53
F2SUM	-0,95	-1,75	-1,75	-0,95	-1,74
F21SUM	-0,19	-0,32	-0,32	-0,19	-0,31
F23SUM	25,61	25,59	10,58	25,61	98,97
F3SUM	-19,86	-19,86	-43,54	-19,86	-19,86
F31SUM	-15,72	-6,92	8,10	-15,72	44,72
F32SUM	0,06	-0,07	-17,28	0,06	80,15

Table A.4 The Relative Difference between the Honeycomb and Regenerated Equivalent Models of CS4-H2 in the First Runs (h=7.938)

CS4 – H2 (Relative Difference, %) (See Table 4.1)					
Total Reaction Force	1	2	3	4	5
F1SUM	-2,20	-2,22	-2,29	-2,29	-2,29
F12SUM	-1,02	-1,04	-1,11	-1,11	-1,11
F13SUM	-98,49	26,93	3,81	8,28	3,81
F2SUM	-2,14	-2,21	-2,27	-2,27	-2,27
F21SUM	-0,25	-0,26	-0,28	-0,28	-0,28
F23SUM	-92,38	106,08	21,86	21,95	21,95
F3SUM	-32,24	-32,23	-32,24	-32,23	-32,24
F31SUM	-100,0	32,42	-21,25	-13,26	-21,25
F32SUM	-100,0	56,51	-6,57	-6,50	-6,50
Total Reaction Force	6	7	8	9	10
F1SUM	-1,26	-2,29	-2,29	-2,24	-2,27
F12SUM	-0,55	-1,11	-1,11	-1,06	-1,08
F13SUM	3,99	8,28	19,15	19,16	26,92
F2SUM	-0,51	-2,27	-2,27	-2,23	-2,25
F21SUM	-0,06	-0,28	-0,29	-0,27	-0,27
F23SUM	21,99	21,95	9,11	9,11	106,07
F3SUM	-32,23	-32,23	-43,67	-43,67	-32,23
F31SUM	-21,18	-13,26	8,61	8,61	32,41
F32SUM	-6,27	-6,50	-19,15	-19,14	56,50

Table A.5 The Relative Difference between the Honeycomb and Regenerated Equivalent Models of CS1-H3 in the First Runs (h=21.813)

CS1 – H3 (Relative Difference, %) (See Table 4.1)					
Total Reaction Force	1	2	3	4	5
F1SUM	-2,02	-1,22	-2,31	-2,31	-2,31
F12SUM	-81,28	-81,21	-81,33	-81,33	-81,33
F13SUM	-98,34	501,19	340,67	368,65	340,27
F2SUM	-2,02	-1,00	-2,41	-2,41	-2,41
F21SUM	967,34	968,53	966,34	966,34	966,34
F23SUM	-93,62	446,90	199,88	199,88	199,88
F3SUM	-71,36	-71,36	-71,36	-71,36	-71,36
F31SUM	-99,96	198,52	91,86	108,54	91,63
F32SUM	-99,96	8,77	-19,47	-19,47	-19,47
Total Reaction Force	6	7	8	9	10
F1SUM	-1,23	-2,31	-2,31	-1,97	-2,23
F12SUM	-81,21	-81,33	-81,33	-81,28	-81,31
F13SUM	341,79	368,65	432,61	432,93	499,57
F2SUM	0,57	-2,41	-2,41	-2,13	-2,35
F21SUM	969,20	966,34	966,32	967,15	966,80
F23SUM	200,09	199,88	156,05	156,11	446,56
F3SUM	-71,36	-71,36	-77,49	-77,49	-71,36
F31SUM	92,16	108,54	135,10	135,22	198,12
F32SUM	-19,25	-19,47	-34,47	-34,41	8,61

Table A.6 The Relative Difference between the Honeycomb and Regenerated Equivalent Models of CS2-H3 in the First Runs (h=21.813)

CS2 – H3 (Relative Difference, %) (See Table 4.1)					
Total Reaction Force	1	2	3	4	5
F1SUM	-2,34	-2,31	-2,40	-2,40	-2,40
F12SUM	-0,95	-0,92	-1,00	-1,00	-1,00
F13SUM	-99,35	18,22	-5,39	0,05	-5,39
F2SUM	-3,09	-3,11	-3,18	-3,18	-3,18
F21SUM	-0,35	-0,35	-0,37	-0,37	-0,37
F23SUM	-96,76	90,74	10,10	10,10	10,10
F3SUM	-19,63	-19,62	-19,63	-19,63	-19,63
F31SUM	-100,0	47,22	-14,53	-3,51	-14,53
F32SUM	-99,99	58,57	-3,77	-3,77	-3,77
Total Reaction Force	6	7	8	9	10
F1SUM	-1,93	-2,40	-2,40	-2,35	-2,39
F12SUM	-0,70	-1,00	-1,01	-0,96	-0,99
F13SUM	-5,31	0,05	7,73	7,74	18,18
F2SUM	-2,49	-3,18	-3,18	-3,14	-3,17
F21SUM	-0,26	-0,37	-0,37	-0,36	-0,36
F23SUM	10,12	10,10	0,85	0,85	90,60
F3SUM	-19,63	-19,63	-51,31	-51,31	-19,63
F31SUM	-14,48	-3,51	8,74	8,75	47,14
F32SUM	-3,61	-3,77	-20,85	-20,83	58,44

Table A.7 The Relative Difference between the Honeycomb and Regenerated Equivalent Models of CS3-H3 in the First Runs (h=21.813)

CS3 – H3 (Relative Difference, %) (See Table 4.1)					
Total Reaction Force	1	2	3	4	5
F1SUM	-2,29	-2,38	-2,47	-2,47	-2,47
F12SUM	-0,86	-0,96	-1,03	-1,03	-1,03
F13SUM	-99,57	19,62	-8,50	-3,29	-8,44
F2SUM	-4,10	-4,29	-4,36	-4,36	-4,36
F21SUM	-0,39	-0,42	-0,44	-0,44	-0,44
F23SUM	-97,54	88,77	-97,58	5,41	5,41
F3SUM	-17,17	-17,16	-17,17	-17,17	-17,17
F31SUM	-99,98	46,20	-9,86	-1,19	-9,74
F32SUM	-99,95	40,53	-100,0	-4,82	-4,82
Total Reaction Force	6	7	8	9	10
F1SUM	-1,50	-2,47	-2,47	-1,50	-2,44
F12SUM	-0,53	-1,03	-1,05	-0,53	-1,00
F13SUM	-8,24	-3,29	5,44	-8,24	19,61
F2SUM	-2,33	-4,36	-4,36	-2,33	-4,34
F21SUM	-0,22	-0,44	-0,45	-0,22	-0,43
F23SUM	5,46	5,41	-9,68	5,46	88,76
F3SUM	-17,17	-17,17	-41,72	-17,17	-17,17
F31SUM	-9,63	-1,19	8,13	-9,63	46,19
F32SUM	-4,55	-4,82	-24,98	-4,55	40,51

Table A.8 The Relative Difference between the Honeycomb and Regenerated Equivalent Models of CS1-H3 in the First Runs (h=21.813)

CS4 – H3 (Relative Difference, %) (See Table 4.1)					
Total Reaction Force	1	2	3	4	5
F1SUM	-2,09	-2,19	-2,38	-2,38	-2,38
F12SUM	-0,84	-0,95	-1,12	-1,12	-1,12
F13SUM	-99,68	24,64	-12,85	-6,44	-12,85
F2SUM	-4,47	-4,68	-4,84	-4,84	-4,84
F21SUM	-0,30	-0,33	-0,39	-0,39	-0,39
F23SUM	-97,46	91,86	3,85	3,94	3,94
F3SUM	-30,24	-30,24	-30,24	-30,24	-30,24
F31SUM	-100,0	25,26	-16,62	-9,77	-16,62
F32SUM	-100,0	4,72	-17,98	-17,94	-17,94
Total Reaction Force	6	7	8	9	10
F1SUM	-1,29	-2,38	-2,38	-2,22	-2,29
F12SUM	-0,47	-1,12	-1,13	-0,99	-1,04
F13SUM	-12,65	-6,44	10,73	10,76	24,61
F2SUM	-1,24	-4,84	-4,84	-4,73	-4,78
F21SUM	-0,11	-0,39	-0,39	-0,34	-0,35
F23SUM	4,03	3,94	-8,46	-8,44	91,84
F3SUM	-30,24	-30,24	-42,08	-42,08	-30,24
F31SUM	-16,48	-9,77	2,93	2,96	25,23
F32SUM	-17,70	-17,94	-30,44	-30,41	4,70

Table A.9 The Relative Difference between the Honeycomb and Regenerated Equivalent Models of CS1-H4 in the First Runs (h=31.750)

CS1 – H4 (Relative Difference, %) (See Table 4.1)					
Total Reaction Force	1	2	3	4	5
F1SUM	-2,05	-1,36	-2,44	-2,44	-2,44
F12SUM	-0,73	-0,40	-1,10	-1,10	-1,10
F13SUM	-99,75	31,42	-7,55	-0,97	-7,64
F2SUM	-5,17	-4,00	-5,67	-5,67	-5,67
F21SUM	-0,41	-0,30	-0,54	-0,54	-0,54
F23SUM	-98,28	94,71	4,89	4,89	4,89
F3SUM	-18,80	-18,79	-18,80	-18,80	-18,80
F31SUM	-99,98	27,97	-13,28	-6,53	-13,37
F32SUM	-99,94	6,42	-14,62	-14,62	-14,62
Total Reaction Force	6	7	8	9	10
F1SUM	-1,38	-2,44	-2,44	-2,05	-2,33
F12SUM	-0,44	-1,10	-1,12	-0,82	-0,99
F13SUM	-7,32	-0,97	14,41	14,49	31,04
F2SUM	-2,33	-5,67	-5,68	-5,32	-5,59
F21SUM	-0,26	-0,54	-0,54	-0,44	-0,48
F23SUM	4,97	4,89	-10,78	-10,75	94,58
F3SUM	-18,80	-18,80	-36,19	-36,18	-18,80
F31SUM	-13,14	-6,53	0,71	0,77	27,80
F32SUM	-14,42	-14,62	-31,13	-31,07	6,28

Table A.10 The Relative Difference between the Honeycomb and Regenerated Equivalent Models of CS2-H4 in the First Runs (h=31.750)

CS2 – H4 (Relative Difference, %) (See Table 4.1)					
Total Reaction Force	1	2	3	4	5
F1SUM	-2,35	-2,31	-2,43	-2,43	-2,43
F12SUM	-0,91	-0,88	-0,98	-0,98	-0,98
F13SUM	-99,58	21,49	-6,80	-0,48	-6,80
F2SUM	-3,82	-3,84	-3,93	-3,93	-3,93
F21SUM	-0,37	-0,36	-0,39	-0,39	-0,39
F23SUM	-97,59	92,31	8,07	8,07	8,07
F3SUM	-19,81	-19,81	-19,81	-19,81	-19,81
F31SUM	-100,0	43,74	-14,71	-4,10	-14,71
F32SUM	-99,99	43,12	-6,95	-6,95	-6,95
Total Reaction Force	6	7	8	9	10
F1SUM	-1,89	-2,43	-2,43	-2,36	-2,42
F12SUM	-0,66	-0,98	-0,99	-0,94	-0,97
F13SUM	-6,70	-0,48	8,64	8,66	21,44
F2SUM	-3,05	-3,93	-3,93	-3,88	-3,92
F21SUM	-0,26	-0,39	-0,39	-0,37	-0,38
F23SUM	8,10	8,07	-1,38	-1,38	92,15
F3SUM	-19,81	-19,81	-51,43	-51,42	-19,81
F31SUM	-14,64	-4,10	4,97	4,98	43,66
F32SUM	-6,76	-6,95	-26,42	-26,40	43,01

Table A.11 The Relative Difference between the Honeycomb and Regenerated Equivalent Models of CS3-H4 in the First Runs (h=31.750)

CS3 – H4 (Relative Difference, %) (See Table 4.1)					
Total Reaction Force	1	2	3	4	5
F1SUM	-2,16	-2,29	-2,40	-2,40	-2,40
F12SUM	-0,80	-0,92	-1,03	-1,03	-1,03
F13SUM	-99,70	21,68	-10,73	-4,93	-10,67
F2SUM	-4,80	-5,03	-5,12	-5,12	-5,12
F21SUM	-0,38	-0,42	-0,44	-0,45	-0,45
F23SUM	-98,16	87,83	-98,20	2,70	2,70
F3SUM	-16,61	-16,61	-16,61	-16,61	-16,61
F31SUM	-99,98	41,85	-9,20	-1,06	-9,10
F32SUM	-99,94	27,04	-99,99	-6,40	-6,40
Total Reaction Force	6	7	8	9	10
F1SUM	-1,45	-2,40	-2,40	-1,45	-2,36
F12SUM	-0,50	-1,03	-1,04	-0,50	-0,98
F13SUM	-10,47	-4,93	5,01	-10,47	21,67
F2SUM	-2,65	-5,12	-5,12	-2,65	-5,09
F21SUM	-0,21	-0,45	-0,45	-0,21	-0,43
F23SUM	2,77	2,70	-12,39	2,77	87,82
F3SUM	-16,61	-16,61	-41,34	-16,61	-16,61
F31SUM	-8,97	-1,06	4,35	-8,97	41,83
F32SUM	-6,15	-6,40	-27,87	-6,15	27,01

Table A.12 The Relative Difference between the Honeycomb and Regenerated Equivalent Models of CS4-H4 in the First Runs (h=31.750)

CS4 – H4 (Relative Difference, %) (See Table 4.1)					
Total Reaction Force	1	2	3	4	5
F1SUM	-1,98	-2,13	-2,37	-2,37	-2,37
F12SUM	-0,76	-0,92	-1,13	-1,13	-1,13
F13SUM	-99,78	26,35	-14,93	-8,09	-14,93
F2SUM	-4,69	-4,96	-5,18	-5,18	-5,18
F21SUM	-0,29	-0,34	-0,42	-0,42	-0,42
F23SUM	-98,09	90,28	1,46	1,55	1,55
F3SUM	-29,95	-29,95	-29,95	-29,95	-29,95
F31SUM	-100,0	17,10	-17,02	-11,14	-17,02
F32SUM	-99,99	-5,61	-20,59	-20,57	-20,57
Total Reaction Force	6	7	8	9	10
F1SUM	-1,27	-2,37	-2,37	-2,17	-2,26
F12SUM	-0,42	-1,13	-1,14	-0,96	-1,02
F13SUM	-14,75	-8,09	10,70	10,72	26,33
F2SUM	-1,30	-5,18	-5,18	-5,03	-5,09
F21SUM	-0,13	-0,42	-0,42	-0,35	-0,36
F23SUM	1,64	1,55	-10,80	-10,78	90,26
F3SUM	-29,95	-29,95	-41,84	-41,84	-29,95
F31SUM	-16,89	-11,14	-3,63	-3,59	17,07
F32SUM	-20,38	-20,57	-33,06	-33,03	-5,63

APPENDIX B

Table B.1 Comparison of the Total Reaction Forces- Shell Modeling and Mixed Modeling of the Honeycomb Structure for CS2-H1

CS2-H1 (h=15.875 mm)				
	Shell (N)	Solid (N)	Difference (N)	Difference (%)
F1SUM (N)	5,702	5,673	0,029	-0,52
F12SUM (N)	0,189	0,188	0,001	-0,40
F13SUM (N)	0,084	0,081	0,003	-3,89
F2SUM (N)	39,740	39,665	0,075	-0,19
F21SUM (N)	10,696	10,692	0,004	-0,04
F23SUM (N)	0,864	0,900	-0,036	4,17
F3SUM (N)	44,899	37,226	7,673	-17,09
F31SUM (N)	8,212	7,171	1,041	-12,67
F32SUM (N)	4,310	4,300	0,009	-0,22

Table B.2 Comparison of the Total Reaction Forces- Shell Modeling and Mixed Modeling of the Honeycomb Structure for CS3-H1

CS3-H1 (h=15.875 mm)				
	Shell (N)	Solid (N)	Difference (N)	Difference (%)
F1SUM (N)	5,718	5,685	0,032	-0,57
F12SUM (N)	0,189	0,188	0,001	-0,42
F13SUM (N)	0,163	0,155	0,008	-4,78
F2SUM (N)	40,139	40,021	0,118	-0,29
F21SUM (N)	10,706	10,702	0,004	-0,04
F23SUM (N)	1,377	1,437	-0,059	4,31
F3SUM (N)	29,612	24,513	5,099	-17,22
F31SUM (N)	5,115	4,515	0,600	-11,72
F32SUM (N)	2,588	2,518	0,070	-2,70

Table B.3 Comparison of the Total Reaction Forces- Shell Modeling and Mixed Modeling of the Honeycomb Structure for CS4-H1

CS4-H1 (h=15.875 mm)				
	Shell (N)	Solid (N)	Difference (N)	Difference (%)
F1SUM (N)	5,698	5,680	0,018	-0,32
F12SUM (N)	0,188	0,188	0,001	-0,33
F13SUM (N)	0,301	0,283	0,018	-5,95
F2SUM (N)	40,384	40,740	-0,356	0,88
F21SUM (N)	10,701	10,700	0,001	-0,01
F23SUM (N)	1,969	2,060	-0,091	4,60
F3SUM (N)	15,241	12,219	3,022	-19,83
F31SUM (N)	2,390	2,121	0,269	-11,24
F32SUM (N)	1,078	0,996	0,082	-7,63

Table B.4 Comparison of the Total Reaction Forces- Shell Modeling and Mixed Modeling of the Honeycomb Structure for CS1-H2

CS1-H2 (h=7.938 mm)				
	Shell (N)	Solid (N)	Difference (N)	Difference (%)
F1SUM (N)	5,709	5,675	0,034	-0,60
F12SUM (N)	0,189	0,188	0,001	-0,41
F13SUM (N)	0,094	0,091	0,003	-3,05
F2SUM (N)	39,803	39,692	0,111	-0,28
F21SUM (N)	10,705	10,702	0,003	-0,03
F23SUM (N)	0,972	0,972	0,001	-0,05
F3SUM (N)	42,340	36,023	6,317	-14,92
F31SUM (N)	7,777	7,009	0,769	-9,88
F32SUM (N)	4,060	4,183	-0,123	3,04

Table B.5 Comparison of the Total Reaction Forces- Shell Modeling and Mixed Modeling of the Honeycomb Structure for CS2-H2

CS2-H2 (h=7.938 mm)				
	Shell (N)	Solid (N)	Difference (N)	Difference (%)
F1SUM (N)	5,674	5,647	0,028	-0,49
F12SUM (N)	0,188	0,188	0,001	-0,37
F13SUM (N)	0,028	0,027	0,001	-1,98
F2SUM (N)	39,323	39,260	0,063	-0,16
F21SUM (N)	10,687	10,684	0,003	-0,03
F23SUM (N)	0,413	0,443	-0,029	7,08
F3SUM (N)	85,973	73,312	12,661	-14,73
F31SUM (N)	17,237	15,016	2,221	-12,89
F32SUM (N)	8,871	9,416	-0,545	6,14

Table B.6 Comparison of the Total Reaction Forces- Shell Modeling and Mixed Modeling of the Honeycomb Structure for CS3-H2

CS3-H2 (h=7.938 mm)				
	Shell (N)	Solid (N)	Difference (N)	Difference (%)
F1SUM (N)	5,692	5,663	0,029	-0,51
F12SUM (N)	0,189	0,188	0,001	-0,39
F13SUM (N)	0,052	0,056	-0,004	7,44
F2SUM (N)	39,530	39,482	0,048	-0,12
F21SUM (N)	10,696	10,693	0,003	-0,03
F23SUM (N)	0,644	0,737	-0,094	14,56
F3SUM (N)	60,293	48,453	11,840	-19,64
F31SUM (N)	11,606	9,663	1,943	-16,74
F32SUM (N)	6,062	5,942	0,120	-1,97

Table B.7 Comparison of the Total Reaction Forces- Shell Modeling and Mixed Modeling of the Honeycomb Structure for CS4-H2

CS4-H2 (h=7.938 mm)				
	Shell (N)	Solid (N)	Difference (N)	Difference (%)
F1SUM (N)	5,709	5,665	0,044	-0,77
F12SUM (N)	0,189	0,188	0,001	-0,53
F13SUM (N)	0,111	0,114	-0,003	2,46
F2SUM (N)	39,750	39,747	0,003	-0,01
F21SUM (N)	10,694	10,694	0,000	0,00
F23SUM (N)	0,978	1,124	-0,146	14,90
F3SUM (N)	37,069	25,125	11,944	-32,22
F31SUM (N)	6,146	4,779	1,367	-22,24
F32SUM (N)	2,989	2,764	0,225	-7,54

Table B.8 Comparison of the Total Reaction Forces- Shell Modeling and Mixed Modeling of the Honeycomb Structure for CS1-H3

CS1-H3 (h=21.813 mm)				
	Shell (N)	Solid (N)	Difference (N)	Difference (%)
F1SUM (N)	5,72	5,682	0,026	-0,60
F12SUM (N)	0,41	0,188	0,001	-0,41
F13SUM (N)	0,19	0,412	-0,301	-3,05
F2SUM (N)	12,18	40,764	-1,014	-0,28
F21SUM (N)	1,91	10,714	-0,020	-0,03
F23SUM (N)	0,81	2,904	-1,926	-0,05
F3SUM (N)	47,91	12,148	24,921	-14,92
F31SUM (N)	11,89	1,909	4,238	-9,88
F32SUM (N)	2,82	0,809	2,181	3,04

Table B.9 Comparison of the Total Reaction Forces- Shell Modeling and Mixed Modeling of the Honeycomb Structure for CS2-H3

CS2-H3 (h=21.813 mm)				
	Shell (N)	Solid (N)	Difference (N)	Difference (%)
F1SUM (N)	5,714	5,684	0,030	-0,53
F12SUM (N)	0,189	0,188	0,001	-0,41
F13SUM (N)	0,157	0,154	0,002	-1,44
F2SUM (N)	40,108	40,001	0,107	-0,27
F21SUM (N)	10,701	10,697	0,004	-0,04
F23SUM (N)	1,320	1,359	-0,039	2,94
F3SUM (N)	30,220	24,785	5,435	-17,98
F31SUM (N)	5,210	4,556	0,654	-12,56
F32SUM (N)	2,648	2,554	0,095	-3,58

Table B.10 Comparison of the Total Reaction Forces- Shell Modeling and Mixed Modeling of the Honeycomb Structure for CS3-H3

CS3-H3 (h=21.813 mm)				
	Shell (N)	Solid (N)	Difference (N)	Difference (%)
F1SUM (N)	5,718	5,684	0,034	-0,59
F12SUM (N)	0,189	0,188	0,001	-0,43
F13SUM (N)	0,301	0,274	0,027	-8,90
F2SUM (N)	40,609	40,442	0,167	-0,41
F21SUM (N)	10,710	10,705	0,005	-0,05
F23SUM (N)	2,109	2,128	-0,018	0,87
F3SUM (N)	19,533	16,319	3,214	-16,45
F31SUM (N)	3,102	2,789	0,312	-10,07
F32SUM (N)	1,430	1,369	0,061	-4,29

Table B.11 Comparison of the Total Reaction Forces- Shell Modeling and Mixed Modeling of the Honeycomb Structure for CS4-H3

CS4-H3 (h=21.813 mm)				
	Shell (N)	Solid (N)	Difference (N)	Difference (%)
F1SUM (N)	5,714	5,664	0,049	-0,86
F12SUM (N)	0,189	0,188	0,001	-0,62
F13SUM (N)	0,539	0,467	0,071	-13,21
F2SUM (N)	40,825	40,590	0,235	-0,58
F21SUM (N)	10,706	10,703	0,003	-0,03
F23SUM (N)	2,952	2,982	-0,030	1,01
F3SUM (N)	12,078	8,434	3,644	-30,17
F31SUM (N)	1,481	1,230	0,251	-16,97
F32SUM (N)	0,564	0,465	0,099	-17,54

Table B.12 Comparison of the Total Reaction Forces- Shell Modeling and Mixed Modeling of the Honeycomb Structure for CS1-H4

CS1-H4 (h=31.750 mm)				
	Shell (N)	Solid (N)	Difference (N)	Difference (%)
F1SUM (N)	5,717	5,680	0,037	-0,65
F12SUM (N)	0,189	0,188	0,001	-0,27
F13SUM (N)	0,645	0,631	0,014	-2,14
F2SUM (N)	41,180	40,988	0,192	-0,47
F21SUM (N)	10,721	10,720	0,001	-0,01
F23SUM (N)	3,737	3,738	-0,001	0,02
F3SUM (N)	11,208	9,112	2,096	-18,70
F31SUM (N)	1,467	1,416	0,051	-3,47
F32SUM (N)	0,527	0,474	0,052	-9,96

Table B.13 Comparison of the Total Reaction Forces- Shell Modeling and Mixed Modeling of the Honeycomb Structure for CS2-H4

CS2-H4 (h=31.750 mm)				
	Shell (N)	Solid (N)	Difference (N)	Difference (%)
F1SUM (N)	5,716	5,684	0,032	-0,55
F12SUM (N)	0,188	0,188	0,001	-0,42
F13SUM (N)	0,240	0,225	0,015	-6,13
F2SUM (N)	40,421	40,295	0,126	-0,31
F21SUM (N)	10,703	10,699	0,004	-0,04
F23SUM (N)	1,777	1,817	-0,040	2,26
F3SUM (N)	22,726	18,525	4,201	-18,49
F31SUM (N)	3,720	3,248	0,473	-12,70
F32SUM (N)	1,791	1,679	0,113	-6,28

Table B.14 Comparison of the Total Reaction Forces- Shell Modeling and Mixed Modeling of the Honeycomb Structure for CS3-H4

CS3-H4 (h=31.750 mm)				
	Shell (N)	Solid (N)	Difference (N)	Difference (%)
F1SUM (N)	5,680	5,714	-0,035	0,61
F12SUM (N)	0,188	0,189	-0,001	0,44
F13SUM (N)	0,403	0,453	-0,050	12,34
F2SUM (N)	40,740	40,935	-0,195	0,48
F21SUM (N)	10,706	10,711	-0,005	0,05
F23SUM (N)	2,816	2,840	-0,024	0,85
F3SUM (N)	12,219	14,561	-2,342	19,17
F31SUM (N)	1,924	2,122	-0,197	10,25
F32SUM (N)	0,824	0,872	-0,049	5,94

Table B.15 Comparison of the Total Reaction Forces- Shell Modeling and Mixed Modeling of the Honeycomb Structure for CS4-H4

CS4-H4 (h=31.750 mm)				
	Shell (N)	Solid (N)	Difference (N)	Difference (%)
F1SUM (N)	5,713	5,664	0,049	-0,86
F12SUM (N)	0,189	0,188	0,001	-0,62
F13SUM (N)	0,778	0,659	0,118	-15,21
F2SUM (N)	40,969	40,704	0,265	-0,65
F21SUM (N)	10,709	10,706	0,003	-0,03
F23SUM (N)	3,928	3,899	0,029	-0,73
F3SUM (N)	9,028	6,327	2,701	-29,91
F31SUM (N)	0,955	0,790	0,165	-17,32
F32SUM (N)	0,311	0,248	0,063	-20,16

APPENDIX C

Table C.1 The Relative Difference between the Honeycomb and
Regenerated Equivalent Models of CS1-H2 in the First Runs (h=7.938)

CS1 – H2 (Relative Difference, %) (See Table 4.1)					
Total Reaction Force	1	2	3	4	5
F1SUM	-1,62	-1,10	-1,72	-1,72	-1,72
F12SUM	-0,59	-0,22	-0,69	-0,69	-0,69
F13SUM	-98,38	19,00	1,52	4,95	1,47
F2SUM	-1,97	-1,59	-2,14	-2,14	-2,14
F21SUM	-0,33	-0,26	-0,37	-0,37	-0,37
F23SUM	-93,50	89,48	15,47	15,47	15,47
F3SUM	0,35	0,38	0,36	0,36	0,36
F31SUM	-99,98	72,43	1,62	11,96	1,48
F32SUM	-99,97	76,21	1,65	1,65	1,65
Total Reaction Force	6	7	8	9	10
F1SUM	-0,88	-1,72	-1,72	-1,58	-1,69
F12SUM	-0,17	-0,69	-0,69	-0,57	-0,66
F13SUM	1,67	4,95	12,14	12,17	18,85
F2SUM	-0,88	-2,14	-2,14	-2,04	-2,12
F21SUM	-0,18	-0,37	-0,37	-0,34	-0,35
F23SUM	15,50	15,47	0,89	0,89	89,43
F3SUM	0,36	0,36	-21,01	-21,01	0,36
F31SUM	1,69	11,96	36,29	36,31	72,35
F32SUM	1,84	1,65	-15,21	-15,18	76,01

Table C.2 The Relative Difference between the Honeycomb and Regenerated Equivalent Models of CS2-H2 in the First Runs (h=7.938)

CS2 – H2 (Relative Difference, %) (See Table 4.1)					
Total Reaction Force	1	2	3	4	5
F1SUM	-1,21	-1,21	-1,24	-1,24	-1,24
F12SUM	-0,52	-0,52	-0,54	-0,54	-0,54
F13SUM	-96,35	13,63	3,17	5,80	3,17
F2SUM	-1,05	-1,06	-1,09	-1,09	-1,09
F21SUM	-0,21	-0,21	-0,21	-0,21	-0,21
F23SUM	-90,35	69,92	14,00	14,01	14,00
F3SUM	-0,92	-0,90	-0,91	-0,91	-0,91
F31SUM	-100,0	74,84	-2,11	11,30	-2,11
F32SUM	-99,99	91,78	2,62	2,62	2,62
Total Reaction Force	6	7	8	9	10
F1SUM	-1,04	-1,24	-1,24	-1,22	-1,23
F12SUM	-0,38	-0,54	-0,55	-0,53	-0,54
F13SUM	3,21	5,80	9,27	9,27	13,62
F2SUM	-0,84	-1,09	-1,09	-1,08	-1,09
F21SUM	-0,17	-0,21	-0,21	-0,21	-0,21
F23SUM	14,01	14,01	6,70	6,70	69,84
F3SUM	-0,91	-0,91	-39,89	-39,89	-0,91
F31SUM	-2,09	11,30	31,68	31,68	74,75
F32SUM	2,66	2,62	-9,55	-9,55	91,61

Table C.3 The Relative Difference between the Honeycomb and Regenerated Equivalent Models of CS3-H2 in the First Runs (h=7.938)

CS3 – H2 (Relative Difference, %) (See Table 4.1)					
Total Reaction Force	1	2	3	4	5
F1SUM	-1,44	-1,48	-1,51	-1,51	-1,51
F12SUM	-0,58	-0,61	-0,64	-0,64	-0,64
F13SUM	-97,81	15,92	1,99	4,91	2,08
F2SUM	-1,50	-1,61	-1,63	-1,63	-1,63
F21SUM	-0,27	-0,28	-0,29	-0,29	-0,29
F23SUM	-93,03	73,67	-93,07	9,62	9,62
F3SUM	-0,29	-0,28	-0,28	-0,28	-0,28
F31SUM	-99,98	73,82	0,95	11,80	1,18
F32SUM	-99,96	83,79	-100,00	1,94	1,94
Total Reaction Force	6	7	8	9	10
F1SUM	-0,94	-1,51	-1,51	-0,94	-1,50
F12SUM	-0,24	-0,64	-0,64	-0,24	-0,63
F13SUM	2,19	4,91	9,38	2,19	15,91
F2SUM	-0,83	-1,63	-1,63	-0,83	-1,62
F21SUM	-0,16	-0,29	-0,29	-0,16	-0,28
F23SUM	9,64	9,62	-3,47	9,64	73,67
F3SUM	-0,28	-0,28	-29,74	-0,28	-0,28
F31SUM	1,23	11,80	29,84	1,23	73,82
F32SUM	2,08	1,94	-15,61	2,08	83,78

Table C.4 The Relative Difference between the Honeycomb and Regenerated Equivalent Models of CS4-H2 in the First Runs (h=7.938)

CS4 – H2 (Relative Difference, %) (See Table 4.1)					
Total Reaction Force	1	2	3	4	5
F1SUM	-1,44	-1,47	-1,54	-1,54	-1,54
F12SUM	-0,49	-0,51	-0,58	-0,58	-0,58
F13SUM	-98,52	23,88	1,31	5,68	1,31
F2SUM	-2,13	-2,20	-2,26	-2,26	-2,26
F21SUM	-0,25	-0,26	-0,28	-0,28	-0,28
F23SUM	-93,36	79,35	6,05	6,13	6,13
F3SUM	-0,03	-0,02	-0,02	-0,02	-0,02
F31SUM	-100,0	70,29	1,27	11,55	1,27
F32SUM	-100,0	69,27	1,05	1,12	1,12
Total Reaction Force	6	7	8	9	10
F1SUM	-0,50	-1,54	-1,54	-1,48	-1,51
F12SUM	-0,02	-0,58	-0,58	-0,53	-0,55
F13SUM	1,49	5,68	16,29	16,30	23,87
F2SUM	-0,50	-2,26	-2,26	-2,22	-2,24
F21SUM	-0,06	-0,28	-0,29	-0,27	-0,27
F23SUM	6,17	6,13	-5,04	-5,04	79,34
F3SUM	-0,02	-0,02	-16,90	-16,90	-0,02
F31SUM	1,37	11,55	39,68	39,68	70,28
F32SUM	1,37	1,12	-12,56	-12,54	69,25

Table C.5 The Relative Difference between the Honeycomb and Regenerated Equivalent Models of CS1-H3 in the First Runs (h=21.813)

CS1 – H3 (Relative Difference, %) (See Table 4.1)					
Total Reaction Force	1	2	3	4	5
F1SUM	-1,55	-0,75	-1,84	-1,84	-1,84
F12SUM	-0,37	0,01	-0,65	-0,65	-0,65
F13SUM	-99,62	36,94	0,38	6,75	0,29
F2SUM	-4,33	-3,34	-4,71	-4,71	-4,71
F21SUM	-0,38	-0,27	-0,47	-0,47	-0,47
F23SUM	-97,80	88,35	3,28	3,28	3,28
F3SUM	-0,19	-0,18	-0,19	-0,19	-0,19
F31SUM	-99,98	56,42	0,53	9,27	0,41
F32SUM	-99,95	34,51	-0,42	-0,42	-0,42
Total Reaction Force	6	7	8	9	10
F1SUM	-0,76	-1,84	-1,84	-1,51	-1,76
F12SUM	-0,04	-0,65	-0,66	-0,41	-0,56
F13SUM	0,63	6,75	21,32	21,39	36,57
F2SUM	-1,80	-4,71	-4,71	-4,44	-4,65
F21SUM	-0,21	-0,47	-0,47	-0,40	-0,43
F23SUM	3,35	3,28	-11,82	-11,80	88,23
F3SUM	-0,19	-0,19	-21,55	-21,54	-0,19
F31SUM	0,69	9,27	23,18	23,25	56,20
F32SUM	-0,14	-0,42	-18,96	-18,89	34,31

Table C.6 The Relative Difference between the Honeycomb and Regenerated Equivalent Models of CS2-H3 in the First Runs (h=21.813)

CS2 – H3 (Relative Difference, %) (See Table 4.1)					
Total Reaction Force	1	2	3	4	5
F1SUM	-1,82	-1,79	-1,88	-1,88	-1,88
F12SUM	-0,54	-0,52	-0,59	-0,59	-0,59
F13SUM	-99,35	19,95	-4,01	1,52	-4,01
F2SUM	-2,84	-2,85	-2,92	-2,92	-2,92
F21SUM	-0,32	-0,31	-0,33	-0,33	-0,33
F23SUM	-96,85	85,30	6,96	6,96	6,96
F3SUM	-2,00	-2,00	-2,00	-2,00	-2,00
F31SUM	-100,0	68,37	-2,25	10,35	-2,25
F32SUM	-99,99	64,46	-0,21	-0,20	-0,21
Total Reaction Force	6	7	8	9	10
F1SUM	-1,41	-1,88	-1,88	-1,83	-1,87
F12SUM	-0,30	-0,59	-0,60	-0,56	-0,58
F13SUM	-3,92	1,52	9,31	9,32	19,91
F2SUM	-2,23	-2,92	-2,92	-2,88	-2,91
F21SUM	-0,22	-0,33	-0,33	-0,32	-0,33
F23SUM	6,98	6,96	-2,03	-2,03	85,16
F3SUM	-2,00	-2,00	-40,63	-40,63	-2,00
F31SUM	-2,20	10,35	24,36	24,37	68,28
F32SUM	-0,03	-0,20	-17,91	-17,90	64,32

Table C.7 The Relative Difference between the Honeycomb and Regenerated Equivalent Models of CS3-H3 in the First Runs (h=21.813)

CS3 – H3 (Relative Difference, %) (See Table 4.1)					
Total Reaction Force	1	2	3	4	5
F1SUM	-1,70	-1,80	-1,89	-1,89	-1,89
F12SUM	-0,43	-0,52	-0,60	-0,60	-0,60
F13SUM	-99,53	31,31	0,44	6,16	0,51
F2SUM	-3,71	-3,90	-3,97	-3,97	-3,97
F21SUM	-0,35	-0,37	-0,39	-0,40	-0,40
F23SUM	-97,56	87,14	-97,60	4,50	4,50
F3SUM	-0,85	-0,85	-0,85	-0,85	-0,85
F31SUM	-99,97	62,57	0,24	9,88	0,36
F32SUM	-99,95	46,82	-99,99	-0,55	-0,55
Total Reaction Force	6	7	8	9	10
F1SUM	-0,91	-1,89	-1,89	-0,91	-1,85
F12SUM	-0,09	-0,60	-0,61	-0,09	-0,57
F13SUM	0,73	6,16	15,75	0,73	31,29
F2SUM	-1,93	-3,97	-3,97	-1,93	-3,94
F21SUM	-0,17	-0,40	-0,40	-0,17	-0,38
F23SUM	4,55	4,50	-10,46	4,55	87,13
F3SUM	-0,85	-0,85	-30,24	-0,85	-0,85
F31SUM	0,49	9,88	20,24	0,49	62,56
F32SUM	-0,27	-0,55	-21,62	-0,27	46,80

Table C.8 The Relative Difference between the Honeycomb and Regenerated Equivalent Models of CS4-H3 in the First Runs (h=21.813)

CS4 – H3 (Relative Difference, %) (See Table 4.1)					
Total Reaction Force	1	2	3	4	5
F1SUM	-1,24	-1,34	-1,53	-1,53	-1,53
F12SUM	-0,23	-0,34	-0,50	-0,50	-0,50
F13SUM	-99,64	43,61	0,42	7,80	0,42
F2SUM	-3,92	-4,13	-4,29	-4,29	-4,29
F21SUM	-0,27	-0,30	-0,36	-0,36	-0,36
F23SUM	-97,49	89,94	2,81	2,89	2,89
F3SUM	-0,10	-0,10	-0,10	-0,10	-0,10
F31SUM	-100,0	50,86	0,43	8,67	0,43
F32SUM	-99,99	26,99	-0,53	-0,49	-0,49
Total Reaction Force	6	7	8	9	10
F1SUM	-0,43	-1,53	-1,53	-1,37	-1,44
F12SUM	0,15	-0,50	-0,51	-0,37	-0,42
F13SUM	0,65	7,80	27,60	27,63	43,59
F2SUM	-0,67	-4,29	-4,29	-4,18	-4,23
F21SUM	-0,08	-0,36	-0,37	-0,31	-0,32
F23SUM	2,99	2,89	-9,38	-9,36	89,92
F3SUM	-0,10	-0,10	-17,05	-17,05	-0,10
F31SUM	0,59	8,67	23,96	24,00	50,82
F32SUM	-0,20	-0,49	-15,65	-15,61	26,96

Table C.9 The Relative Difference between the Honeycomb and Regenerated Equivalent Models of CS1-H4 in the First Runs (h=31.750)

CS1 – H4 (Relative Difference, %) (See Table 4.1)					
Total Reaction Force	1	2	3	4	5
F1SUM	-1,41	-0,71	-1,80	-1,80	-1,80
F12SUM	-0,46	-0,13	-0,83	-0,83	-0,83
F13SUM	-99,75	34,30	-5,52	1,19	-5,62
F2SUM	-4,73	-3,55	-5,23	-5,23	-5,23
F21SUM	-0,40	-0,30	-0,53	-0,53	-0,53
F23SUM	-98,28	94,67	4,87	4,87	4,87
F3SUM	-0,12	-0,11	-0,12	-0,12	-0,12
F31SUM	-99,98	32,57	-10,16	-3,17	-10,26
F32SUM	-99,94	18,19	-5,18	-5,18	-5,18
Total Reaction Force	6	7	8	9	10
F1SUM	-0,74	-1,80	-1,80	-1,41	-1,69
F12SUM	-0,17	-0,83	-0,85	-0,55	-0,73
F13SUM	-5,29	1,19	16,91	17,00	33,91
F2SUM	-1,88	-5,23	-5,23	-4,88	-5,15
F21SUM	-0,25	-0,53	-0,53	-0,43	-0,47
F23SUM	4,95	4,87	-10,80	-10,77	94,54
F3SUM	-0,12	-0,12	-21,51	-21,50	-0,12
F31SUM	-10,02	-3,17	4,32	4,39	32,40
F32SUM	-4,96	-5,18	-23,51	-23,44	18,04

Table C.10 The Relative Difference between the Honeycomb and Regenerated Equivalent Models of CS2-H4 in the First Runs (h=31.750)

CS2 – H4 (Relative Difference, %) (See Table 4.1)					
Total Reaction Force	1	2	3	4	5
F1SUM	-1,81	-1,77	-1,89	-1,89	-1,89
F12SUM	-0,50	-0,46	-0,56	-0,56	-0,56
F13SUM	-99,55	29,42	-0,72	6,02	-0,72
F2SUM	-3,52	-3,54	-3,63	-3,63	-3,63
F21SUM	-0,33	-0,33	-0,35	-0,35	-0,35
F23SUM	-97,64	88,05	5,68	5,68	5,68
F3SUM	-1,63	-1,62	-1,63	-1,63	-1,63
F31SUM	-100,0	64,66	-2,30	9,86	-2,30
F32SUM	-99,99	52,71	-0,71	-0,71	-0,71
Total Reaction Force	6	7	8	9	10
F1SUM	-1,35	-1,89	-1,89	-1,82	-1,88
F12SUM	-0,25	-0,56	-0,58	-0,52	-0,55
F13SUM	-0,61	6,02	15,74	15,75	29,37
F2SUM	-2,74	-3,63	-3,63	-3,58	-3,62
F21SUM	-0,22	-0,35	-0,35	-0,34	-0,34
F23SUM	5,71	5,68	-3,56	-3,56	87,90
F3SUM	-1,63	-1,63	-40,41	-40,41	-1,63
F31SUM	-2,22	9,86	20,25	20,26	64,57
F32SUM	-0,51	-0,71	-21,49	-21,47	52,59

Table C.11 The Relative Difference between the Honeycomb and Regenerated Equivalent Models of CS3-H4 in the First Runs (h=31.750)

CS3 – H4 (Relative Difference, %) (See Table 4.1)					
Total Reaction Force	1	2	3	4	5
F1SUM	-1,56	-1,69	-1,81	-1,81	-1,81
F12SUM	-0,36	-0,49	-0,59	-0,59	-0,59
F13SUM	-99,67	36,70	0,28	6,80	0,35
F2SUM	-4,34	-4,58	-4,67	-4,67	-4,67
F21SUM	-0,34	-0,37	-0,39	-0,41	-0,41
F23SUM	-98,14	89,42	-98,18	3,57	3,57
F3SUM	-0,63	-0,63	-0,63	-0,63	-0,63
F31SUM	-99,97	56,39	0,11	9,08	0,22
F32SUM	-99,94	34,58	-99,99	-0,84	-0,84
Total Reaction Force	6	7	8	9	10
F1SUM	-0,85	-1,81	-1,81	-0,85	-1,76
F12SUM	-0,06	-0,59	-0,60	-0,06	-0,54
F13SUM	0,58	6,80	17,97	0,58	36,68
F2SUM	-2,19	-4,67	-4,67	-2,19	-4,63
F21SUM	-0,17	-0,41	-0,41	-0,17	-0,38
F23SUM	3,64	3,57	-11,65	3,64	89,41
F3SUM	-0,63	-0,63	-30,09	-0,63	-0,63
F31SUM	0,37	9,08	15,05	0,37	56,37
F32SUM	-0,58	-0,84	-23,59	-0,58	34,55

Table C.12 The Relative Difference between the Honeycomb and Regenerated Equivalent Models of CS4-H4 in the First Runs (h=31.750)

CS4 – H4 (Relative Difference, %) (See Table 4.1)					
Total Reaction Force	1	2	3	4	5
F1SUM	-1,13	-1,28	-1,52	-1,52	-1,52
F12SUM	-0,14	-0,30	-0,51	-0,50	-0,51
F13SUM	-99,74	49,03	0,33	8,40	0,33
F2SUM	-4,07	-4,34	-4,56	-4,56	-4,56
F21SUM	-0,27	-0,31	-0,39	-0,39	-0,39
F23SUM	-98,07	91,67	2,20	2,29	2,29
F3SUM	-0,05	-0,05	-0,05	-0,05	-0,05
F31SUM	-100,0	41,64	0,37	7,48	0,37
F32SUM	-99,99	18,22	-0,54	-0,51	-0,51
Total Reaction Force	6	7	8	9	10
F1SUM	-0,41	-1,52	-1,52	-1,32	-1,41
F12SUM	0,21	-0,50	-0,52	-0,34	-0,40
F13SUM	0,55	8,40	30,56	30,59	48,99
F2SUM	-0,66	-4,56	-4,56	-4,41	-4,48
F21SUM	-0,10	-0,39	-0,39	-0,32	-0,33
F23SUM	2,39	2,29	-10,14	-10,13	91,65
F3SUM	-0,05	-0,05	-17,02	-17,02	-0,05
F31SUM	0,53	7,48	16,57	16,61	41,60
F32SUM	-0,27	-0,51	-16,15	-16,12	18,20

APPENDIX D

Table D.1 The Relative Difference between the Honeycomb and
Regenerated Equivalent Models of CS1-H2 in the Third Runs

CS1 – H2 (h=7.938mm)				
Total Reaction Force	11	12	13	14
F1SUM	-0,59	-0,57	-0,58	-1,70
F12SUM	-0,04	-0,05	-0,05	-0,67
F13SUM	5,19	5,20	1,75	4,96
F2SUM	-0,33	0,08	0,08	-2,12
F21SUM	-0,11	-0,06	-0,07	-0,35
F23SUM	15,52	15,53	15,52	15,47
F3SUM	0,36	0,36	0,36	0,36
F31SUM	12,05	12,06	1,72	11,96
F32SUM	1,90	1,93	1,93	1,65

Table D.2 The Relative Difference between the Honeycomb and
Regenerated Equivalent Models of CS2-H2 in the Third Runs

CS2 – H2 (h=7.938mm)				
Total Reaction Force	11	12	13	14
F1SUM	-1,04	-1,09	-1,09	-1,23
F12SUM	-0,38	-0,42	-0,42	-0,54
F13SUM	7,16	5,83	3,74	5,80
F2SUM	-0,84	-0,87	-0,87	-1,09
F21SUM	-0,17	-0,17	-0,17	-0,21
F23SUM	14,02	14,02	14,01	14,01
F3SUM	-0,91	-0,91	-0,91	-0,91
F31SUM	19,15	11,31	0,45	11,30
F32SUM	2,67	2,66	2,66	2,62

Table D.3 The Relative Difference between the Honeycomb and Regenerated Equivalent Models of CS3-H2 in the Third Runs

CS3 – H2 (h=7.938mm)				
Total Reaction Force	11	12	13	14
F1SUM	-0,94	-1,02	-1,02	-1,51
F12SUM	-0,24	-0,29	-0,29	-0,63
F13SUM	5,03	5,01	2,18	4,91
F2SUM	-0,82	-0,82	-0,82	-1,62
F21SUM	-0,16	-0,15	-0,16	-0,28
F23SUM	9,64	9,64	9,64	9,62
F3SUM	-0,28	-0,28	-0,28	-0,28
F31SUM	11,85	11,84	1,22	11,80
F32SUM	2,08	2,08	2,07	1,94

Table D.4 The Relative Difference between the Honeycomb and Regenerated Equivalent Models of CS4-H2 in the Third Runs

CS4 – H2 (h=7.938mm)				
Total Reaction Force	11	12	13	14
F1SUM	-0,50	-0,51	-0,51	-1,52
F12SUM	-0,02	-0,04	-0,04	-0,56
F13SUM	5,88	5,88	1,50	5,69
F2SUM	-0,49	-0,11	-0,12	-2,24
F21SUM	-0,05	0,00	-0,01	-0,27
F23SUM	6,17	6,18	6,18	6,13
F3SUM	-0,02	-0,02	-0,02	-0,02
F31SUM	11,65	11,66	1,37	11,55
F32SUM	1,37	1,40	1,40	1,12

Table D.5 The Relative Difference between the Honeycomb and Regenerated Equivalent Models of CS1-H3 in the Third Runs

CS1 – H3 (h=23.813 mm)				
Total Reaction Force	11	12	13	14
F1SUM	-0,52	-0,56	-0,57	-1,78
F12SUM	0,09	0,08	0,07	-0,59
F13SUM	7,13	7,14	0,71	6,76
F2SUM	-0,71	0,13	0,06	-4,65
F21SUM	-0,14	-0,05	-0,09	-0,43
F23SUM	3,36	3,37	3,37	3,28
F3SUM	-0,19	-0,19	-0,19	-0,19
F31SUM	9,45	9,45	0,70	9,28
F32SUM	-0,10	-0,08	-0,08	-0,40

Table D.6 The Relative Difference between the Honeycomb and Regenerated Equivalent Models of CS2-H3 in the Third Runs

CS2 – H3 (h=23.813 mm)				
Total Reaction Force	11	12	13	14
F1SUM	-1,41	-1,52	-1,52	-1,87
F12SUM	-0,30	-0,36	-0,36	-0,59
F13SUM	4,52	1,59	-2,83	1,52
F2SUM	-2,23	-2,30	-2,31	-2,91
F21SUM	-0,22	-0,23	-0,23	-0,33
F23SUM	6,98	6,98	6,98	6,96
F3SUM	-2,00	-2,00	-2,00	-2,00
F31SUM	17,72	10,40	0,20	10,35
F32SUM	-0,03	-0,05	-0,05	-0,20

Table D.7 The Relative Difference between the Honeycomb and Regenerated Equivalent Models of CS3-H3 in the Third Runs

CS3 – H3 (h=23.813 mm)				
Total Reaction Force	11	12	13	14
F1SUM	-0,91	-1,04	-1,04	-1,86
F12SUM	-0,09	-0,15	-0,16	-0,58
F13SUM	6,41	6,38	0,70	6,17
F2SUM	-1,91	-1,88	-1,89	-3,94
F21SUM	-0,17	-0,15	-0,17	-0,38
F23SUM	4,55	4,55	4,55	4,50
F3SUM	-0,85	-0,85	-0,85	-0,85
F31SUM	10,01	10,00	0,48	9,88
F32SUM	-0,27	-0,27	-0,28	-0,55

Table D.8 The Relative Difference between the Honeycomb and Regenerated Equivalent Models of CS4-H3 in the Third Runs

CS4 – H3 (h=23.813 mm)				
Total Reaction Force	11	12	13	14
F1SUM	-0,43	-0,46	-0,46	-1,47
F12SUM	0,15	0,14	0,14	-0,44
F13SUM	8,07	8,07	0,65	7,81
F2SUM	-0,61	0,11	0,04	-4,23
F21SUM	-0,08	0,00	-0,01	-0,32
F23SUM	2,99	3,00	2,99	2,90
F3SUM	-0,10	-0,10	-0,10	-0,10
F31SUM	8,84	8,84	0,59	8,68
F32SUM	-0,20	-0,18	-0,18	-0,48

Table D.9 The Relative Difference between the Honeycomb and Regenerated Equivalent Models of CS1-H4 in the Third Runs

CS1 – H4 (h=31.750 mm)				
Total Reaction Force	11	12	13	14
F1SUM	-0,50	-0,53	-0,53	-1,72
F12SUM	-0,04	-0,05	-0,06	-0,76
F13SUM	1,54	1,54	-5,22	1,20
F2SUM	-0,74	0,16	0,06	-5,15
F21SUM	-0,19	-0,09	-0,14	-0,47
F23SUM	4,96	4,97	4,97	4,87
F3SUM	-0,12	-0,12	-0,12	-0,12
F31SUM	-3,01	-3,02	-10,0	-3,16
F32SUM	-4,92	-4,90	-4,90	-5,17

Table D.10 The Relative Difference between the Honeycomb and Regenerated Equivalent Models of CS2-H4 in the Third Runs

CS2 – H4 (h=31.750 mm)				
Total Reaction Force	11	12	13	14
F1SUM	11	12	13	14
F12SUM	-1,35	-1,46	-1,46	-1,88
F13SUM	-0,25	-0,31	-0,31	-0,56
F2SUM	9,73	6,11	0,71	6,02
F21SUM	-2,74	-2,84	-2,84	-3,62
F23SUM	-0,22	-0,23	-0,23	-0,34
F3SUM	5,71	5,71	5,70	5,68
F31SUM	-1,63	-1,63	-1,63	-1,63
F32SUM	16,94	9,92	0,09	9,86

Table D.11 The Relative Difference between the Honeycomb and Regenerated Equivalent Models of CS3-H4 in the Third Runs

CS3 – H4 (h=31.750 mm)				
Total Reaction Force	11	12	13	14
F1SUM	-0,84	-0,97	-0,97	-1,77
F12SUM	-0,05	-0,11	-0,12	-0,56
F13SUM	7,07	7,04	0,55	6,81
F2SUM	-2,17	-2,12	-2,14	-4,64
F21SUM	-0,16	-0,14	-0,16	-0,38
F23SUM	3,64	3,64	3,64	3,57
F3SUM	-0,63	-0,63	-0,63	-0,63
F31SUM	9,24	9,22	0,36	9,09
F32SUM	-0,58	-0,58	-0,58	-0,84

Table D.12 The Relative Difference between the Honeycomb and Regenerated Equivalent Models of CS4-H4 in the Third Runs

CS4 – H4 (h=31.750 mm)				
Total Reaction Force	11	12	13	14
F1SUM	-0,41	-0,44	-0,44	-1,44
F12SUM	0,21	0,20	0,20	-0,43
F13SUM	8,65	8,65	0,54	8,41
F2SUM	-0,59	0,16	0,07	-4,48
F21SUM	-0,09	-0,01	-0,01	-0,33
F23SUM	2,39	2,39	2,39	2,30
F3SUM	-0,05	-0,05	-0,05	-0,05
F31SUM	7,64	7,63	0,53	7,50
F32SUM	-0,27	-0,25	-0,25	-0,50

APPENDIX E

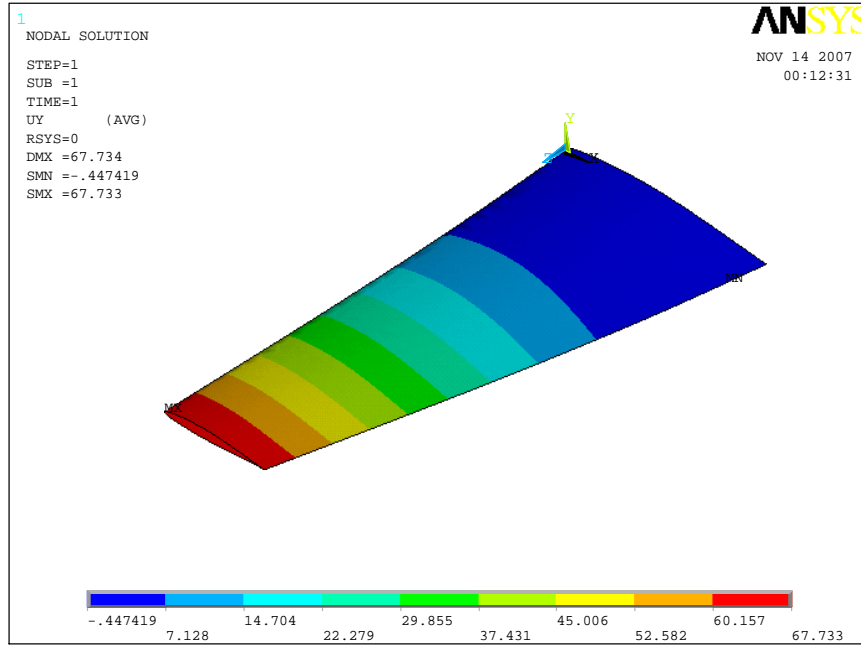


Figure E.1 Displacement of Wing Alternative 1

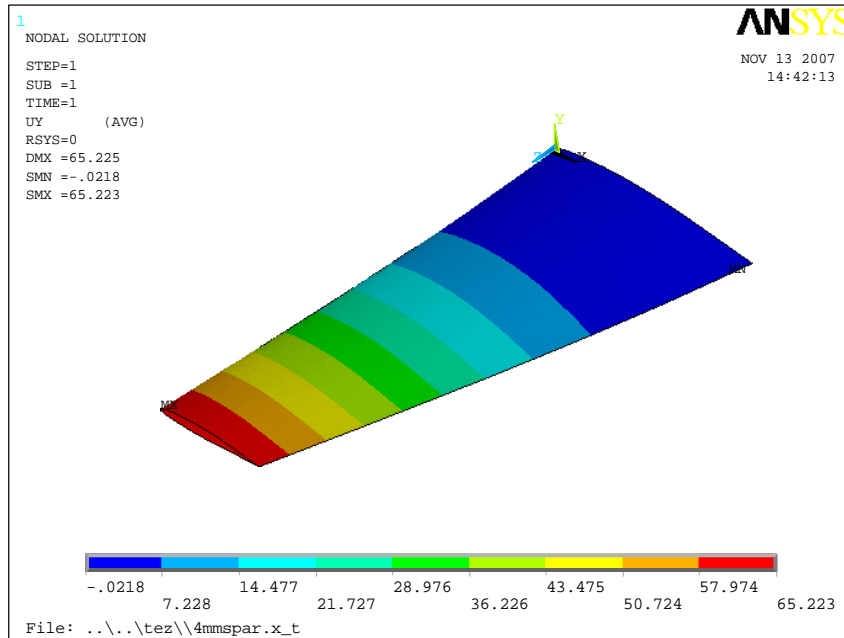


Figure E.2 Displacement of Wing Alternative 2

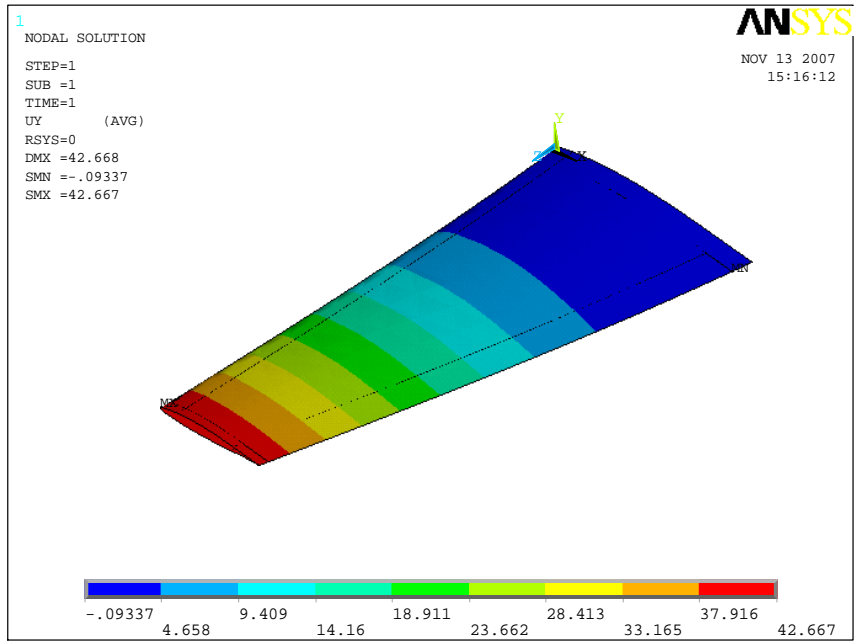


Figure E.3 Displacement of Wing Alternative 3